A study of dipole localization accuracy for MEG and EEG using a human skull phantom

R. M. Leahy[+], J. C. Mosher[*], M. E. Spencer[++], M. X. Huang[**], and J. D. Lewine[***]

[+]Signal & Image Processing Institute, University of Southern California, Los Angeles, CA 90089

[*]Los Alamos National Laboratory, Biophysics Group, Los Alamos, NM 87545

[++]Signal Processing Solutions, Inc., Redondo Beach, CA 90277

[**]Department of Radiology, University of New Mexico, Albuquerque, NM 87131

[***]Department of Radiology, University of Utah, Salt Lake City, UT 84132

Corresponding Author:

Richard M. Leahy, Ph.D.
Signal and Image Processing Institute
University of Southern California
Los Angeles, CA 90089-2564
Tel: (213) 740 4659
Fax: (213) 740 4651
e-mail: leahy@sipi.usc.edu

Printed: 4/1/98

A study of dipole localization accuracy for MEG and EEG using a human skull phantom

R. M. Leahy[+], J. C. Mosher[*], M. E. Spencer[++], M. X. Huang[**], and J. D. Lewine[***]

[+]Signal & Image Processing Institute, University of Southern California, Los Angeles, CA 90089

[*]Los Alamos National Laboratory, Biophysics Group, Los Alamos, NM 87545

[++]Signal Processing Solutions, Inc., Redondo Beach, CA 90277

[**]Department of Radiology, University of New Mexico, Albuquerque, NM 87131

[***]Department of Radiology, University of Utah, Salt Lake City, UT 84132

Corresponding Author:

Richard M. Leahy, Ph.D.
Signal and Image Processing Institute
University of Southern California
Los Angeles, CA 90089-2564
Tel: (213) 740 4659
Fax: (213) 740 4651
e-mail: leahy@sipi.usc.edu

Printed: 4/1/98

A study of dipole localization accuracy for MEG and EEG using a human skull phantom

R. M. Leahy[+], J. C. Mosher[*], M. E. Spencer[++], M. X. Huang[**], and J. D. Lewine[***]

[+]Signal & Image Processing Institute, University of Southern California, Los Angeles, CA 90089

[*]Los Alamos National Laboratory, Biophysics Group, Los Alamos, NM 87545

[++]Signal Processing Solutions, Inc., Redondo Beach, CA 90277

[**]Department of Radiology, University of New Mexico, Albuquerque, NM 87131

[***]Department of Radiology, University of Utah, Salt Lake City, UT 84132

Corresponding Author:

Richard M. Leahy, Ph.D.
Signal and Image Processing Institute
University of Southern California
Los Angeles, CA 90089-2564
Tel: (213) 740 4659
Fax: (213) 740 4651
e-mail: leahy@sipi.usc.edu

Printed: 4/1/98

A study of dipole localization accuracy for MEG and EEG using a human skull phantom

R. M. Leahy[+], J. C. Mosher[*], M. E. Spencer[++], M. X. Huang[**], and J. Lewine[***]

[+]University of Southern California, Los Angeles, CA 90089
[*]Los Alamos National Laboratory, Biophysics Group, Los Alamos, NM 87545
[++]Signal Processing Solutions, Inc., Redondo Beach, CA 90277
[**]Department of Radiology, University of New Mexico, Albuquerque, NM 87131
[***]Department of Radiology, University of Utah, Salt Lake City, UT 84132

Abstract

Objective: to investigate the accuracy of forward and inverse techniques for EEG and MEG dipole localization. Design and Methods: a human skull phantom was constructed with brain, skull and scalp layers and realistic relative conductivities. Thirty two independent current dipoles were distributed within the "brain" region and EEG and MEG data collected separately for each dipole. The true dipole locations and orientations and the morphology of the brain, skull and scalp layers were extracted from X-ray CT data. The location of each dipole was estimated from the EEG and MEG data using the R-MUSIC inverse method and forward models based on spherical and realistic head geometries. Additional computer simulations were performed to investigate the factors affecting localization accuracy. Results: localization errors using the relatively simpler locally fitted sphere approach are only slightly greater than those using a BEM approach. The average localization error over the 32 dipoles was 7 – 8 mm for EEG and 3 mm for MEG. Conclusion: The superior performance of MEG over EEG appears to be because the latter is more sensitive to errors in the forward model arising from simplifying assumptions concerning the conductivity of the skull, scalp and brain.

Key words: MEG, EEG, dipole localization, phantom, boundary element methods, locally fitted spheres.

This work is supported by the National Institute of Mental Health Grant R01-MH53213, and by Los Alamos National Laboratory, operated by the University of California for the United States Department of Energy under contract W-7405-ENG-36

A study of dipole localization accuracy for MEG and EEG using a human skull phantom

R. M. Leahy[+], J. C. Mosher[*], M. E. Spencer[++], M. X. Huang[**], and J. Lewine[***]

[+]University of Southern California, Los Angeles, CA 90089
[*]Los Alamos National Laboratory, Biophysics Group, Los Alamos, NM 87545
[++]Signal Processing Solutions, Inc., Redondo Beach, CA 90277
[**]Department of Radiology, University of New Mexico, Albuquerque, NM 87131
[***]Department of Radiology, University of Utah, Salt Lake City, UT 84132

Abstract

Objective: to investigate the accuracy of forward and inverse techniques for EEG and MEG dipole localization. Design and Methods: a human skull phantom was constructed with brain, skull and scalp layers and realistic relative conductivities. Thirty two independent current dipoles were distributed within the "brain" region and EEG and MEG data collected separately for each dipole. The true dipole locations and orientations and the morphology of the brain, skull and scalp layers were extracted from X-ray CT data. The location of each dipole was estimated from the EEG and MEG data using the R-MUSIC inverse method and forward models based on spherical and realistic head geometries. Additional computer simulations were performed to investigate the factors affecting localization accuracy. Results: localization errors using the relatively simpler locally fitted sphere approach are only slightly greater than those using a BEM approach. The average localization error over the 32 dipoles was 7 – 8 mm for EEG and 3 mm for MEG. Conclusion: The superior performance of MEG over EEG appears to be because the latter is more sensitive to errors in the forward model arising from simplifying assumptions concerning the conductivity of the skull, scalp and brain.

Key words: MEG, EEG, dipole localization, phantom, boundary element methods, locally fitted spheres.

This work is supported by the National Institute of Mental Health Grant R01-MH53213, and by Los Alamos National Laboratory, operated by the University of California for the United States Department of Energy under contract W-7405-ENG-36

A study of dipole localization accuracy for MEG and EEG using a human skull phantom

R. M. Leahy[+], J. C. Mosher[*], M. E. Spencer[++], M. X. Huang[**], and J. Lewine[***]

[+]University of Southern California, Los Angeles, CA 90089
[*]Los Alamos National Laboratory, Biophysics Group, Los Alamos, NM 87545
[++]Signal Processing Solutions, Inc., Redondo Beach, CA 90277
[**]Department of Radiology, University of New Mexico, Albuquerque, NM 87131
[***]Department of Radiology, University of Utah, Salt Lake City, UT 84132

Abstract

Objective: to investigate the accuracy of forward and inverse techniques for EEG and MEG dipole localization. Design and Methods: a human skull phantom was constructed with brain, skull and scalp layers and realistic relative conductivities. Thirty two independent current dipoles were distributed within the "brain" region and EEG and MEG data collected separately for each dipole. The true dipole locations and orientations and the morphology of the brain, skull and scalp layers were extracted from X-ray CT data. The location of each dipole was estimated from the EEG and MEG data using the R-MUSIC inverse method and forward models based on spherical and realistic head geometries. Additional computer simulations were performed to investigate the factors affecting localization accuracy. Results: localization errors using the relatively simpler locally fitted sphere approach are only slightly greater than those using a BEM approach. The average localization error over the 32 dipoles was 7 – 8 mm for EEG and 3 mm for MEG. Conclusion: The superior performance of MEG over EEG appears to be because the latter is more sensitive to errors in the forward model arising from simplifying assumptions concerning the conductivity of the skull, scalp and brain.

Key words: MEG, EEG, dipole localization, phantom, boundary element methods, locally fitted spheres.

This work is supported by the National Institute of Mental Health Grant R01-MH53213, and by Los Alamos National Laboratory, operated by the University of California for the United States Department of Energy under contract W-7405-ENG-36

1. Introduction

Electroencephalography (EEG) and magentoencephalography (MEG) can be used, respectively, to measure scalp surface potentials and external magnetic fields produced by the neural current sources associated with sensory, motor and cognitive activity. Inverse procedures in EEG and MEG are used to estimate the spatial distribution of the underlying, possibly focal, neural sources. The equivalent current dipole, and clusters of such dipoles, are a widely used source model for representing focal neural activity. For this model the inverse procedure must estimate the locations and amplitudes of the equivalent dipoles.

An important step in assessing the accuracy with which these sources can be estimated is to perform experimental studies in which the true location and temporal activity of the dipoles are known. In this way we can study the effect on accuracy of errors in the head and sensor models and of noise in the data. Studies of this type can be performed using computer simulation; however, the majority of published results that use computer simulations assume simplified models for the head, instrumentation and noise. Typical simulations use a spherical head with point measurements of the scalp potential or magnetic field and additive white Gaussian noise (cf. Mosher et al. 1993). To establish practical limits on the accuracy with which dipolar sources can be estimated, the models should take into account the non-ideal nature of the sensors, realistic head geometries and correlations in the noise. Furthermore, we must also consider the effects of inaccuracies in the forward model associated with uncertainties in the estimated conductivities in the head and the effect of simplifications and numerical errors associated with either spherical head approximations or boundary element methods based on more realistic head geometries.

While more elaborate simulations could be developed to include these factors, evaluation using data collected directly from a physical system has the advantage that the results can more closely reflect *in vivo* performance since they include factors that cannot readily be included in simulations, such as environmental noise and deviations of the physical system from our model. Such studies have been performed using dipolar sources implanted in epilepsy patients (Cohen et al. 1990); however, the procedures required to implant these sources, including making holes in the skull,

1. Introduction

Electroencephalography (EEG) and magentoencephalography (MEG) can be used, respectively, to measure scalp surface potentials and external magnetic fields produced by the neural current sources associated with sensory, motor and cognitive activity. Inverse procedures in EEG and MEG are used to estimate the spatial distribution of the underlying, possibly focal, neural sources. The equivalent current dipole, and clusters of such dipoles, are a widely used source model for representing focal neural activity. For this model the inverse procedure must estimate the locations and amplitudes of the equivalent dipoles.

An important step in assessing the accuracy with which these sources can be estimated is to perform experimental studies in which the true location and temporal activity of the dipoles are known. In this way we can study the effect on accuracy of errors in the head and sensor models and of noise in the data. Studies of this type can be performed using computer simulation; however, the majority of published results that use computer simulations assume simplified models for the head, instrumentation and noise. Typical simulations use a spherical head with point measurements of the scalp potential or magnetic field and additive white Gaussian noise (cf. Mosher et al. 1993). To establish practical limits on the accuracy with which dipolar sources can be estimated, the models should take into account the non-ideal nature of the sensors, realistic head geometries and correlations in the noise. Furthermore, we must also consider the effects of inaccuracies in the forward model associated with uncertainties in the estimated conductivities in the head and the effect of simplifications and numerical errors associated with either spherical head approximations or boundary element methods based on more realistic head geometries.

While more elaborate simulations could be developed to include these factors, evaluation using data collected directly from a physical system has the advantage that the results can more closely reflect *in vivo* performance since they include factors that cannot readily be included in simulations, such as environmental noise and deviations of the physical system from our model. Such studies have been performed using dipolar sources implanted in epilepsy patients (Cohen et al. 1990); however, the procedures required to implant these sources, including making holes in the skull,

1. Introduction

Electroencephalography (EEG) and magentoencephalography (MEG) can be used, respectively, to measure scalp surface potentials and external magnetic fields produced by the neural current sources associated with sensory, motor and cognitive activity. Inverse procedures in EEG and MEG are used to estimate the spatial distribution of the underlying, possibly focal, neural sources. The equivalent current dipole, and clusters of such dipoles, are a widely used source model for representing focal neural activity. For this model the inverse procedure must estimate the locations and amplitudes of the equivalent dipoles.

An important step in assessing the accuracy with which these sources can be estimated is to perform experimental studies in which the true location and temporal activity of the dipoles are known. In this way we can study the effect on accuracy of errors in the head and sensor models and of noise in the data. Studies of this type can be performed using computer simulation; however, the majority of published results that use computer simulations assume simplified models for the head, instrumentation and noise. Typical simulations use a spherical head with point measurements of the scalp potential or magnetic field and additive white Gaussian noise (cf. Mosher et al. 1993). To establish practical limits on the accuracy with which dipolar sources can be estimated, the models should take into account the non-ideal nature of the sensors, realistic head geometries and correlations in the noise. Furthermore, we must also consider the effects of inaccuracies in the forward model associated with uncertainties in the estimated conductivities in the head and the effect of simplifications and numerical errors associated with either spherical head approximations or boundary element methods based on more realistic head geometries.

While more elaborate simulations could be developed to include these factors, evaluation using data collected directly from a physical system has the advantage that the results can more closely reflect *in vivo* performance since they include factors that cannot readily be included in simulations, such as environmental noise and deviations of the physical system from our model. Such studies have been performed using dipolar sources implanted in epilepsy patients (Cohen et al. 1990); however, the procedures required to implant these sources, including making holes in the skull,

may result in severe distortion of volume currents. While such studies are important, they are not ideal for evaluation of general forward and inverse methods. The other functional modalities (fMRI and PET) offer the potential for providing ground truth for clinical and volunteer studies; however, the relationship between hemodynamic and electrophysiological processes are currently not sufficiently well understood to provide reliable cross-validation.

A multiple dipole phantom was used in (Phillips et al 1997) for evaluation of several MEG imaging methods. This “dry” phantom is based on the theoretical description in (Ilmoniemi et al. 1985) in which the resulting fields are shown to be identical to those produced by a current dipole in a uniformly conducting medium. The major limitations of this phantom are its inability to generate the volume currents associated with realistic head geometries and its unsuitability for EEG. Interesting studies have been performed with dipoles implanted in a cadaver head (Barth et al. 1986) and gelatin filled skulls by (Greenblatt and Robinson 1994, Lewine et al. 1995) and more recently by (Baillet et al. 1997). Here we build on these studies using a large number of dipoles implanted in a human skull phantom.

Motivated by the desire to produce realistic data corresponding to complex spatio-temporal current sources and to include the effects of realistic head geometries, we designed and fabricated a multiple dipole phantom consisting of 32 independently programmable and isolated dipoles which can be inserted in a skull mount and used to collect both EEG and MEG data. The design of the phantom was first described in (Spencer 1996). Here we report on the design of this phantom and include the results of a localization study using EEG and MEG. The design of the phantom and data collection procedures are described in Section 2. In Section 3 we describe our data processing methods that include registration of the MEG and phantom-based coordinate systems, forward head modeling for EEG and MEG, and current dipole fitting. Experimental results are reported in Section 4. These include tabulations of the localization errors for each of the dipoles using EEG and MEG data with spherical and realistic head models. In the discussion in Section 5 we include the results of several simulations that are compared with the experimental data in order to assess

may result in severe distortion of volume currents. While such studies are important, they are not ideal for evaluation of general forward and inverse methods. The other functional modalities (fMRI and PET) offer the potential for providing ground truth for clinical and volunteer studies; however, the relationship between hemodynamic and electrophysiological processes are currently not sufficiently well understood to provide reliable cross-validation.

A multiple dipole phantom was used in (Phillips et al 1997) for evaluation of several MEG imaging methods. This “dry” phantom is based on the theoretical description in (Ilmoniemi et al. 1985) in which the resulting fields are shown to be identical to those produced by a current dipole in a uniformly conducting medium. The major limitations of this phantom are its inability to generate the volume currents associated with realistic head geometries and its unsuitability for EEG. Interesting studies have been performed with dipoles implanted in a cadaver head (Barth et al. 1986) and gelatin filled skulls by (Greenblatt and Robinson 1994, Lewine et al. 1995) and more recently by (Baillet et al. 1997). Here we build on these studies using a large number of dipoles implanted in a human skull phantom.

Motivated by the desire to produce realistic data corresponding to complex spatio-temporal current sources and to include the effects of realistic head geometries, we designed and fabricated a multiple dipole phantom consisting of 32 independently programmable and isolated dipoles which can be inserted in a skull mount and used to collect both EEG and MEG data. The design of the phantom was first described in (Spencer 1996). Here we report on the design of this phantom and include the results of a localization study using EEG and MEG. The design of the phantom and data collection procedures are described in Section 2. In Section 3 we describe our data processing methods that include registration of the MEG and phantom-based coordinate systems, forward head modeling for EEG and MEG, and current dipole fitting. Experimental results are reported in Section 4. These include tabulations of the localization errors for each of the dipoles using EEG and MEG data with spherical and realistic head models. In the discussion in Section 5 we include the results of several simulations that are compared with the experimental data in order to assess

may result in severe distortion of volume currents. While such studies are important, they are not ideal for evaluation of general forward and inverse methods. The other functional modalities (fMRI and PET) offer the potential for providing ground truth for clinical and volunteer studies; however, the relationship between hemodynamic and electrophysiological processes are currently not sufficiently well understood to provide reliable cross-validation.

A multiple dipole phantom was used in (Phillips et al 1997) for evaluation of several MEG imaging methods. This “dry” phantom is based on the theoretical description in (Ilmoniemi et al. 1985) in which the resulting fields are shown to be identical to those produced by a current dipole in a uniformly conducting medium. The major limitations of this phantom are its inability to generate the volume currents associated with realistic head geometries and its unsuitability for EEG. Interesting studies have been performed with dipoles implanted in a cadaver head (Barth et al. 1986) and gelatin filled skulls by (Greenblatt and Robinson 1994, Lewine et al. 1995) and more recently by (Baillet et al. 1997). Here we build on these studies using a large number of dipoles implanted in a human skull phantom.

Motivated by the desire to produce realistic data corresponding to complex spatio-temporal current sources and to include the effects of realistic head geometries, we designed and fabricated a multiple dipole phantom consisting of 32 independently programmable and isolated dipoles which can be inserted in a skull mount and used to collect both EEG and MEG data. The design of the phantom was first described in (Spencer 1996). Here we report on the design of this phantom and include the results of a localization study using EEG and MEG. The design of the phantom and data collection procedures are described in Section 2. In Section 3 we describe our data processing methods that include registration of the MEG and phantom-based coordinate systems, forward head modeling for EEG and MEG, and current dipole fitting. Experimental results are reported in Section 4. These include tabulations of the localization errors for each of the dipoles using EEG and MEG data with spherical and realistic head models. In the discussion in Section 5 we include the results of several simulations that are compared with the experimental data in order to assess

the impact of different error sources on the total localization error. Final conclusions are drawn in Section 6.

2. Experimental Design and Data Acquisition

2.1. Phantom Design

The phantom design consists of three components: (i) a 32-element current dipole array; (ii) a personal computer (PC) controlled dipole driver with 32 isolated channels allowing independent control of each dipole; and (iii) a human-skull mount in which the dipole array is placed. We describe each of these three components below.

2.1.1. Dipole Array

The dipoles were constructed from semi-rigid coaxial cable (UT-034-SS-SS, Micro-Coax, UTI, Collegeville, PA) consisting of a 0.84 mm outside diameter shield made from stainless steel alloy (#304) tubing, a Teflon PTFE (Polytetrafluoroethylene) insulator and an inner stainless steel conductor. The semi-rigid coax was insulated using standard 3/64 inch heat shrinkable tubing and then striped back to expose 1 mm of the shield and 1 mm of the inner conductor to the volume conducting medium, as illustrated in Fig. 1. Thirty-two dipoles were constructed and arranged to approximately follow a pair of sulcal folds. Sixteen of these dipoles were distributed along, and arranged normally to, a nominal left central sulcus. Another fourteen dipoles were arranged along a nominal left calcerine fissure. The remaining dipoles were positioned to represent a pair of frontal sources. The semi-rigid nature of the cable allows us to bend the cable to individually position the dipoles for the desired locations and orientations.

2.1.2. Driver Design

The dipoles are driven by isolated current sources which in turn are controlled through a special purpose interface to a DOS-based PC. Arbitrary waveforms can be generated simultaneously at each of the 32 dipoles. These waveforms are designed using MATLAB software (The Mathworks, Natick, MA) on the PC and directed to the dipole drivers. The disk file on the PC can contain data

the impact of different error sources on the total localization error. Final conclusions are drawn in Section 6.

2. Experimental Design and Data Acquisition

2.1. Phantom Design

The phantom design consists of three components: (i) a 32-element current dipole array; (ii) a personal computer (PC) controlled dipole driver with 32 isolated channels allowing independent control of each dipole; and (iii) a human-skull mount in which the dipole array is placed. We describe each of these three components below.

2.1.1. Dipole Array

The dipoles were constructed from semi-rigid coaxial cable (UT-034-SS-SS, Micro-Coax, UTI, Collegeville, PA) consisting of a 0.84 mm outside diameter shield made from stainless steel alloy (#304) tubing, a Teflon PTFE (Polytetrafluoroethylene) insulator and an inner stainless steel conductor. The semi-rigid coax was insulated using standard 3/64 inch heat shrinkable tubing and then striped back to expose 1 mm of the shield and 1 mm of the inner conductor to the volume conducting medium, as illustrated in Fig. 1. Thirty-two dipoles were constructed and arranged to approximately follow a pair of sulcal folds. Sixteen of these dipoles were distributed along, and arranged normally to, a nominal left central sulcus. Another fourteen dipoles were arranged along a nominal left calcerine fissure. The remaining dipoles were positioned to represent a pair of frontal sources. The semi-rigid nature of the cable allows us to bend the cable to individually position the dipoles for the desired locations and orientations.

2.1.2. Driver Design

The dipoles are driven by isolated current sources which in turn are controlled through a special purpose interface to a DOS-based PC. Arbitrary waveforms can be generated simultaneously at each of the 32 dipoles. These waveforms are designed using MATLAB software (The Mathworks, Natick, MA) on the PC and directed to the dipole drivers. The disk file on the PC can contain data

the impact of different error sources on the total localization error. Final conclusions are drawn in Section 6.

2. Experimental Design and Data Acquisition

2.1. Phantom Design

The phantom design consists of three components: (i) a 32-element current dipole array; (ii) a personal computer (PC) controlled dipole driver with 32 isolated channels allowing independent control of each dipole; and (iii) a human-skull mount in which the dipole array is placed. We describe each of these three components below.

2.1.1. Dipole Array

The dipoles were constructed from semi-rigid coaxial cable (UT-034-SS-SS, Micro-Coax, UTI, Collegeville, PA) consisting of a 0.84 mm outside diameter shield made from stainless steel alloy (#304) tubing, a Teflon PTFE (Polytetrafluoroethylene) insulator and an inner stainless steel conductor. The semi-rigid coax was insulated using standard 3/64 inch heat shrinkable tubing and then striped back to expose 1 mm of the shield and 1 mm of the inner conductor to the volume conducting medium, as illustrated in Fig. 1. Thirty-two dipoles were constructed and arranged to approximately follow a pair of sulcal folds. Sixteen of these dipoles were distributed along, and arranged normally to, a nominal left central sulcus. Another fourteen dipoles were arranged along a nominal left calcerine fissure. The remaining dipoles were positioned to represent a pair of frontal sources. The semi-rigid nature of the cable allows us to bend the cable to individually position the dipoles for the desired locations and orientations.

2.1.2. Driver Design

The dipoles are driven by isolated current sources which in turn are controlled through a special purpose interface to a DOS-based PC. Arbitrary waveforms can be generated simultaneously at each of the 32 dipoles. These waveforms are designed using MATLAB software (The Mathworks, Natick, MA) on the PC and directed to the dipole drivers. The disk file on the PC can contain data

to drive all dipoles for as long as one hour with a sampling rate of 1000 samples per second per channel. “Streamer” software and a PDMA-16 Digital DMA Board (Keithley Metrabyte, Taunton, MA 02780) in the PC are used to clock the data at a constant rate in 16 bit words to the external dipole driver chassis.

In the external chassis, a parallel interface and clock generator format the digital data for 32 electrically-isolated Digital-to-Analog (D/A) converters. The 32 channels are electrically isolated from the ground and each other, and each channel can generate a fully bipolar signal. Each channel has optical isolators for the serial data, clock and load signals and has a transformer isolated DC-to-DC power converter. The digital data is converted to an analog signal using a 12 bit D/A converter (Linear Technology, LTC1257). The signal from the D/A converter is then filtered with a second order bandpass filter with a passband of 1 Hz to 200 Hz and a transconductance amplifier is used to convert the voltage signal to a current in the dipole. The dipole is driven with a current source so that the resulting dipole current is independent of the impedance of the dipole. For epoch-based acquisition, a synchronization signal formed by dividing the clock signal by 1000 is supplied from the dipole driver chassis to the EEG or MEG machine.

2.1.3. The Skull Mount

To study the irregular, eccentric morphology of the head, a human skull mount was built. The whole skull was boiled in saline solution and gelatin to impregnate the bone and achieve an appropriate conductivity relative to the interior volume. The skull was then filled with a saline-gelatin mixture to represent the brain volume. To provide a scalp layer, the outside of the skull was coated with forty layers of rubber latex molding compound (GP 306, Gerisch Products, Torrance, CA) to an approximately uniform thickness of 5 mm. The latex was mixed with sodium chloride to achieve the desired conductivity. To determine the relative conductivities of the brain, skull and scalp layers, separate 3 cm x 3 cm samples, each approximately 3 mm thick, where prepared for each layer and the impedance measured using a pair of 2 mm diameter cylindrical Ag/AgCl electrodes. The

to drive all dipoles for as long as one hour with a sampling rate of 1000 samples per second per channel. “Streamer” software and a PDMA-16 Digital DMA Board (Keithley Metrabyte, Taunton, MA 02780) in the PC are used to clock the data at a constant rate in 16 bit words to the external dipole driver chassis.

In the external chassis, a parallel interface and clock generator format the digital data for 32 electrically-isolated Digital-to-Analog (D/A) converters. The 32 channels are electrically isolated from the ground and each other, and each channel can generate a fully bipolar signal. Each channel has optical isolators for the serial data, clock and load signals and has a transformer isolated DC-to-DC power converter. The digital data is converted to an analog signal using a 12 bit D/A converter (Linear Technology, LTC1257). The signal from the D/A converter is then filtered with a second order bandpass filter with a passband of 1 Hz to 200 Hz and a transconductance amplifier is used to convert the voltage signal to a current in the dipole. The dipole is driven with a current source so that the resulting dipole current is independent of the impedance of the dipole. For epoch-based acquisition, a synchronization signal formed by dividing the clock signal by 1000 is supplied from the dipole driver chassis to the EEG or MEG machine.

2.1.3. The Skull Mount

To study the irregular, eccentric morphology of the head, a human skull mount was built. The whole skull was boiled in saline solution and gelatin to impregnate the bone and achieve an appropriate conductivity relative to the interior volume. The skull was then filled with a saline-gelatin mixture to represent the brain volume. To provide a scalp layer, the outside of the skull was coated with forty layers of rubber latex molding compound (GP 306, Gerisch Products, Torrance, CA) to an approximately uniform thickness of 5 mm. The latex was mixed with sodium chloride to achieve the desired conductivity. To determine the relative conductivities of the brain, skull and scalp layers, separate 3 cm x 3 cm samples, each approximately 3 mm thick, where prepared for each layer and the impedance measured using a pair of 2 mm diameter cylindrical Ag/AgCl electrodes. The

to drive all dipoles for as long as one hour with a sampling rate of 1000 samples per second per channel. “Streamer” software and a PDMA-16 Digital DMA Board (Keithley Metrabyte, Taunton, MA 02780) in the PC are used to clock the data at a constant rate in 16 bit words to the external dipole driver chassis.

In the external chassis, a parallel interface and clock generator format the digital data for 32 electrically-isolated Digital-to-Analog (D/A) converters. The 32 channels are electrically isolated from the ground and each other, and each channel can generate a fully bipolar signal. Each channel has optical isolators for the serial data, clock and load signals and has a transformer isolated DC-to-DC power converter. The digital data is converted to an analog signal using a 12 bit D/A converter (Linear Technology, LTC1257). The signal from the D/A converter is then filtered with a second order bandpass filter with a passband of 1 Hz to 200 Hz and a transconductance amplifier is used to convert the voltage signal to a current in the dipole. The dipole is driven with a current source so that the resulting dipole current is independent of the impedance of the dipole. For epoch-based acquisition, a synchronization signal formed by dividing the clock signal by 1000 is supplied from the dipole driver chassis to the EEG or MEG machine.

2.1.3. The Skull Mount

To study the irregular, eccentric morphology of the head, a human skull mount was built. The whole skull was boiled in saline solution and gelatin to impregnate the bone and achieve an appropriate conductivity relative to the interior volume. The skull was then filled with a saline-gelatin mixture to represent the brain volume. To provide a scalp layer, the outside of the skull was coated with forty layers of rubber latex molding compound (GP 306, Gerisch Products, Torrance, CA) to an approximately uniform thickness of 5 mm. The latex was mixed with sodium chloride to achieve the desired conductivity. To determine the relative conductivities of the brain, skull and scalp layers, separate 3 cm x 3 cm samples, each approximately 3 mm thick, where prepared for each layer and the impedance measured using a pair of 2 mm diameter cylindrical Ag/AgCl electrodes. The

ratio of the conductivities measured using this method was approximately 53:1:100 for scalp:skull:brain.

The skull phantom was attached to a plexi-glass base containing the dipole array using a rubber flange glued to the enlarged base of the skull. The base has a fill/drain plug for filling the brain volume of the phantom. A pressurized air volume in the neck of the base pushes on a membrane, which is in contact with the conducting medium, in order to compensate for volume loss due to evaporation. Without volume compensation, evaporative losses through the skull and scalp layers can cause air gaps to form between the brain and skull layers and interrupt volume currents in the skull. All materials in the base and phantoms were nonferrous for MEG sensor compatibility.

2.1.4. Electrode Placement

Sixty-five 2 mm diameter Ag/AgCl electrodes (In Vivo Metric Inc., Healdsburg, CA) were affixed to the scalp layer of the phantom. Most of the EEG electrodes were placed at the left and back portions of the phantom scalp surface, with a few placed at other regions. For this electrode placement, the angular distance between two nearby electrodes is about 10 degrees relative to the center of a spherical approximation to the scalp. The reference electrode was placed at the center of the electrode array. This distribution of electrodes provided denser sampling of the scalp potentials close to the actual dipole locations than would have been achieved with a more uniform distribution of sensors.

2.2. Data Acquisition

2.2.1. CT Scanning

To obtain ground truth information on the locations of the electrodes and coaxial dipoles and to extract the shape of the skull and scalp, the phantom was scanned using a Siemens Somatom Plus X-ray CT scanner. The original CT volume data consisted of 2 mm thick coronal slices with a pixel size of 0.29×0.29 mm. The original volume data was then resampled as a $256 \times 256 \times 325$ voxel isotropic volume using the AIR (Automatic Imaging Registration) software package (Woods et al. 1992). The voxel size of the interpolated CT data was $0.58 \times 0.58 \times 0.58$ mm. An X-ray pro-

ratio of the conductivities measured using this method was approximately 53:1:100 for scalp:skull:brain.

The skull phantom was attached to a plexi-glass base containing the dipole array using a rubber flange glued to the enlarged base of the skull. The base has a fill/drain plug for filling the brain volume of the phantom. A pressurized air volume in the neck of the base pushes on a membrane, which is in contact with the conducting medium, in order to compensate for volume loss due to evaporation. Without volume compensation, evaporative losses through the skull and scalp layers can cause air gaps to form between the brain and skull layers and interrupt volume currents in the skull. All materials in the base and phantoms were nonferrous for MEG sensor compatibility.

2.1.4. Electrode Placement

Sixty-five 2 mm diameter Ag/AgCl electrodes (In Vivo Metric Inc., Healdsburg, CA) were affixed to the scalp layer of the phantom. Most of the EEG electrodes were placed at the left and back portions of the phantom scalp surface, with a few placed at other regions. For this electrode placement, the angular distance between two nearby electrodes is about 10 degrees relative to the center of a spherical approximation to the scalp. The reference electrode was placed at the center of the electrode array. This distribution of electrodes provided denser sampling of the scalp potentials close to the actual dipole locations than would have been achieved with a more uniform distribution of sensors.

2.2. Data Acquisition

2.2.1. CT Scanning

To obtain ground truth information on the locations of the electrodes and coaxial dipoles and to extract the shape of the skull and scalp, the phantom was scanned using a Siemens Somatom Plus X-ray CT scanner. The original CT volume data consisted of 2 mm thick coronal slices with a pixel size of 0.29×0.29 mm. The original volume data was then resampled as a $256 \times 256 \times 325$ voxel isotropic volume using the AIR (Automatic Imaging Registration) software package (Woods et al. 1992). The voxel size of the interpolated CT data was $0.58 \times 0.58 \times 0.58$ mm. An X-ray pro-

ratio of the conductivities measured using this method was approximately 53:1:100 for scalp:skull:brain.

The skull phantom was attached to a plexi-glass base containing the dipole array using a rubber flange glued to the enlarged base of the skull. The base has a fill/drain plug for filling the brain volume of the phantom. A pressurized air volume in the neck of the base pushes on a membrane, which is in contact with the conducting medium, in order to compensate for volume loss due to evaporation. Without volume compensation, evaporative losses through the skull and scalp layers can cause air gaps to form between the brain and skull layers and interrupt volume currents in the skull. All materials in the base and phantoms were nonferrous for MEG sensor compatibility.

2.1.4. Electrode Placement

Sixty-five 2 mm diameter Ag/AgCl electrodes (In Vivo Metric Inc., Healdsburg, CA) were affixed to the scalp layer of the phantom. Most of the EEG electrodes were placed at the left and back portions of the phantom scalp surface, with a few placed at other regions. For this electrode placement, the angular distance between two nearby electrodes is about 10 degrees relative to the center of a spherical approximation to the scalp. The reference electrode was placed at the center of the electrode array. This distribution of electrodes provided denser sampling of the scalp potentials close to the actual dipole locations than would have been achieved with a more uniform distribution of sensors.

2.2. Data Acquisition

2.2.1. CT Scanning

To obtain ground truth information on the locations of the electrodes and coaxial dipoles and to extract the shape of the skull and scalp, the phantom was scanned using a Siemens Somatom Plus X-ray CT scanner. The original CT volume data consisted of 2 mm thick coronal slices with a pixel size of 0.29×0.29 mm. The original volume data was then resampled as a $256 \times 256 \times 325$ voxel isotropic volume using the AIR (Automatic Imaging Registration) software package (Woods et al. 1992). The voxel size of the interpolated CT data was $0.58 \times 0.58 \times 0.58$ mm. An X-ray pro-

jection of the phantom is shown in Fig. 2 and a single CT slice in Fig. 3. The geometric surfaces of the scalp and outer and inner skull were found by thresholding the images followed by manual editing of the boundaries in each of the resampled CT slices. Renderings of each of the three surfaces are shown in Fig. 4.

The electrode and dipole locations were found by viewing the interpolated CT slices. The dipole orientations were found from the CT coordinates of several points along the tip of the coaxial dipole using a best straight line fit. Since MEG is blind to the radial component and most sensitive to tangential dipoles, it is important for this comparative study of MEG and EEG localization errors that the study be conducted over a range of orientations. In Fig. 5 we show the deviation from a radial orientation of each of the 32 dipoles. Since the dipoles are neither predominantly radial or tangential, there appears to be no *a priori* bias in this study towards superior performance of either MEG or EEG.

The 3-D coordinates of the dipoles in CT space, after scaling for voxel size, are our "ground truth" data. The EEG electrode locations extracted from the CT data are also available in these ground truth coordinates, as well as in coordinates established by a probe position indicator system provided with the MEG equipment. Thus these CT-extracted EEG electrode locations were also used to register the MEG coordinate system to ground truth, as we will describe below.

2.2.2. MEG and EEG Acquisition

The MEG data were collected using the Neuromag-122 (Neuromag Ltd., Helsinki, Finland) whole head system at the New Mexico Institute of Neuroimaging in Albuquerque, New Mexico. This machine contains 61 dual-channel planar-gradiometer sensors giving a total of 122 spatial measurements. The EEG data were collected separately using a 32-channel Synamps (Neuroscan Inc., Sterling, Virginia) EEG system at the University of Southern California Signal & Image Processing Institute. Since our Synamps is limited to 32 channels simultaneously, we acquired data over the 64 EEG electrodes in two separate but identical runs. As an extra precaution against increased contact impedance due to separation of the brain volume from the skull, the EEG data

jection of the phantom is shown in Fig. 2 and a single CT slice in Fig. 3. The geometric surfaces of the scalp and outer and inner skull were found by thresholding the images followed by manual editing of the boundaries in each of the resampled CT slices. Renderings of each of the three surfaces are shown in Fig. 4.

The electrode and dipole locations were found by viewing the interpolated CT slices. The dipole orientations were found from the CT coordinates of several points along the tip of the coaxial dipole using a best straight line fit. Since MEG is blind to the radial component and most sensitive to tangential dipoles, it is important for this comparative study of MEG and EEG localization errors that the study be conducted over a range of orientations. In Fig. 5 we show the deviation from a radial orientation of each of the 32 dipoles. Since the dipoles are neither predominantly radial or tangential, there appears to be no *a priori* bias in this study towards superior performance of either MEG or EEG.

The 3-D coordinates of the dipoles in CT space, after scaling for voxel size, are our "ground truth" data. The EEG electrode locations extracted from the CT data are also available in these ground truth coordinates, as well as in coordinates established by a probe position indicator system provided with the MEG equipment. Thus these CT-extracted EEG electrode locations were also used to register the MEG coordinate system to ground truth, as we will describe below.

2.2.2. MEG and EEG Acquisition

The MEG data were collected using the Neuromag-122 (Neuromag Ltd., Helsinki, Finland) whole head system at the New Mexico Institute of Neuroimaging in Albuquerque, New Mexico. This machine contains 61 dual-channel planar-gradiometer sensors giving a total of 122 spatial measurements. The EEG data were collected separately using a 32-channel Synamps (Neuroscan Inc., Sterling, Virginia) EEG system at the University of Southern California Signal & Image Processing Institute. Since our Synamps is limited to 32 channels simultaneously, we acquired data over the 64 EEG electrodes in two separate but identical runs. As an extra precaution against increased contact impedance due to separation of the brain volume from the skull, the EEG data

jection of the phantom is shown in Fig. 2 and a single CT slice in Fig. 3. The geometric surfaces of the scalp and outer and inner skull were found by thresholding the images followed by manual editing of the boundaries in each of the resampled CT slices. Renderings of each of the three surfaces are shown in Fig. 4.

The electrode and dipole locations were found by viewing the interpolated CT slices. The dipole orientations were found from the CT coordinates of several points along the tip of the coaxial dipole using a best straight line fit. Since MEG is blind to the radial component and most sensitive to tangential dipoles, it is important for this comparative study of MEG and EEG localization errors that the study be conducted over a range of orientations. In Fig. 5 we show the deviation from a radial orientation of each of the 32 dipoles. Since the dipoles are neither predominantly radial or tangential, there appears to be no *a priori* bias in this study towards superior performance of either MEG or EEG.

The 3-D coordinates of the dipoles in CT space, after scaling for voxel size, are our "ground truth" data. The EEG electrode locations extracted from the CT data are also available in these ground truth coordinates, as well as in coordinates established by a probe position indicator system provided with the MEG equipment. Thus these CT-extracted EEG electrode locations were also used to register the MEG coordinate system to ground truth, as we will describe below.

2.2.2. MEG and EEG Acquisition

The MEG data were collected using the Neuromag-122 (Neuromag Ltd., Helsinki, Finland) whole head system at the New Mexico Institute of Neuroimaging in Albuquerque, New Mexico. This machine contains 61 dual-channel planar-gradiometer sensors giving a total of 122 spatial measurements. The EEG data were collected separately using a 32-channel Synamps (Neuroscan Inc., Sterling, Virginia) EEG system at the University of Southern California Signal & Image Processing Institute. Since our Synamps is limited to 32 channels simultaneously, we acquired data over the 64 EEG electrodes in two separate but identical runs. As an extra precaution against increased contact impedance due to separation of the brain volume from the skull, the EEG data

were collected with the skull inverted. In the results presented below, localization accuracies are compared for 122 channels of MEG data and 64 channels of EEG. To ensure that differences in performance are not simply due to the difference in the number of channels, simulations studies of the effect of increasing the number of channels were also conducted (see Section 5).

Using the Head Position Indicator (HPI) system provided with the Neuromag-122, we placed three standard magnetic dipole fiducials on the skull and calibrated a "patient coordinate system" (PCS) on the skull. The PCS was established by selecting and marking on the phantom a nominal nasion and two prearicular points. The 64 EEG electrodes, the reference electrode and the system ground electrode were also located in the PCS coordinate system with the HPI. The skull phantom was then placed under the Dewar and the locations of the three magnetic dipole fiducials were measured relative to the helmet array, thereby establishing the location of the MEG sensor coils in the PCS coordinate system.

A period of 60 seconds of "pre-stim" data containing no activation were collected, followed by 120 seconds of signal generation, then finally another 60 seconds of quiescent data. This bracketing of the signal generation by quiescent periods provides measurements of the background noise for each channel, from which variance and correlation statistics can be computed. For this study, we generated a 10 Hz sine wave for one second for each dipole, with each dipole fired successively with no overlap. The sinusodial waveforms were digitally generated in MATLAB at 1000 samples per second, with a peak amplitude of 100 microampere. Since the coaxial sources have an exposed region of 2-3 mm, the dipolar sources had amplitudes of 200 - 300 nA-m.

A 0.1 Hz highpass filter and a 100 Hz low pass filter were applied to the MEG data before sampling at 500 samples per second. The standard equipment gain setting was used, yielding approximately 25 fT per bit. The EEG data were passed through a 0.3 Hz high pass and 50 Hz low pass, as well as a 60 Hz notch, before digitally sampling at 250 samples per second. The equipment gains and sampling yielded about 0.017 uV per bit.

were collected with the skull inverted. In the results presented below, localization accuracies are compared for 122 channels of MEG data and 64 channels of EEG. To ensure that differences in performance are not simply due to the difference in the number of channels, simulations studies of the effect of increasing the number of channels were also conducted (see Section 5).

Using the Head Position Indicator (HPI) system provided with the Neuromag-122, we placed three standard magnetic dipole fiducials on the skull and calibrated a "patient coordinate system" (PCS) on the skull. The PCS was established by selecting and marking on the phantom a nominal nasion and two prearicular points. The 64 EEG electrodes, the reference electrode and the system ground electrode were also located in the PCS coordinate system with the HPI. The skull phantom was then placed under the Dewar and the locations of the three magnetic dipole fiducials were measured relative to the helmet array, thereby establishing the location of the MEG sensor coils in the PCS coordinate system.

A period of 60 seconds of "pre-stim" data containing no activation were collected, followed by 120 seconds of signal generation, then finally another 60 seconds of quiescent data. This bracketing of the signal generation by quiescent periods provides measurements of the background noise for each channel, from which variance and correlation statistics can be computed. For this study, we generated a 10 Hz sine wave for one second for each dipole, with each dipole fired successively with no overlap. The sinusodial waveforms were digitally generated in MATLAB at 1000 samples per second, with a peak amplitude of 100 microampere. Since the coaxial sources have an exposed region of 2-3 mm, the dipolar sources had amplitudes of 200 - 300 nA-m.

A 0.1 Hz highpass filter and a 100 Hz low pass filter were applied to the MEG data before sampling at 500 samples per second. The standard equipment gain setting was used, yielding approximately 25 fT per bit. The EEG data were passed through a 0.3 Hz high pass and 50 Hz low pass, as well as a 60 Hz notch, before digitally sampling at 250 samples per second. The equipment gains and sampling yielded about 0.017 uV per bit.

were collected with the skull inverted. In the results presented below, localization accuracies are compared for 122 channels of MEG data and 64 channels of EEG. To ensure that differences in performance are not simply due to the difference in the number of channels, simulations studies of the effect of increasing the number of channels were also conducted (see Section 5).

Using the Head Position Indicator (HPI) system provided with the Neuromag-122, we placed three standard magnetic dipole fiducials on the skull and calibrated a "patient coordinate system" (PCS) on the skull. The PCS was established by selecting and marking on the phantom a nominal nasion and two prearicular points. The 64 EEG electrodes, the reference electrode and the system ground electrode were also located in the PCS coordinate system with the HPI. The skull phantom was then placed under the Dewar and the locations of the three magnetic dipole fiducials were measured relative to the helmet array, thereby establishing the location of the MEG sensor coils in the PCS coordinate system.

A period of 60 seconds of "pre-stim" data containing no activation were collected, followed by 120 seconds of signal generation, then finally another 60 seconds of quiescent data. This bracketing of the signal generation by quiescent periods provides measurements of the background noise for each channel, from which variance and correlation statistics can be computed. For this study, we generated a 10 Hz sine wave for one second for each dipole, with each dipole fired successively with no overlap. The sinusodial waveforms were digitally generated in MATLAB at 1000 samples per second, with a peak amplitude of 100 microampere. Since the coaxial sources have an exposed region of 2-3 mm, the dipolar sources had amplitudes of 200 - 300 nA-m.

A 0.1 Hz highpass filter and a 100 Hz low pass filter were applied to the MEG data before sampling at 500 samples per second. The standard equipment gain setting was used, yielding approximately 25 fT per bit. The EEG data were passed through a 0.3 Hz high pass and 50 Hz low pass, as well as a 60 Hz notch, before digitally sampling at 250 samples per second. The equipment gains and sampling yielded about 0.017 uV per bit.

3. Data Processing

3.1. Data Registration

Ordinarily, only a few fiducial markers are available between different modalities to provide data alignment, but the EEG sensors affixed to the phantom scalp provided a rich set of markers which were used for registration. The MEG and EEG sensor locations were found relative to the patient coordinate system (PCS) using the head position indicators (HPI) as described above. The EEG sensor locations were also manually identified and extracted from the CT images. The EEG sensor locations in the PCS, measured using the HPI, and the CT identified locations of the same EEG electrodes, provided a set of 64 correspondence points from which the coordinate transformation between PCS and CT coordinates was computed. Using this transformation, the MEG sensor locations were found in the CT coordinate system so that they were in register with the phantom surface geometry and the dipole and electrode locations.

The registration was performed by computing a least-squares fit of a rotation, translation and global scaling parameter between the two coordinate systems. A closed form solution to this problem can be found using the Procrustes method (Sibson 1978, Golub and Van Loan 1983). Four of the 64 electrode points were not used due to uncertainty about the correspondence between the two modalities. The resulting root mean square error was 2.26 mm between the HPI and CT based locations. The fit produced a scaling factor of 1.0027 between the two modalities indicating very little calibration error in the absolute coordinates in either PCS or CT coordinate systems. In the EEG dipole fitting described below, the electrode locations that were extracted from the CT data were used in solving the forward problem, rather than those obtained by transforming the HPI locations from PCS to CT coordinates.

3.2. Forward Modeling

To find the locations of the dipoles from the measured EEG or MEG data, we must first solve the forward problem. This problem involves calculating the electric potential or magnetic field generated by known current sources for a given head model. The typical model used in MEG and EEG

3. Data Processing

3.1. Data Registration

Ordinarily, only a few fiducial markers are available between different modalities to provide data alignment, but the EEG sensors affixed to the phantom scalp provided a rich set of markers which were used for registration. The MEG and EEG sensor locations were found relative to the patient coordinate system (PCS) using the head position indicators (HPI) as described above. The EEG sensor locations were also manually identified and extracted from the CT images. The EEG sensor locations in the PCS, measured using the HPI, and the CT identified locations of the same EEG electrodes, provided a set of 64 correspondence points from which the coordinate transformation between PCS and CT coordinates was computed. Using this transformation, the MEG sensor locations were found in the CT coordinate system so that they were in register with the phantom surface geometry and the dipole and electrode locations.

The registration was performed by computing a least-squares fit of a rotation, translation and global scaling parameter between the two coordinate systems. A closed form solution to this problem can be found using the Procrustes method (Sibson 1978, Golub and Van Loan 1983). Four of the 64 electrode points were not used due to uncertainty about the correspondence between the two modalities. The resulting root mean square error was 2.26 mm between the HPI and CT based locations. The fit produced a scaling factor of 1.0027 between the two modalities indicating very little calibration error in the absolute coordinates in either PCS or CT coordinate systems. In the EEG dipole fitting described below, the electrode locations that were extracted from the CT data were used in solving the forward problem, rather than those obtained by transforming the HPI locations from PCS to CT coordinates.

3.2. Forward Modeling

To find the locations of the dipoles from the measured EEG or MEG data, we must first solve the forward problem. This problem involves calculating the electric potential or magnetic field generated by known current sources for a given head model. The typical model used in MEG and EEG

3. Data Processing

3.1. Data Registration

Ordinarily, only a few fiducial markers are available between different modalities to provide data alignment, but the EEG sensors affixed to the phantom scalp provided a rich set of markers which were used for registration. The MEG and EEG sensor locations were found relative to the patient coordinate system (PCS) using the head position indicators (HPI) as described above. The EEG sensor locations were also manually identified and extracted from the CT images. The EEG sensor locations in the PCS, measured using the HPI, and the CT identified locations of the same EEG electrodes, provided a set of 64 correspondence points from which the coordinate transformation between PCS and CT coordinates was computed. Using this transformation, the MEG sensor locations were found in the CT coordinate system so that they were in register with the phantom surface geometry and the dipole and electrode locations.

The registration was performed by computing a least-squares fit of a rotation, translation and global scaling parameter between the two coordinate systems. A closed form solution to this problem can be found using the Procrustes method (Sibson 1978, Golub and Van Loan 1983). Four of the 64 electrode points were not used due to uncertainty about the correspondence between the two modalities. The resulting root mean square error was 2.26 mm between the HPI and CT based locations. The fit produced a scaling factor of 1.0027 between the two modalities indicating very little calibration error in the absolute coordinates in either PCS or CT coordinate systems. In the EEG dipole fitting described below, the electrode locations that were extracted from the CT data were used in solving the forward problem, rather than those obtained by transforming the HPI locations from PCS to CT coordinates.

3.2. Forward Modeling

To find the locations of the dipoles from the measured EEG or MEG data, we must first solve the forward problem. This problem involves calculating the electric potential or magnetic field generated by known current sources for a given head model. The typical model used in MEG and EEG

analysis is that the head consists of a set of connected volumes, typically representing the scalp, skull and brain. If the conductivities within each of these regions are isotropic and constant, the electric potentials can be expressed in terms of surface integrals. The forward EEG and MEG problems can then be solved using a boundary element method (BEM). If, in addition, the regions of constant conductivity can be modeled as concentric spheres, then analytic solutions exist for EEG and MEG.

The BEM method used in this study was a linear collocation method (Mosher et al. 1997a, Mosher et. al. 1997b) for solving the electric potentials, an approach similar to the one introduced by (Schlitt et al. 1995). The approach of (Ferguson et al. 1994) was used for calculating the magnetic field values from the surface potentials. Instabilities due to the large conductivity differences between brain and skull were minimized using the isolated skull approach of (Hämäläinen and Sarvas 1989).

The BEM requires a tessellated representation of the inner and outer skull and scalp surfaces. The surface tessellation procedure that we used is straightforward: each surface of the phantom was first approximated using a pre-tessellated sphere, then the radii of the triangles on the pre-tessellated sphere were adjusted to match the real surface obtained from CT, while the elevation and azimuth angles were preserved. The number of triangles on each of the three tessellated surface meshes was 2,292, corresponding to 1,148 vertices. With this tessellation the triangles were about 6--8 mm on a side with a small variability. Several nodes were manually adjusted in the vicinity of the eye sockets, nose, and jaw to prevent intersection of the surfaces.

We also approximated the skull using a locally fitted sphere, for which closed-form solutions are available (Brody et al. 1973, Sarvas 1987, Zhang 1995). The 32 dipoles formed two main clusters that represented the somatosensory and visual areas; for each cluster a locally fitted sphere model was built. In the EEG case the model was obtained by fitting three concentric spheres to the local curvature of the scalp, outermost skull, and innermost skull. For MEG a single sphere was fitted to the innermost skull. The forward models used in the MEG data included the gradiometer effects

analysis is that the head consists of a set of connected volumes, typically representing the scalp, skull and brain. If the conductivities within each of these regions are isotropic and constant, the electric potentials can be expressed in terms of surface integrals. The forward EEG and MEG problems can then be solved using a boundary element method (BEM). If, in addition, the regions of constant conductivity can be modeled as concentric spheres, then analytic solutions exist for EEG and MEG.

The BEM method used in this study was a linear collocation method (Mosher et al. 1997a, Mosher et. al. 1997b) for solving the electric potentials, an approach similar to the one introduced by (Schlitt et al. 1995). The approach of (Ferguson et al. 1994) was used for calculating the magnetic field values from the surface potentials. Instabilities due to the large conductivity differences between brain and skull were minimized using the isolated skull approach of (Hämäläinen and Sarvas 1989).

The BEM requires a tessellated representation of the inner and outer skull and scalp surfaces. The surface tessellation procedure that we used is straightforward: each surface of the phantom was first approximated using a pre-tessellated sphere, then the radii of the triangles on the pre-tessellated sphere were adjusted to match the real surface obtained from CT, while the elevation and azimuth angles were preserved. The number of triangles on each of the three tessellated surface meshes was 2,292, corresponding to 1,148 vertices. With this tessellation the triangles were about 6--8 mm on a side with a small variability. Several nodes were manually adjusted in the vicinity of the eye sockets, nose, and jaw to prevent intersection of the surfaces.

We also approximated the skull using a locally fitted sphere, for which closed-form solutions are available (Brody et al. 1973, Sarvas 1987, Zhang 1995). The 32 dipoles formed two main clusters that represented the somatosensory and visual areas; for each cluster a locally fitted sphere model was built. In the EEG case the model was obtained by fitting three concentric spheres to the local curvature of the scalp, outermost skull, and innermost skull. For MEG a single sphere was fitted to the innermost skull. The forward models used in the MEG data included the gradiometer effects

analysis is that the head consists of a set of connected volumes, typically representing the scalp, skull and brain. If the conductivities within each of these regions are isotropic and constant, the electric potentials can be expressed in terms of surface integrals. The forward EEG and MEG problems can then be solved using a boundary element method (BEM). If, in addition, the regions of constant conductivity can be modeled as concentric spheres, then analytic solutions exist for EEG and MEG.

The BEM method used in this study was a linear collocation method (Mosher et al. 1997a, Mosher et. al. 1997b) for solving the electric potentials, an approach similar to the one introduced by (Schlitt et al. 1995). The approach of (Ferguson et al. 1994) was used for calculating the magnetic field values from the surface potentials. Instabilities due to the large conductivity differences between brain and skull were minimized using the isolated skull approach of (Hämäläinen and Sarvas 1989).

The BEM requires a tessellated representation of the inner and outer skull and scalp surfaces. The surface tessellation procedure that we used is straightforward: each surface of the phantom was first approximated using a pre-tessellated sphere, then the radii of the triangles on the pre-tessellated sphere were adjusted to match the real surface obtained from CT, while the elevation and azimuth angles were preserved. The number of triangles on each of the three tessellated surface meshes was 2,292, corresponding to 1,148 vertices. With this tessellation the triangles were about 6--8 mm on a side with a small variability. Several nodes were manually adjusted in the vicinity of the eye sockets, nose, and jaw to prevent intersection of the surfaces.

We also approximated the skull using a locally fitted sphere, for which closed-form solutions are available (Brody et al. 1973, Sarvas 1987, Zhang 1995). The 32 dipoles formed two main clusters that represented the somatosensory and visual areas; for each cluster a locally fitted sphere model was built. In the EEG case the model was obtained by fitting three concentric spheres to the local curvature of the scalp, outermost skull, and innermost skull. For MEG a single sphere was fitted to the innermost skull. The forward models used in the MEG data included the gradiometer effects

and true sensor orientation, and in the EEG included differential measurements relative to the reference electrode.

3.3. Source Localization using R-MUSIC

MEG and EEG data were processed using the R-MUSIC source localization method (Mosher and Leahy 1996). This method is a variant of the MUSIC method applied to MEG and EEG data as described in (Mosher et al. 1992). The MUSIC methods are based on estimation of a signal subspace from a set of spatio-temporal data using a singular value decomposition (SVD) (Golub and Van Loan 1983). The source locations are then found as the 3-D locations for which some orientation of a dipolar source at that point produces a forward model ("gain") vector that lies approximately in the signal subspace. The measure of the distance between this gain vector and the estimated signal subspace is computed as the first principle angle (Golub and Van Loan 1983) between the gain matrix for a source at that point and the signal subspace. Once the source locations are found, the dipole orientation is then computed as we describe in (Mosher et al. 1992). The R-MUSIC method used here differs from the original MUSIC method primarily by performing a recursive search in which we localize only one source at each recursion. We have found that this method improves the robustness of the MUSIC approach. In the results we present below we show the cosine of the principal angles, also known as canonical or subspace correlations, since these are a useful measure of how well the main dipole model fits the estimated signal subspace (a value $s_1 = 1$ indicates a perfect fit). As such, subspace correlation is a good measure of whether the data produced are truly dipolar, and is robust, to some degree, to the presence of additional non-dipolar sources and noise. In contrast, the "percent variance explained" of a least-squares fit shows the total difference between the data corresponding to the estimated source(s) and the true data, which does not distinguish between contributions from source modeling error and those from noise. We include both functions below.

In our study, we generated a grid throughout the brain volume comprising 1100 dipolar locations, with locations nearest the inner skull more densely arranged. We then pre-calculated the forward model for this grid into EEG and MEG gain matrices, using both our BEM and the locally

and true sensor orientation, and in the EEG included differential measurements relative to the reference electrode.

3.3. Source Localization using R-MUSIC

MEG and EEG data were processed using the R-MUSIC source localization method (Mosher and Leahy 1996). This method is a variant of the MUSIC method applied to MEG and EEG data as described in (Mosher et al. 1992). The MUSIC methods are based on estimation of a signal subspace from a set of spatio-temporal data using a singular value decomposition (SVD) (Golub and Van Loan 1983). The source locations are then found as the 3-D locations for which some orientation of a dipolar source at that point produces a forward model ("gain") vector that lies approximately in the signal subspace. The measure of the distance between this gain vector and the estimated signal subspace is computed as the first principle angle (Golub and Van Loan 1983) between the gain matrix for a source at that point and the signal subspace. Once the source locations are found, the dipole orientation is then computed as we describe in (Mosher et al. 1992). The R-MUSIC method used here differs from the original MUSIC method primarily by performing a recursive search in which we localize only one source at each recursion. We have found that this method improves the robustness of the MUSIC approach. In the results we present below we show the cosine of the principal angles, also known as canonical or subspace correlations, since these are a useful measure of how well the main dipole model fits the estimated signal subspace (a value $s_1 = 1$ indicates a perfect fit). As such, subspace correlation is a good measure of whether the data produced are truly dipolar, and is robust, to some degree, to the presence of additional non-dipolar sources and noise. In contrast, the "percent variance explained" of a least-squares fit shows the total difference between the data corresponding to the estimated source(s) and the true data, which does not distinguish between contributions from source modeling error and those from noise. We include both functions below.

In our study, we generated a grid throughout the brain volume comprising 1100 dipolar locations, with locations nearest the inner skull more densely arranged. We then pre-calculated the forward model for this grid into EEG and MEG gain matrices, using both our BEM and the locally

and true sensor orientation, and in the EEG included differential measurements relative to the reference electrode.

3.3. Source Localization using R-MUSIC

MEG and EEG data were processed using the R-MUSIC source localization method (Mosher and Leahy 1996). This method is a variant of the MUSIC method applied to MEG and EEG data as described in (Mosher et al. 1992). The MUSIC methods are based on estimation of a signal subspace from a set of spatio-temporal data using a singular value decomposition (SVD) (Golub and Van Loan 1983). The source locations are then found as the 3-D locations for which some orientation of a dipolar source at that point produces a forward model ("gain") vector that lies approximately in the signal subspace. The measure of the distance between this gain vector and the estimated signal subspace is computed as the first principle angle (Golub and Van Loan 1983) between the gain matrix for a source at that point and the signal subspace. Once the source locations are found, the dipole orientation is then computed as we describe in (Mosher et al. 1992). The R-MUSIC method used here differs from the original MUSIC method primarily by performing a recursive search in which we localize only one source at each recursion. We have found that this method improves the robustness of the MUSIC approach. In the results we present below we show the cosine of the principal angles, also known as canonical or subspace correlations, since these are a useful measure of how well the main dipole model fits the estimated signal subspace (a value $s_1 = 1$ indicates a perfect fit). As such, subspace correlation is a good measure of whether the data produced are truly dipolar, and is robust, to some degree, to the presence of additional non-dipolar sources and noise. In contrast, the "percent variance explained" of a least-squares fit shows the total difference between the data corresponding to the estimated source(s) and the true data, which does not distinguish between contributions from source modeling error and those from noise. We include both functions below.

In our study, we generated a grid throughout the brain volume comprising 1100 dipolar locations, with locations nearest the inner skull more densely arranged. We then pre-calculated the forward model for this grid into EEG and MEG gain matrices, using both our BEM and the locally

fitted sphere model. The R-MUSIC program was then run through the grid to find the grid point with the highest subspace correlation. Starting with this grid point, a Nelder-Mead simplex method was used to refine the dipole location by locally maximizing the subspace correlation. Once the first source was found, the R-MUSIC procedure was repeated to search for a second and third dipolar source as described in (Mosher and Leahy 1996).

4. Experimental Results for the Skull Phantom

4.1. The Data

The MEG and EEG data corresponding to each of the 32 dipoles were used to compute estimates of the dipole locations, orientations and time series. Before presenting the results of the localization study, we first investigate the signal to noise ratios (SNRs) of the two data sets. In Fig. 6 we have plotted the SNR for each MEG and EEG data set. Here, we define SNR as the root mean square (RMS) value of the measured signal across all the measurement channels and time slices divided by the RMS noise level estimated from the pre-stim data. Our recorded EEG SNR was about two to three times larger than that for MEG (i.e., four to nine times more signal power).

For both MEG and EEG, the original data were collected continuously for the 32 sequentially fired dipoles. Each dipole was fired individually as a 10 Hz sine wave for 1000 ms. To avoid transient effects, we used only the central 600 ms of data in our analysis, representing six full sine wave cycles and 150 (300) time slices for the EEG (respectively, MEG) data. Fig. 7(a) and (b) show the measured MEG and EEG waveforms for a representative dipole. Both EEG and MEG waveforms clearly contain measurement noise, with the EEG data visibly less noisy than the MEG.

For dipole localization using R-MUSIC processing, we need to estimate the signal subspace as described in (Mosher et al. 1992). If the only signal measured by the EEG/MEG system is due to a single dipole, we would expect a rank one signal subspace. This would be indicated by a single large singular value in an SVD of the data matrix. The singular values plotted in Fig. 7(c) and (d) for a typical data matrix (dipole #1), show additional complexity. In addition to the large first singular value, the second and third singular values also appear to contain significant energy, espe-

fitted sphere model. The R-MUSIC program was then run through the grid to find the grid point with the highest subspace correlation. Starting with this grid point, a Nelder-Mead simplex method was used to refine the dipole location by locally maximizing the subspace correlation. Once the first source was found, the R-MUSIC procedure was repeated to search for a second and third dipolar source as described in (Mosher and Leahy 1996).

4. Experimental Results for the Skull Phantom

4.1. The Data

The MEG and EEG data corresponding to each of the 32 dipoles were used to compute estimates of the dipole locations, orientations and time series. Before presenting the results of the localization study, we first investigate the signal to noise ratios (SNRs) of the two data sets. In Fig. 6 we have plotted the SNR for each MEG and EEG data set. Here, we define SNR as the root mean square (RMS) value of the measured signal across all the measurement channels and time slices divided by the RMS noise level estimated from the pre-stim data. Our recorded EEG SNR was about two to three times larger than that for MEG (i.e., four to nine times more signal power).

For both MEG and EEG, the original data were collected continuously for the 32 sequentially fired dipoles. Each dipole was fired individually as a 10 Hz sine wave for 1000 ms. To avoid transient effects, we used only the central 600 ms of data in our analysis, representing six full sine wave cycles and 150 (300) time slices for the EEG (respectively, MEG) data. Fig. 7(a) and (b) show the measured MEG and EEG waveforms for a representative dipole. Both EEG and MEG waveforms clearly contain measurement noise, with the EEG data visibly less noisy than the MEG.

For dipole localization using R-MUSIC processing, we need to estimate the signal subspace as described in (Mosher et al. 1992). If the only signal measured by the EEG/MEG system is due to a single dipole, we would expect a rank one signal subspace. This would be indicated by a single large singular value in an SVD of the data matrix. The singular values plotted in Fig. 7(c) and (d) for a typical data matrix (dipole #1), show additional complexity. In addition to the large first singular value, the second and third singular values also appear to contain significant energy, espe-

fitted sphere model. The R-MUSIC program was then run through the grid to find the grid point with the highest subspace correlation. Starting with this grid point, a Nelder-Mead simplex method was used to refine the dipole location by locally maximizing the subspace correlation. Once the first source was found, the R-MUSIC procedure was repeated to search for a second and third dipolar source as described in (Mosher and Leahy 1996).

4. Experimental Results for the Skull Phantom

4.1. The Data

The MEG and EEG data corresponding to each of the 32 dipoles were used to compute estimates of the dipole locations, orientations and time series. Before presenting the results of the localization study, we first investigate the signal to noise ratios (SNRs) of the two data sets. In Fig. 6 we have plotted the SNR for each MEG and EEG data set. Here, we define SNR as the root mean square (RMS) value of the measured signal across all the measurement channels and time slices divided by the RMS noise level estimated from the pre-stim data. Our recorded EEG SNR was about two to three times larger than that for MEG (i.e., four to nine times more signal power).

For both MEG and EEG, the original data were collected continuously for the 32 sequentially fired dipoles. Each dipole was fired individually as a 10 Hz sine wave for 1000 ms. To avoid transient effects, we used only the central 600 ms of data in our analysis, representing six full sine wave cycles and 150 (300) time slices for the EEG (respectively, MEG) data. Fig. 7(a) and (b) show the measured MEG and EEG waveforms for a representative dipole. Both EEG and MEG waveforms clearly contain measurement noise, with the EEG data visibly less noisy than the MEG.

For dipole localization using R-MUSIC processing, we need to estimate the signal subspace as described in (Mosher et al. 1992). If the only signal measured by the EEG/MEG system is due to a single dipole, we would expect a rank one signal subspace. This would be indicated by a single large singular value in an SVD of the data matrix. The singular values plotted in Fig. 7(c) and (d) for a typical data matrix (dipole #1), show additional complexity. In addition to the large first singular value, the second and third singular values also appear to contain significant energy, espe-

cially for the EEG data. The fact that the signal subspace is greater than rank one indicates that there are other "sources" contributing to the measurements. These sources may be due either to additional current fields inside the phantom or to external noise sources which produce measurements across the sensors that are strongly spatially correlated. Provided that these sources are not fully coherent with our dipolar source, then the true source subspace should remain identifiable within the higher dimensional signal subspace. MUSIC techniques are particularly robust to overspecifying the dimension of the signal subspace, so for each of the 32 EEG/MEG data sets, we attempted to localize three dipoles in an eight-dimensional signal subspace using R-MUSIC (Mosher and Leahy, 1996).

4.2. EEG Results using BEM and Locally Fitted Sphere Approximation

Fig. 8 shows the EEG localization errors for all 32 dipoles using the BEM approach and the locally fitted sphere model. As we summarize in Table 1, the mean error in localizing each source for the BEM approach is 7.62 mm. Using the two locally fitted spheres model, the mean error increased only slightly to 8.00 mm. The corresponding average errors in the tangential component of the dipole moment were 10.0^o and 8.8^o for the spherical and BEM models, respectively. We observe from Fig. 8 that the performance varies for different dipoles, with each forward model outperforming the other in individual cases. In particular, as shown in Fig. 2, dipole #12 is a deep frontal-temporal source, near regions where the shape of the skull is highly irregular and the 64 EEG channels do not have good coverage. This poor electrode coverage results in the low SNR shown in Fig. 6. If we exclude this dipole, the mean error using BEM decreases to 7.20 mm and that for locally fitted spheres goes down to 7.39 mm.

In Fig. 9(a)-(c), the EEG subspace correlations of the 32 dipolar sources are plotted. Fig. 9(a) shows the subspace correlation of the first dipole with the rank eight signal subspace for both the BEM and two-sphere models. The high degree of correlation indicates an excellent agreement between the dipole model and all of our sources. The second dipole is found by holding the first dipole location and orientation fixed and searching for the second dipole location as that which maximizes the second subspace correlation. The good subspace fit for this second dipole, as

cially for the EEG data. The fact that the signal subspace is greater than rank one indicates that there are other "sources" contributing to the measurements. These sources may be due either to additional current fields inside the phantom or to external noise sources which produce measurements across the sensors that are strongly spatially correlated. Provided that these sources are not fully coherent with our dipolar source, then the true source subspace should remain identifiable within the higher dimensional signal subspace. MUSIC techniques are particularly robust to overspecifying the dimension of the signal subspace, so for each of the 32 EEG/MEG data sets, we attempted to localize three dipoles in an eight-dimensional signal subspace using R-MUSIC (Mosher and Leahy, 1996).

4.2. EEG Results using BEM and Locally Fitted Sphere Approximation

Fig. 8 shows the EEG localization errors for all 32 dipoles using the BEM approach and the locally fitted sphere model. As we summarize in Table 1, the mean error in localizing each source for the BEM approach is 7.62 mm. Using the two locally fitted spheres model, the mean error increased only slightly to 8.00 mm. The corresponding average errors in the tangential component of the dipole moment were 10.0^o and 8.8^o for the spherical and BEM models, respectively. We observe from Fig. 8 that the performance varies for different dipoles, with each forward model outperforming the other in individual cases. In particular, as shown in Fig. 2, dipole #12 is a deep frontal-temporal source, near regions where the shape of the skull is highly irregular and the 64 EEG channels do not have good coverage. This poor electrode coverage results in the low SNR shown in Fig. 6. If we exclude this dipole, the mean error using BEM decreases to 7.20 mm and that for locally fitted spheres goes down to 7.39 mm.

In Fig. 9(a)-(c), the EEG subspace correlations of the 32 dipolar sources are plotted. Fig. 9(a) shows the subspace correlation of the first dipole with the rank eight signal subspace for both the BEM and two-sphere models. The high degree of correlation indicates an excellent agreement between the dipole model and all of our sources. The second dipole is found by holding the first dipole location and orientation fixed and searching for the second dipole location as that which maximizes the second subspace correlation. The good subspace fit for this second dipole, as

cially for the EEG data. The fact that the signal subspace is greater than rank one indicates that there are other "sources" contributing to the measurements. These sources may be due either to additional current fields inside the phantom or to external noise sources which produce measurements across the sensors that are strongly spatially correlated. Provided that these sources are not fully coherent with our dipolar source, then the true source subspace should remain identifiable within the higher dimensional signal subspace. MUSIC techniques are particularly robust to overspecifying the dimension of the signal subspace, so for each of the 32 EEG/MEG data sets, we attempted to localize three dipoles in an eight-dimensional signal subspace using R-MUSIC (Mosher and Leahy, 1996).

4.2. EEG Results using BEM and Locally Fitted Sphere Approximation

Fig. 8 shows the EEG localization errors for all 32 dipoles using the BEM approach and the locally fitted sphere model. As we summarize in Table 1, the mean error in localizing each source for the BEM approach is 7.62 mm. Using the two locally fitted spheres model, the mean error increased only slightly to 8.00 mm. The corresponding average errors in the tangential component of the dipole moment were 10.0^o and 8.8^o for the spherical and BEM models, respectively. We observe from Fig. 8 that the performance varies for different dipoles, with each forward model outperforming the other in individual cases. In particular, as shown in Fig. 2, dipole #12 is a deep frontal-temporal source, near regions where the shape of the skull is highly irregular and the 64 EEG channels do not have good coverage. This poor electrode coverage results in the low SNR shown in Fig. 6. If we exclude this dipole, the mean error using BEM decreases to 7.20 mm and that for locally fitted spheres goes down to 7.39 mm.

In Fig. 9(a)-(c), the EEG subspace correlations of the 32 dipolar sources are plotted. Fig. 9(a) shows the subspace correlation of the first dipole with the rank eight signal subspace for both the BEM and two-sphere models. The high degree of correlation indicates an excellent agreement between the dipole model and all of our sources. The second dipole is found by holding the first dipole location and orientation fixed and searching for the second dipole location as that which maximizes the second subspace correlation. The good subspace fit for this second dipole, as

reflected in the second subspace correlations shown in Fig. 9(b), indicates that a second dipole is apparently present. Conversely, the poor correlations shown for the third dipole model in Fig. 9(c) indicate that there is little evidence for a third dipolar source.

As a comparison to a more conventional measure of performance, we also calculated the "percent variance explained" (PVE) by the identified three-dipole spatio-temporal model fit; this is plotted in Fig. 9(d). For most of the dipoles the PVE exceeds 90%, with the two deep frontal dipoles (#5 and #12) having the lowest PVE. In most cases, the first identified dipole dominates the PVE, with the identified second dipole contributing about 10% to the PVE; the poorly correlated third dipole contributes at most 2%.

Fig. 10(a) shows the true locations and orientations of the 32 dipoles overlaid on a transparent rendering of the tessellated inner skull surface. The fitted dipole locations and orientations using BEM and locally fitted sphere approximation are plotted in Fig. 10(b) and (c), respectively. We observe qualitatively in these figures the general concurrence among the true and estimated dipole locations and orientations. We again note dipole #12, the deep frontal source shown in Fig. 2, which is the dipole in Fig. 10(b) and (c) that is localized outside the surface.

In Fig. 10(d), we show the locations and orientations of the second dipolar source for all 32 data sets for both the spherical and BEM models. These dipolar sources are oriented approximately radially and are located very close to the reference electrode used for all channels. Examination of the channel impedances indicated a possible mismatch with the reference channel, adding an apparently spatially correlated noise component across all channels. Interestingly, the EEG forward model can apparently compensate for this type of correlated noise by placing a small radial dipolar source at the electrode, which, as we noted, accounts for about 10% of the PVE. Since the presence of a second source can impact on the accuracy of localization of the first (Mosher et al. 1993), we ran simulation studies to determine the potential impact of this second source on the first. We used a similar configuration to that in the true phantom with and without the second source for each of the 32 dipole locations. White noise was added to the simulated data at an SNR to match that of the true phantom data. The time series were set equal to those extracted from the experimen-

reflected in the second subspace correlations shown in Fig. 9(b), indicates that a second dipole is apparently present. Conversely, the poor correlations shown for the third dipole model in Fig. 9(c) indicate that there is little evidence for a third dipolar source.

As a comparison to a more conventional measure of performance, we also calculated the "percent variance explained" (PVE) by the identified three-dipole spatio-temporal model fit; this is plotted in Fig. 9(d). For most of the dipoles the PVE exceeds 90%, with the two deep frontal dipoles (#5 and #12) having the lowest PVE. In most cases, the first identified dipole dominates the PVE, with the identified second dipole contributing about 10% to the PVE; the poorly correlated third dipole contributes at most 2%.

Fig. 10(a) shows the true locations and orientations of the 32 dipoles overlaid on a transparent rendering of the tessellated inner skull surface. The fitted dipole locations and orientations using BEM and locally fitted sphere approximation are plotted in Fig. 10(b) and (c), respectively. We observe qualitatively in these figures the general concurrence among the true and estimated dipole locations and orientations. We again note dipole #12, the deep frontal source shown in Fig. 2, which is the dipole in Fig. 10(b) and (c) that is localized outside the surface.

In Fig. 10(d), we show the locations and orientations of the second dipolar source for all 32 data sets for both the spherical and BEM models. These dipolar sources are oriented approximately radially and are located very close to the reference electrode used for all channels. Examination of the channel impedances indicated a possible mismatch with the reference channel, adding an apparently spatially correlated noise component across all channels. Interestingly, the EEG forward model can apparently compensate for this type of correlated noise by placing a small radial dipolar source at the electrode, which, as we noted, accounts for about 10% of the PVE. Since the presence of a second source can impact on the accuracy of localization of the first (Mosher et al. 1993), we ran simulation studies to determine the potential impact of this second source on the first. We used a similar configuration to that in the true phantom with and without the second source for each of the 32 dipole locations. White noise was added to the simulated data at an SNR to match that of the true phantom data. The time series were set equal to those extracted from the experimen-

reflected in the second subspace correlations shown in Fig. 9(b), indicates that a second dipole is apparently present. Conversely, the poor correlations shown for the third dipole model in Fig. 9(c) indicate that there is little evidence for a third dipolar source.

As a comparison to a more conventional measure of performance, we also calculated the "percent variance explained" (PVE) by the identified three-dipole spatio-temporal model fit; this is plotted in Fig. 9(d). For most of the dipoles the PVE exceeds 90%, with the two deep frontal dipoles (#5 and #12) having the lowest PVE. In most cases, the first identified dipole dominates the PVE, with the identified second dipole contributing about 10% to the PVE; the poorly correlated third dipole contributes at most 2%.

Fig. 10(a) shows the true locations and orientations of the 32 dipoles overlaid on a transparent rendering of the tessellated inner skull surface. The fitted dipole locations and orientations using BEM and locally fitted sphere approximation are plotted in Fig. 10(b) and (c), respectively. We observe qualitatively in these figures the general concurrence among the true and estimated dipole locations and orientations. We again note dipole #12, the deep frontal source shown in Fig. 2, which is the dipole in Fig. 10(b) and (c) that is localized outside the surface.

In Fig. 10(d), we show the locations and orientations of the second dipolar source for all 32 data sets for both the spherical and BEM models. These dipolar sources are oriented approximately radially and are located very close to the reference electrode used for all channels. Examination of the channel impedances indicated a possible mismatch with the reference channel, adding an apparently spatially correlated noise component across all channels. Interestingly, the EEG forward model can apparently compensate for this type of correlated noise by placing a small radial dipolar source at the electrode, which, as we noted, accounts for about 10% of the PVE. Since the presence of a second source can impact on the accuracy of localization of the first (Mosher et al. 1993), we ran simulation studies to determine the potential impact of this second source on the first. We used a similar configuration to that in the true phantom with and without the second source for each of the 32 dipole locations. White noise was added to the simulated data at an SNR to match that of the true phantom data. The time series were set equal to those extracted from the experimen-

tal dipole fits. We found that the error in the localization of the true current dipole, averaged over the 32 dipoles, was affected by less than 0.3mm.

4.3. MEG Results using BEM and Locally Fitted Sphere Approximation

The localization errors for the MEG data using the BEM and locally fitted sphere models are plotted in Fig. 11. Again, performance is similar for the two forward models with the exception of the frontal-temporal dipole #12, in which the BEM outperforms the locally fitted sphere model. The two spheres used apparently did not account well for this deep source or the other frontal source, dipole #5, also marked in Fig. 2. As summarized in Table 1, the average localization error using the BEM approach is 3.40 mm, while for two locally fitted spheres the average is 4.14 mm. If we exclude the two poorest dipoles, the mean error for BEM becomes 3.03 mm and that for the locally fitted sphere model only slightly greater at 3.47 mm. The corresponding errors in the tangential components of the dipole moments, averaged over all 32 dipoles, were 6.8^o and 7.7^o for the spherical and BEM models, respectively.

Analogous to Fig. 9, Fig. 12(a)-(c) show the subspace correlations of the first, second, and the third fitted dipoles for all 32 MEG data sets, for both head models, again using a rank eight signal subspace. From Fig. 12(a), the first identified dipole again shows high subspace correlations, but these correlations are not as high as in the EEG case (cf. Fig. 9(a)). We also note that a second dipole did not correlate well with the remaining signal subspace, nor obviously did a third. The locations of these secondary dipoles appear random and do not form a cluster as in the EEG case.

The lower correlation of the first dipole is probably due to the significantly poorer SNR of the MEG data, yielding larger subspace estimation errors. Similarly, the PVE shown in Fig. 12(d) is significantly poorer than the comparable EEG PVE shown in Fig. 9(d). The first fitted dipoles again dominate the PVE, while the contributions from the second and third dipoles are only a few percent. Nonetheless, the poorer SNR MEG data yielded excellent localization results, and the locations of the fitted dipoles using the BEM approach and the locally fitted sphere model are plotted in Fig. 13(a) and (b), respectively. The strong similarity among these two sets of locations and the CT identified dipole locations (Fig. 10(a)) is clear.

tal dipole fits. We found that the error in the localization of the true current dipole, averaged over the 32 dipoles, was affected by less than 0.3mm.

4.3. MEG Results using BEM and Locally Fitted Sphere Approximation

The localization errors for the MEG data using the BEM and locally fitted sphere models are plotted in Fig. 11. Again, performance is similar for the two forward models with the exception of the frontal-temporal dipole #12, in which the BEM outperforms the locally fitted sphere model. The two spheres used apparently did not account well for this deep source or the other frontal source, dipole #5, also marked in Fig. 2. As summarized in Table 1, the average localization error using the BEM approach is 3.40 mm, while for two locally fitted spheres the average is 4.14 mm. If we exclude the two poorest dipoles, the mean error for BEM becomes 3.03 mm and that for the locally fitted sphere model only slightly greater at 3.47 mm. The corresponding errors in the tangential components of the dipole moments, averaged over all 32 dipoles, were 6.8^o and 7.7^o for the spherical and BEM models, respectively.

Analogous to Fig. 9, Fig. 12(a)-(c) show the subspace correlations of the first, second, and the third fitted dipoles for all 32 MEG data sets, for both head models, again using a rank eight signal subspace. From Fig. 12(a), the first identified dipole again shows high subspace correlations, but these correlations are not as high as in the EEG case (cf. Fig. 9(a)). We also note that a second dipole did not correlate well with the remaining signal subspace, nor obviously did a third. The locations of these secondary dipoles appear random and do not form a cluster as in the EEG case.

The lower correlation of the first dipole is probably due to the significantly poorer SNR of the MEG data, yielding larger subspace estimation errors. Similarly, the PVE shown in Fig. 12(d) is significantly poorer than the comparable EEG PVE shown in Fig. 9(d). The first fitted dipoles again dominate the PVE, while the contributions from the second and third dipoles are only a few percent. Nonetheless, the poorer SNR MEG data yielded excellent localization results, and the locations of the fitted dipoles using the BEM approach and the locally fitted sphere model are plotted in Fig. 13(a) and (b), respectively. The strong similarity among these two sets of locations and the CT identified dipole locations (Fig. 10(a)) is clear.

tal dipole fits. We found that the error in the localization of the true current dipole, averaged over the 32 dipoles, was affected by less than 0.3mm.

4.3. MEG Results using BEM and Locally Fitted Sphere Approximation

The localization errors for the MEG data using the BEM and locally fitted sphere models are plotted in Fig. 11. Again, performance is similar for the two forward models with the exception of the frontal-temporal dipole #12, in which the BEM outperforms the locally fitted sphere model. The two spheres used apparently did not account well for this deep source or the other frontal source, dipole #5, also marked in Fig. 2. As summarized in Table 1, the average localization error using the BEM approach is 3.40 mm, while for two locally fitted spheres the average is 4.14 mm. If we exclude the two poorest dipoles, the mean error for BEM becomes 3.03 mm and that for the locally fitted sphere model only slightly greater at 3.47 mm. The corresponding errors in the tangential components of the dipole moments, averaged over all 32 dipoles, were 6.8^o and 7.7^o for the spherical and BEM models, respectively.

Analogous to Fig. 9, Fig. 12(a)-(c) show the subspace correlations of the first, second, and the third fitted dipoles for all 32 MEG data sets, for both head models, again using a rank eight signal subspace. From Fig. 12(a), the first identified dipole again shows high subspace correlations, but these correlations are not as high as in the EEG case (cf. Fig. 9(a)). We also note that a second dipole did not correlate well with the remaining signal subspace, nor obviously did a third. The locations of these secondary dipoles appear random and do not form a cluster as in the EEG case.

The lower correlation of the first dipole is probably due to the significantly poorer SNR of the MEG data, yielding larger subspace estimation errors. Similarly, the PVE shown in Fig. 12(d) is significantly poorer than the comparable EEG PVE shown in Fig. 9(d). The first fitted dipoles again dominate the PVE, while the contributions from the second and third dipoles are only a few percent. Nonetheless, the poorer SNR MEG data yielded excellent localization results, and the locations of the fitted dipoles using the BEM approach and the locally fitted sphere model are plotted in Fig. 13(a) and (b), respectively. The strong similarity among these two sets of locations and the CT identified dipole locations (Fig. 10(a)) is clear.

5. Discussion

The results presented above show that MEG dipole localization errors are as small as could be expected (~3 mm) given the various sources of registration error between the true dipole locations, the CT extracted locations and the HPI-based localization of the MEG sensors. In contrast the errors for EEG localization are significantly larger (~7–8 mm), although still well within bounds that could be considered useful in clinical and research localization studies. Here we discuss the factors that contribute to these localization errors and present the results of several simulations designed to further investigate these factors.

The small MEG localization errors are comparable in magnitude to our registration errors. The average registration error observed between CT and HPI-based coordinate systems for the EEG electrode array was 2.26 mm, and consequently we can expect a similar misregistration between the CT-extracted dipole locations and the HPI-based MEG sensor locations. Additional localization errors of up to 1 mm can be attributed to the finite voxel size in the original CT data (0.29 mm by 0.29 mm pixels and a 2 mm thick slice) and manual identification of the dipole locations in the isotropically resampled CT images.

The EEG data were of higher SNR and gave higher correlations between the dipole models and the estimated signal subspace than for MEG (compare Fig. 9(a) and Fig. 12(a)); however, the localization errors were worse for EEG than MEG. By comparing the localization errors for EEG when using BEM to those using locally fitted spheres model, we note that there is a relatively small advantage gained from using the considerably more complex BEM method, i.e. a difference on average of less than 0.5 mm in a total error in excess of 7 mm. These localization errors are summarized in Table 1.

One distinct advantage of EEG for source localization is that it is sensitive to the radial component of the dipole while MEG is not. Provided that the dipole has some tangential component, then it can be localized using either modality. In this study the dipoles had orientations ranging from near radial to near tangential as shown in Fig. 5. There is no strong correlation between the localization errors in the two modalities and the dipole orientations. This is because, provided the tan-

5. Discussion

The results presented above show that MEG dipole localization errors are as small as could be expected (~3 mm) given the various sources of registration error between the true dipole locations, the CT extracted locations and the HPI-based localization of the MEG sensors. In contrast the errors for EEG localization are significantly larger (~7–8 mm), although still well within bounds that could be considered useful in clinical and research localization studies. Here we discuss the factors that contribute to these localization errors and present the results of several simulations designed to further investigate these factors.

The small MEG localization errors are comparable in magnitude to our registration errors. The average registration error observed between CT and HPI-based coordinate systems for the EEG electrode array was 2.26 mm, and consequently we can expect a similar misregistration between the CT-extracted dipole locations and the HPI-based MEG sensor locations. Additional localization errors of up to 1 mm can be attributed to the finite voxel size in the original CT data (0.29 mm by 0.29 mm pixels and a 2 mm thick slice) and manual identification of the dipole locations in the isotropically resampled CT images.

The EEG data were of higher SNR and gave higher correlations between the dipole models and the estimated signal subspace than for MEG (compare Fig. 9(a) and Fig. 12(a)); however, the localization errors were worse for EEG than MEG. By comparing the localization errors for EEG when using BEM to those using locally fitted spheres model, we note that there is a relatively small advantage gained from using the considerably more complex BEM method, i.e. a difference on average of less than 0.5 mm in a total error in excess of 7 mm. These localization errors are summarized in Table 1.

One distinct advantage of EEG for source localization is that it is sensitive to the radial component of the dipole while MEG is not. Provided that the dipole has some tangential component, then it can be localized using either modality. In this study the dipoles had orientations ranging from near radial to near tangential as shown in Fig. 5. There is no strong correlation between the localization errors in the two modalities and the dipole orientations. This is because, provided the tan-

5. Discussion

The results presented above show that MEG dipole localization errors are as small as could be expected (~3 mm) given the various sources of registration error between the true dipole locations, the CT extracted locations and the HPI-based localization of the MEG sensors. In contrast the errors for EEG localization are significantly larger (~7–8 mm), although still well within bounds that could be considered useful in clinical and research localization studies. Here we discuss the factors that contribute to these localization errors and present the results of several simulations designed to further investigate these factors.

The small MEG localization errors are comparable in magnitude to our registration errors. The average registration error observed between CT and HPI-based coordinate systems for the EEG electrode array was 2.26 mm, and consequently we can expect a similar misregistration between the CT-extracted dipole locations and the HPI-based MEG sensor locations. Additional localization errors of up to 1 mm can be attributed to the finite voxel size in the original CT data (0.29 mm by 0.29 mm pixels and a 2 mm thick slice) and manual identification of the dipole locations in the isotropically resampled CT images.

The EEG data were of higher SNR and gave higher correlations between the dipole models and the estimated signal subspace than for MEG (compare Fig. 9(a) and Fig. 12(a)); however, the localization errors were worse for EEG than MEG. By comparing the localization errors for EEG when using BEM to those using locally fitted spheres model, we note that there is a relatively small advantage gained from using the considerably more complex BEM method, i.e. a difference on average of less than 0.5 mm in a total error in excess of 7 mm. These localization errors are summarized in Table 1.

One distinct advantage of EEG for source localization is that it is sensitive to the radial component of the dipole while MEG is not. Provided that the dipole has some tangential component, then it can be localized using either modality. In this study the dipoles had orientations ranging from near radial to near tangential as shown in Fig. 5. There is no strong correlation between the localization errors in the two modalities and the dipole orientations. This is because, provided the tan-

gential component is sufficiently large to produce a reasonable SNR, other factors such as forward model accuracy dominate the localization errors. The relative importance of these factors are investigated below. Since MEG cannot reliably estimate the radial component of the dipole moment, we compare only the tangential components, while acknowledging that EEG is obviously superior in estimating the radial component. The average errors in the tangential components for MEG and EEG using spherical and BEM forward models are all within 10^o. Since our uncertainty in the estimated orientations is also on the order of 10^o, there is no evidence in our data for significant differences in tangential orientation estimation between MEG and EEG. In concluding this discusison of dipole orientation, we note that with a widely distribed range of orientations, both MEG and EEG are able to produce reasonably accurate source localizations. This may indicate that some of the concerns expressed in the literature over the blindness of MEG to radial sources are possibly exagerated, since this is likely to affect only the relatively small proportion of the cortical surface where the surface normals are strongly radial.

To investigate the difference between EEG and MEG performance in our phantom data, we performed a series of computer simulations. We considered the effects of the BEM approximations and sensor coverage in both noiseless data and data with noise levels comparable to the experimental data. To investigate the effects arising from the approximations and numerical errors in our BEM methods, we used a three concentric spheres simulation so that the true fields could be computed exactly. The configuration of the spherical simulation was designed to mimic the pattern of the skull phantom in terms of the angular placement of the dipoles and sensors, and the distance between the dipoles and the inner skull boundary. The simulated forward data were computed analytically for each source location. For the noisy simulations, white Gaussian noise was added to yield SNR levels comparable to the experimental levels shown in Fig. 6. The BEM approach was then used to localize each dipole using the same tessellation pattern as used in the phantom data.

The first simulation study used the same array pattern as the phantom data. The simulated head geometry was based on fitting the real phantom using 3 concentric spheres representing the simulated scalp, outermost skull, and innermost skull surfaces. For the simulated MEG we used the true

gential component is sufficiently large to produce a reasonable SNR, other factors such as forward model accuracy dominate the localization errors. The relative importance of these factors are investigated below. Since MEG cannot reliably estimate the radial component of the dipole moment, we compare only the tangential components, while acknowledging that EEG is obviously superior in estimating the radial component. The average errors in the tangential components for MEG and EEG using spherical and BEM forward models are all within 10^o. Since our uncertainty in the estimated orientations is also on the order of 10^o, there is no evidence in our data for significant differences in tangential orientation estimation between MEG and EEG. In concluding this discusison of dipole orientation, we note that with a widely distribed range of orientations, both MEG and EEG are able to produce reasonably accurate source localizations. This may indicate that some of the concerns expressed in the literature over the blindness of MEG to radial sources are possibly exagerated, since this is likely to affect only the relatively small proportion of the cortical surface where the surface normals are strongly radial.

To investigate the difference between EEG and MEG performance in our phantom data, we performed a series of computer simulations. We considered the effects of the BEM approximations and sensor coverage in both noiseless data and data with noise levels comparable to the experimental data. To investigate the effects arising from the approximations and numerical errors in our BEM methods, we used a three concentric spheres simulation so that the true fields could be computed exactly. The configuration of the spherical simulation was designed to mimic the pattern of the skull phantom in terms of the angular placement of the dipoles and sensors, and the distance between the dipoles and the inner skull boundary. The simulated forward data were computed analytically for each source location. For the noisy simulations, white Gaussian noise was added to yield SNR levels comparable to the experimental levels shown in Fig. 6. The BEM approach was then used to localize each dipole using the same tessellation pattern as used in the phantom data.

The first simulation study used the same array pattern as the phantom data. The simulated head geometry was based on fitting the real phantom using 3 concentric spheres representing the simulated scalp, outermost skull, and innermost skull surfaces. For the simulated MEG we used the true

gential component is sufficiently large to produce a reasonable SNR, other factors such as forward model accuracy dominate the localization errors. The relative importance of these factors are investigated below. Since MEG cannot reliably estimate the radial component of the dipole moment, we compare only the tangential components, while acknowledging that EEG is obviously superior in estimating the radial component. The average errors in the tangential components for MEG and EEG using spherical and BEM forward models are all within 10^o. Since our uncertainty in the estimated orientations is also on the order of 10^o, there is no evidence in our data for significant differences in tangential orientation estimation between MEG and EEG. In concluding this discusison of dipole orientation, we note that with a widely distribed range of orientations, both MEG and EEG are able to produce reasonably accurate source localizations. This may indicate that some of the concerns expressed in the literature over the blindness of MEG to radial sources are possibly exagerated, since this is likely to affect only the relatively small proportion of the cortical surface where the surface normals are strongly radial.

To investigate the difference between EEG and MEG performance in our phantom data, we performed a series of computer simulations. We considered the effects of the BEM approximations and sensor coverage in both noiseless data and data with noise levels comparable to the experimental data. To investigate the effects arising from the approximations and numerical errors in our BEM methods, we used a three concentric spheres simulation so that the true fields could be computed exactly. The configuration of the spherical simulation was designed to mimic the pattern of the skull phantom in terms of the angular placement of the dipoles and sensors, and the distance between the dipoles and the inner skull boundary. The simulated forward data were computed analytically for each source location. For the noisy simulations, white Gaussian noise was added to yield SNR levels comparable to the experimental levels shown in Fig. 6. The BEM approach was then used to localize each dipole using the same tessellation pattern as used in the phantom data.

The first simulation study used the same array pattern as the phantom data. The simulated head geometry was based on fitting the real phantom using 3 concentric spheres representing the simulated scalp, outermost skull, and innermost skull surfaces. For the simulated MEG we used the true

Neuromag-122 MEG sensor array geometry. The EEG electrodes were found by radially mapping the phantom electrode locations onto the sphere. Similarly, to simulate the dipole locations, we radially mapped them inside the innermost sphere so that the distance to the innermost surface remained about the same as in the phantom data. The orientations of the dipoles were also set to approximate those of the phantom.

To test the effects of electrode placement, we also simulated two other EEG array patterns. The first simulated pattern was generated by mapping each of the 61 Neuromag MEG dual-channel sensor locations along their radii onto the simulated spherical scalp surface. These locations were then used for an EEG array with spatial coverage comparable to that of the MEG Neuromag-122. The final simulated pattern was 148 EEG sensor sites about the upper hemisphere, representing the sort of dense array coverage not usually seen in practice. These sensor patterns are shown in Fig. 14.

R-MUSIC (Mosher and Leahy 1996) was again used to localize the dipoles for the simulated data, and the average localization errors are summarized in Table 1. The localization errors per dipole are plotted in Fig. 15(a) for all of the EEG and MEG simulations. For comparison, we have also replotted the skull phantom EEG and MEG results in Fig. 15(b). We observe that for the majority of dipoles, the EEG localization errors exhibit only minor differences due to the specific EEG array pattern, including both noisy and noiseless simulations. The MEG localization errors are submillimeter, indicating a strong robustness to our BEM approximations, which is to be expected since the near radial orientation of the MEG sensors makes the measurement relatively insensitive to volume currents. The larger errors for the EEG dipole fits are due to the fact that EEG forward calculations are more sensitive to the approximations and numerical errors in the BEM method than is the forward model in MEG.

In conclusion, the observed MEG phantom errors can probably be attributed primarily to registration errors, since the BEM simulation errors appear to be very small. The EEG BEM simulation errors appear to be comparable to registration errors, yet both are markedly lower than the EEG skull phantom localization errors. The simulations also indicate that the presence of noise in the data and EEG array coverage do not appear to be significant factors in this larger error. Our suppo-

Neuromag-122 MEG sensor array geometry. The EEG electrodes were found by radially mapping the phantom electrode locations onto the sphere. Similarly, to simulate the dipole locations, we radially mapped them inside the innermost sphere so that the distance to the innermost surface remained about the same as in the phantom data. The orientations of the dipoles were also set to approximate those of the phantom.

To test the effects of electrode placement, we also simulated two other EEG array patterns. The first simulated pattern was generated by mapping each of the 61 Neuromag MEG dual-channel sensor locations along their radii onto the simulated spherical scalp surface. These locations were then used for an EEG array with spatial coverage comparable to that of the MEG Neuromag-122. The final simulated pattern was 148 EEG sensor sites about the upper hemisphere, representing the sort of dense array coverage not usually seen in practice. These sensor patterns are shown in Fig. 14.

R-MUSIC (Mosher and Leahy 1996) was again used to localize the dipoles for the simulated data, and the average localization errors are summarized in Table 1. The localization errors per dipole are plotted in Fig. 15(a) for all of the EEG and MEG simulations. For comparison, we have also replotted the skull phantom EEG and MEG results in Fig. 15(b). We observe that for the majority of dipoles, the EEG localization errors exhibit only minor differences due to the specific EEG array pattern, including both noisy and noiseless simulations. The MEG localization errors are submillimeter, indicating a strong robustness to our BEM approximations, which is to be expected since the near radial orientation of the MEG sensors makes the measurement relatively insensitive to volume currents. The larger errors for the EEG dipole fits are due to the fact that EEG forward calculations are more sensitive to the approximations and numerical errors in the BEM method than is the forward model in MEG.

In conclusion, the observed MEG phantom errors can probably be attributed primarily to registration errors, since the BEM simulation errors appear to be very small. The EEG BEM simulation errors appear to be comparable to registration errors, yet both are markedly lower than the EEG skull phantom localization errors. The simulations also indicate that the presence of noise in the data and EEG array coverage do not appear to be significant factors in this larger error. Our suppo-

Neuromag-122 MEG sensor array geometry. The EEG electrodes were found by radially mapping the phantom electrode locations onto the sphere. Similarly, to simulate the dipole locations, we radially mapped them inside the innermost sphere so that the distance to the innermost surface remained about the same as in the phantom data. The orientations of the dipoles were also set to approximate those of the phantom.

To test the effects of electrode placement, we also simulated two other EEG array patterns. The first simulated pattern was generated by mapping each of the 61 Neuromag MEG dual-channel sensor locations along their radii onto the simulated spherical scalp surface. These locations were then used for an EEG array with spatial coverage comparable to that of the MEG Neuromag-122. The final simulated pattern was 148 EEG sensor sites about the upper hemisphere, representing the sort of dense array coverage not usually seen in practice. These sensor patterns are shown in Fig. 14.

R-MUSIC (Mosher and Leahy 1996) was again used to localize the dipoles for the simulated data, and the average localization errors are summarized in Table 1. The localization errors per dipole are plotted in Fig. 15(a) for all of the EEG and MEG simulations. For comparison, we have also replotted the skull phantom EEG and MEG results in Fig. 15(b). We observe that for the majority of dipoles, the EEG localization errors exhibit only minor differences due to the specific EEG array pattern, including both noisy and noiseless simulations. The MEG localization errors are submillimeter, indicating a strong robustness to our BEM approximations, which is to be expected since the near radial orientation of the MEG sensors makes the measurement relatively insensitive to volume currents. The larger errors for the EEG dipole fits are due to the fact that EEG forward calculations are more sensitive to the approximations and numerical errors in the BEM method than is the forward model in MEG.

In conclusion, the observed MEG phantom errors can probably be attributed primarily to registration errors, since the BEM simulation errors appear to be very small. The EEG BEM simulation errors appear to be comparable to registration errors, yet both are markedly lower than the EEG skull phantom localization errors. The simulations also indicate that the presence of noise in the data and EEG array coverage do not appear to be significant factors in this larger error. Our suppo-

sition is that the larger error lies in the forward model itself, i.e. errors in the estimated conductivities for the phantom and discrepancies between the piece-wise isotropic and homogeneous conductor model and the true nature of the brain, skull and scalp layers in the phantom. While we expect that the gelatin "brain" volume in the phantom is approximately isotropic, this may not be the case for the scalp layer which is formed by repeated application of a thin layer of conducting latex. Furthermore, our model of the skull does not include considerations of the conductivity variations. We expect these to be particularly pronounced in regions where there are substantial fractions of the skull volume occupied by the diploic space - these regions are clearly visible in the CT slice of Fig. 3. A more accurate model that considers the effect of the diploic space should lead to better localization of the dipolar sources. We note, however, that the conductivity properties of a human head are far more complex than those of our phantom. Unless we can produce high-resolution images of spatially varying conductivities *in vivo*, it is unlikely that forward models for human subjects can be made much more accurate than the forward model used for the phantom described here. Consequently we conjecture that it will very difficult to localize dipoles in human subjects using EEG with accuracies much better than the 7–8 mm reported here.

6. Conclusions

We have presented a study of MEG and EEG dipole localization accuracy using a human skull phantom containing 32 independently programmable and isolated dipolar sources. This phantom provides insights not readily obtainable from either simulation or experimental human data: i) the skull phantom provides realistic bone structure and morphology; ii) the EEG and MEG data can be collected on commercial systems, adding the uncertainties of instrumental and environmental noise; iii) the sources are known to be piecewise dipolar and can also be grouped to form more complex sources; iv) a ground-truth for the sources and surfaces can be readily obtained using X-ray CT; v) the relatively large number of dipoles allows a "macro" study of the effects of processing trade-offs, without unduly emphasizing any one dipole location; vi) the multiple-modality compatibility allows registration errors to be examined and the EEG and MEG modalities compared.

sition is that the larger error lies in the forward model itself, i.e. errors in the estimated conductivities for the phantom and discrepancies between the piece-wise isotropic and homogeneous conductor model and the true nature of the brain, skull and scalp layers in the phantom. While we expect that the gelatin "brain" volume in the phantom is approximately isotropic, this may not be the case for the scalp layer which is formed by repeated application of a thin layer of conducting latex. Furthermore, our model of the skull does not include considerations of the conductivity variations. We expect these to be particularly pronounced in regions where there are substantial fractions of the skull volume occupied by the diploic space - these regions are clearly visible in the CT slice of Fig. 3. A more accurate model that considers the effect of the diploic space should lead to better localization of the dipolar sources. We note, however, that the conductivity properties of a human head are far more complex than those of our phantom. Unless we can produce high-resolution images of spatially varying conductivities *in vivo*, it is unlikely that forward models for human subjects can be made much more accurate than the forward model used for the phantom described here. Consequently we conjecture that it will very difficult to localize dipoles in human subjects using EEG with accuracies much better than the 7–8 mm reported here.

6. Conclusions

We have presented a study of MEG and EEG dipole localization accuracy using a human skull phantom containing 32 independently programmable and isolated dipolar sources. This phantom provides insights not readily obtainable from either simulation or experimental human data: i) the skull phantom provides realistic bone structure and morphology; ii) the EEG and MEG data can be collected on commercial systems, adding the uncertainties of instrumental and environmental noise; iii) the sources are known to be piecewise dipolar and can also be grouped to form more complex sources; iv) a ground-truth for the sources and surfaces can be readily obtained using X-ray CT; v) the relatively large number of dipoles allows a "macro" study of the effects of processing trade-offs, without unduly emphasizing any one dipole location; vi) the multiple-modality compatibility allows registration errors to be examined and the EEG and MEG modalities compared.

sition is that the larger error lies in the forward model itself, i.e. errors in the estimated conductivities for the phantom and discrepancies between the piece-wise isotropic and homogeneous conductor model and the true nature of the brain, skull and scalp layers in the phantom. While we expect that the gelatin "brain" volume in the phantom is approximately isotropic, this may not be the case for the scalp layer which is formed by repeated application of a thin layer of conducting latex. Furthermore, our model of the skull does not include considerations of the conductivity variations. We expect these to be particularly pronounced in regions where there are substantial fractions of the skull volume occupied by the diploic space - these regions are clearly visible in the CT slice of Fig. 3. A more accurate model that considers the effect of the diploic space should lead to better localization of the dipolar sources. We note, however, that the conductivity properties of a human head are far more complex than those of our phantom. Unless we can produce high-resolution images of spatially varying conductivities *in vivo*, it is unlikely that forward models for human subjects can be made much more accurate than the forward model used for the phantom described here. Consequently we conjecture that it will very difficult to localize dipoles in human subjects using EEG with accuracies much better than the 7–8 mm reported here.

6. Conclusions

We have presented a study of MEG and EEG dipole localization accuracy using a human skull phantom containing 32 independently programmable and isolated dipolar sources. This phantom provides insights not readily obtainable from either simulation or experimental human data: i) the skull phantom provides realistic bone structure and morphology; ii) the EEG and MEG data can be collected on commercial systems, adding the uncertainties of instrumental and environmental noise; iii) the sources are known to be piecewise dipolar and can also be grouped to form more complex sources; iv) a ground-truth for the sources and surfaces can be readily obtained using X-ray CT; v) the relatively large number of dipoles allows a "macro" study of the effects of processing trade-offs, without unduly emphasizing any one dipole location; vi) the multiple-modality compatibility allows registration errors to be examined and the EEG and MEG modalities compared.

In order to validate the design of the phantom and examine some fundamental localization issues, we restricted this study to single dipole sources. The mis-localizations of both EEG and MEG were quite small, in general below one cm; however, the MEG localization errors were on average half the size of the EEG errors, and indeed, the MEG localization errors were comparable to the probable registration errors. The mean errors in the tangential components of the dipole orientation for MEG and EEG were within 10^o, with little significant difference between the two. modalities. Simulation results demonstrated that the EEG localization suffers from errors (~1–2 mm) due to the BEM technique applied; in contrast the MEG simulation errors were sub-millimeter. The simulation errors for EEG, however, were still markedly less than for the phantom, indicating that the largest sources of error are discrepancies between the homogenous isotropic shell models used in our forward computations and the true, probably anisotropic, nature of the phantom itself.

In addition to comparing EEG and MEG localization errors, the phantom data were also used to examine the differences between two forward head modeling techniques, namely, a boundary element method and a locally fitted sphere approach. The results show that the boundary element method, on average, gives slightly less localization error than the locally fitted sphere model for both EEG and MEG data. This marginal improvement, however, is gained at the expense of significantly higher computational cost, in both time and memory. The locally fitted sphere model results indicate that this approximation may yield acceptable accuracy for both MEG and EEG data.

7. Acknowledgments

We would like to thank Bijan Timsari and Tong Zhang of the Signal and Image Processing Institute at the University of Southern California for their assistance in the X-ray CT surface extraction and data registration. Also, we thank Charles C. Wood of the Biophysics Group at Los Alamos National Laboratory for reviewing a draft of this manuscript and providing helpful suggestions.

In order to validate the design of the phantom and examine some fundamental localization issues, we restricted this study to single dipole sources. The mis-localizations of both EEG and MEG were quite small, in general below one cm; however, the MEG localization errors were on average half the size of the EEG errors, and indeed, the MEG localization errors were comparable to the probable registration errors. The mean errors in the tangential components of the dipole orientation for MEG and EEG were within 10^o, with little significant difference between the two. modalities. Simulation results demonstrated that the EEG localization suffers from errors (~1–2 mm) due to the BEM technique applied; in contrast the MEG simulation errors were sub-millimeter. The simulation errors for EEG, however, were still markedly less than for the phantom, indicating that the largest sources of error are discrepancies between the homogenous isotropic shell models used in our forward computations and the true, probably anisotropic, nature of the phantom itself.

In addition to comparing EEG and MEG localization errors, the phantom data were also used to examine the differences between two forward head modeling techniques, namely, a boundary element method and a locally fitted sphere approach. The results show that the boundary element method, on average, gives slightly less localization error than the locally fitted sphere model for both EEG and MEG data. This marginal improvement, however, is gained at the expense of significantly higher computational cost, in both time and memory. The locally fitted sphere model results indicate that this approximation may yield acceptable accuracy for both MEG and EEG data.

7. Acknowledgments

We would like to thank Bijan Timsari and Tong Zhang of the Signal and Image Processing Institute at the University of Southern California for their assistance in the X-ray CT surface extraction and data registration. Also, we thank Charles C. Wood of the Biophysics Group at Los Alamos National Laboratory for reviewing a draft of this manuscript and providing helpful suggestions.

In order to validate the design of the phantom and examine some fundamental localization issues, we restricted this study to single dipole sources. The mis-localizations of both EEG and MEG were quite small, in general below one cm; however, the MEG localization errors were on average half the size of the EEG errors, and indeed, the MEG localization errors were comparable to the probable registration errors. The mean errors in the tangential components of the dipole orientation for MEG and EEG were within 10^o, with little significant difference between the two. modalities. Simulation results demonstrated that the EEG localization suffers from errors (~1–2 mm) due to the BEM technique applied; in contrast the MEG simulation errors were sub-millimeter. The simulation errors for EEG, however, were still markedly less than for the phantom, indicating that the largest sources of error are discrepancies between the homogenous isotropic shell models used in our forward computations and the true, probably anisotropic, nature of the phantom itself.

In addition to comparing EEG and MEG localization errors, the phantom data were also used to examine the differences between two forward head modeling techniques, namely, a boundary element method and a locally fitted sphere approach. The results show that the boundary element method, on average, gives slightly less localization error than the locally fitted sphere model for both EEG and MEG data. This marginal improvement, however, is gained at the expense of significantly higher computational cost, in both time and memory. The locally fitted sphere model results indicate that this approximation may yield acceptable accuracy for both MEG and EEG data.

7. Acknowledgments

We would like to thank Bijan Timsari and Tong Zhang of the Signal and Image Processing Institute at the University of Southern California for their assistance in the X-ray CT surface extraction and data registration. Also, we thank Charles C. Wood of the Biophysics Group at Los Alamos National Laboratory for reviewing a draft of this manuscript and providing helpful suggestions.

8. References

Baillet S., Marin G., le Rudulier F., Garnero L, Evoked potentials from a real skull phantom-head: an experimental step to the validation of methods for solving the forward and inverse problems of brain cortical imaging, submitted to *Human Brain Mapping*, Nov., 1997.

Barth, D., Sutherling, W., Broffman, J., Beatty, J., Magnetic localization of a dipolar current source implanted in a sphere and a human cranium. *Electroenceph. Clin. Neurophysiol.*, 1986, 63: 260-273.

Brody DA, Terry FH, Ideker RE, Eccentric dipole in a spherical medium: Generalized expression for surface potentials, *IEEE Trans. Biomed. Eng.*, pp. 141–143, March 1973.

Cohen, D., Cuffin, B.N., Yunokuchi, K., Maniewski, R., Purcell, C., Cosgrove, G.R., Ives, J., Kennedy, J.G., Schomer, D.L. MEG versus EEG localization test using implanted sources in the human brain. *Ann. Neurol.*, 1990, 28: 811-817.

Ferguson, A.S., Zhang, X., Stroink, G., A complete linear discretization for calculating the magnetic field using the boundary element method. *IEEE Trans. Biomed. Eng.*, 1994, 41:455-459.

Golub, G.H., Van Loan, C.F., *Matrix Computations*. Baltimore, Maryland: The Johns Hopkins University Press, 1983.

Greenblatt, R.E., Robinson, S.E., A simple head shape approximation for the 3 shell model. *Brain Topography*, 1994, 6(4):331.

Hämäläinen, M.S., Sarvas, J., Realistic conductor geometry model of the human head for interpretation of neuromagnetic data. *IEEE Trans. Biomed. Eng.*, 1989, 36: 165-171

.Ilmoniemi, R.J., Hamalainen, M.S., Knuutila, J., 1985, The forward and inverse problems in the spherical model. In: H. Weinberg, G. Stroink, and H. Katila (Eds.), *Biomagnetism: Application*. New York, Pergamon, 1985: 278-282..

Lewine, J.D., Edgar, J.C., Repa, K., Paulson, K., Asture, R.S., Orrison, W.W. Jr. A physical phantom for simulating the impact of pathology on magnetic source imaging. In: C. Baumgartner, L. Deecke, G. Stroink, S.J. Williamson (Eds.), *Biomagnetism: Fundamental Research and Clinical Applications*. Elsevier,1995: 368-372.

Mosher, J.C., Lewis, P.S., and Leahy, R.M. Multiple dipole modeling and localization from spatio-temporal MEG data. *IEEE Trans. Biomedical Eng.*, 1992, 39: 541-557.

Mosher JC, Spencer ME, Leahy RM, Lewis PS, “Error bounds for EEG and MEG dipole source localization,” *Electroenceph. and clin. Neurophys*. 1993, vol. 86, pp. 303 – 320.

8. References

Baillet S., Marin G., le Rudulier F., Garnero L, Evoked potentials from a real skull phantom-head: an experimental step to the validation of methods for solving the forward and inverse problems of brain cortical imaging, submitted to *Human Brain Mapping*, Nov., 1997.

Barth, D., Sutherling, W., Broffman, J., Beatty, J., Magnetic localization of a dipolar current source implanted in a sphere and a human cranium. *Electroenceph. Clin. Neurophysiol.*, 1986, 63: 260-273.

Brody DA, Terry FH, Ideker RE, Eccentric dipole in a spherical medium: Generalized expression for surface potentials, *IEEE Trans. Biomed. Eng.*, pp. 141–143, March 1973.

Cohen, D., Cuffin, B.N., Yunokuchi, K., Maniewski, R., Purcell, C., Cosgrove, G.R., Ives, J., Kennedy, J.G., Schomer, D.L. MEG versus EEG localization test using implanted sources in the human brain. *Ann. Neurol.*, 1990, 28: 811-817.

Ferguson, A.S., Zhang, X., Stroink, G., A complete linear discretization for calculating the magnetic field using the boundary element method. *IEEE Trans. Biomed. Eng.*, 1994, 41:455-459.

Golub, G.H., Van Loan, C.F., *Matrix Computations*. Baltimore, Maryland: The Johns Hopkins University Press, 1983.

Greenblatt, R.E., Robinson, S.E., A simple head shape approximation for the 3 shell model. *Brain Topography*, 1994, 6(4):331.

Hämäläinen, M.S., Sarvas, J., Realistic conductor geometry model of the human head for interpretation of neuromagnetic data. *IEEE Trans. Biomed. Eng.*, 1989, 36: 165-171

.Ilmoniemi, R.J., Hamalainen, M.S., Knuutila, J., 1985, The forward and inverse problems in the spherical model. In: H. Weinberg, G. Stroink, and H. Katila (Eds.), *Biomagnetism: Application*. New York, Pergamon, 1985: 278-282..

Lewine, J.D., Edgar, J.C., Repa, K., Paulson, K., Asture, R.S., Orrison, W.W. Jr. A physical phantom for simulating the impact of pathology on magnetic source imaging. In: C. Baumgartner, L. Deecke, G. Stroink, S.J. Williamson (Eds.), *Biomagnetism: Fundamental Research and Clinical Applications*. Elsevier,1995: 368-372.

Mosher, J.C., Lewis, P.S., and Leahy, R.M. Multiple dipole modeling and localization from spatio-temporal MEG data. *IEEE Trans. Biomedical Eng.*, 1992, 39: 541-557.

Mosher JC, Spencer ME, Leahy RM, Lewis PS, “Error bounds for EEG and MEG dipole source localization,” *Electroenceph. and clin. Neurophys*. 1993, vol. 86, pp. 303 – 320.

8. References

Baillet S., Marin G., le Rudulier F., Garnero L, Evoked potentials from a real skull phantom-head: an experimental step to the validation of methods for solving the forward and inverse problems of brain cortical imaging, submitted to *Human Brain Mapping*, Nov., 1997.

Barth, D., Sutherling, W., Broffman, J., Beatty, J., Magnetic localization of a dipolar current source implanted in a sphere and a human cranium. *Electroenceph. Clin. Neurophysiol.*, 1986, 63: 260-273.

Brody DA, Terry FH, Ideker RE, Eccentric dipole in a spherical medium: Generalized expression for surface potentials, *IEEE Trans. Biomed. Eng.*, pp. 141–143, March 1973.

Cohen, D., Cuffin, B.N., Yunokuchi, K., Maniewski, R., Purcell, C., Cosgrove, G.R., Ives, J., Kennedy, J.G., Schomer, D.L. MEG versus EEG localization test using implanted sources in the human brain. *Ann. Neurol.*, 1990, 28: 811-817.

Ferguson, A.S., Zhang, X., Stroink, G., A complete linear discretization for calculating the magnetic field using the boundary element method. *IEEE Trans. Biomed. Eng.*, 1994, 41:455-459.

Golub, G.H., Van Loan, C.F., *Matrix Computations*. Baltimore, Maryland: The Johns Hopkins University Press, 1983.

Greenblatt, R.E., Robinson, S.E., A simple head shape approximation for the 3 shell model. *Brain Topography*, 1994, 6(4):331.

Hämäläinen, M.S., Sarvas, J., Realistic conductor geometry model of the human head for interpretation of neuromagnetic data. *IEEE Trans. Biomed. Eng.*, 1989, 36: 165-171

.Ilmoniemi, R.J., Hamalainen, M.S., Knuutila, J., 1985, The forward and inverse problems in the spherical model. In: H. Weinberg, G. Stroink, and H. Katila (Eds.), *Biomagnetism: Application*. New York, Pergamon, 1985: 278-282..

Lewine, J.D., Edgar, J.C., Repa, K., Paulson, K., Asture, R.S., Orrison, W.W. Jr. A physical phantom for simulating the impact of pathology on magnetic source imaging. In: C. Baumgartner, L. Deecke, G. Stroink, S.J. Williamson (Eds.), *Biomagnetism: Fundamental Research and Clinical Applications*. Elsevier,1995: 368-372.

Mosher, J.C., Lewis, P.S., and Leahy, R.M. Multiple dipole modeling and localization from spatio-temporal MEG data. *IEEE Trans. Biomedical Eng.*, 1992, 39: 541-557.

Mosher JC, Spencer ME, Leahy RM, Lewis PS, “Error bounds for EEG and MEG dipole source localization,” *Electroenceph. and clin. Neurophys*. 1993, vol. 86, pp. 303 – 320.

Mosher, JC, Leahy, RM, EEG and MEG source localization using recursively applied (RAP) MUSIC, *IEEE Proc. 30th Asilomar Conf. on Signals, Systems, and Computers*, Pacific Grove, CA, November 1996, pp. 1201-1207.

Mosher, J.C., Chang, C.H., Leahy, R.M., Comparison of the constant and linear boundary element method for EEG and MEG forward modeling. In: C. Aine, Y. Okada, G. Stoink, S. Swithenby, and C. Wood (Eds.), *Biomag96: Advances in Biomagnetism Research*, Springer-Verlag, New York, 1997a.

Mosher, JC, Leahy, RM, Lewis, PS, Matrix kernels for EEG and MEG source modeling, *Los Alamos Technical Report* LAUR-97-3812, September 1997b.

Phillips, JW, Leahy, RM, Mosher, JC, MEG-based imaging of focal neuronal current sources, IEEE Trans. on Medical Imaging, June,1997, pp 338-348.

Sarvas, J. Basic mathematical and electromagnetic concepts of the bio-magnetic inverse problems. *Phys. Med. Biol*., 1987, 32: 11-22.

Schlitt, H.A., Heller, L. , Aaron, R., Best, E., Ranken, D. M., Evaluation of boundary element method for the EEG forward problem: Effect of linear interpolation, *IEEE Trans. Biomed. Eng*, 1995, 42: 52-57.

Sibson, R. Studies in the robustness of Multidimensional scaling: procrustes statistics. *J. R. Statist. Soc. B*, 1978, 40: 234-238.

Spencer M., Leahy R., Mosher J., A Skull-Based Multiple Dipole Phantom for EEG and MEG Studies, In Aine, C.J., Flynn, E.R., Okada, Y., Stroink, G., Swithenby, S.J., and Wood, C.C. (Eds.) *Biomag96: Advances in Biomagnetism Research*, Springer-Verlag, New York, (in press)

Woods, R.P., Cherry, S.R., Mazziotta, J.C. Rapid automated algorithm for aligning and reslicing PET images. *J. Comput. Assist. Tomogr*., 1992, 16: 620-633.

Zhang, Z. A fast method to compute surface potentials generated by dipoles within multilayer anisotropic spheres. *Phys. Med. Biol*., 1995, 40: 335-349.

Mosher, JC, Leahy, RM, EEG and MEG source localization using recursively applied (RAP) MUSIC, *IEEE Proc. 30th Asilomar Conf. on Signals, Systems, and Computers*, Pacific Grove, CA, November 1996, pp. 1201-1207.

Mosher, J.C., Chang, C.H., Leahy, R.M., Comparison of the constant and linear boundary element method for EEG and MEG forward modeling. In: C. Aine, Y. Okada, G. Stoink, S. Swithenby, and C. Wood (Eds.), *Biomag96: Advances in Biomagnetism Research*, Springer-Verlag, New York, 1997a.

Mosher, JC, Leahy, RM, Lewis, PS, Matrix kernels for EEG and MEG source modeling, *Los Alamos Technical Report* LAUR-97-3812, September 1997b.

Phillips, JW, Leahy, RM, Mosher, JC, MEG-based imaging of focal neuronal current sources, IEEE Trans. on Medical Imaging, June,1997, pp 338-348.

Sarvas, J. Basic mathematical and electromagnetic concepts of the bio-magnetic inverse problems. *Phys. Med. Biol*., 1987, 32: 11-22.

Schlitt, H.A., Heller, L. , Aaron, R., Best, E., Ranken, D. M., Evaluation of boundary element method for the EEG forward problem: Effect of linear interpolation, *IEEE Trans. Biomed. Eng*, 1995, 42: 52-57.

Sibson, R. Studies in the robustness of Multidimensional scaling: procrustes statistics. *J. R. Statist. Soc. B*, 1978, 40: 234-238.

Spencer M., Leahy R., Mosher J., A Skull-Based Multiple Dipole Phantom for EEG and MEG Studies, In Aine, C.J., Flynn, E.R., Okada, Y., Stroink, G., Swithenby, S.J., and Wood, C.C. (Eds.) *Biomag96: Advances in Biomagnetism Research*, Springer-Verlag, New York, (in press)

Woods, R.P., Cherry, S.R., Mazziotta, J.C. Rapid automated algorithm for aligning and reslicing PET images. *J. Comput. Assist. Tomogr*., 1992, 16: 620-633.

Zhang, Z. A fast method to compute surface potentials generated by dipoles within multilayer anisotropic spheres. *Phys. Med. Biol*., 1995, 40: 335-349.

Mosher, JC, Leahy, RM, EEG and MEG source localization using recursively applied (RAP) MUSIC, *IEEE Proc. 30th Asilomar Conf. on Signals, Systems, and Computers*, Pacific Grove, CA, November 1996, pp. 1201-1207.

Mosher, J.C., Chang, C.H., Leahy, R.M., Comparison of the constant and linear boundary element method for EEG and MEG forward modeling. In: C. Aine, Y. Okada, G. Stoink, S. Swithenby, and C. Wood (Eds.), *Biomag96: Advances in Biomagnetism Research*, Springer-Verlag, New York, 1997a.

Mosher, JC, Leahy, RM, Lewis, PS, Matrix kernels for EEG and MEG source modeling, *Los Alamos Technical Report* LAUR-97-3812, September 1997b.

Phillips, JW, Leahy, RM, Mosher, JC, MEG-based imaging of focal neuronal current sources, IEEE Trans. on Medical Imaging, June,1997, pp 338-348.

Sarvas, J. Basic mathematical and electromagnetic concepts of the bio-magnetic inverse problems. *Phys. Med. Biol*., 1987, 32: 11-22.

Schlitt, H.A., Heller, L. , Aaron, R., Best, E., Ranken, D. M., Evaluation of boundary element method for the EEG forward problem: Effect of linear interpolation, *IEEE Trans. Biomed. Eng*, 1995, 42: 52-57.

Sibson, R. Studies in the robustness of Multidimensional scaling: procrustes statistics. *J. R. Statist. Soc. B*, 1978, 40: 234-238.

Spencer M., Leahy R., Mosher J., A Skull-Based Multiple Dipole Phantom for EEG and MEG Studies, In Aine, C.J., Flynn, E.R., Okada, Y., Stroink, G., Swithenby, S.J., and Wood, C.C. (Eds.) *Biomag96: Advances in Biomagnetism Research*, Springer-Verlag, New York, (in press)

Woods, R.P., Cherry, S.R., Mazziotta, J.C. Rapid automated algorithm for aligning and reslicing PET images. *J. Comput. Assist. Tomogr*., 1992, 16: 620-633.

Zhang, Z. A fast method to compute surface potentials generated by dipoles within multilayer anisotropic spheres. *Phys. Med. Biol*., 1995, 40: 335-349.

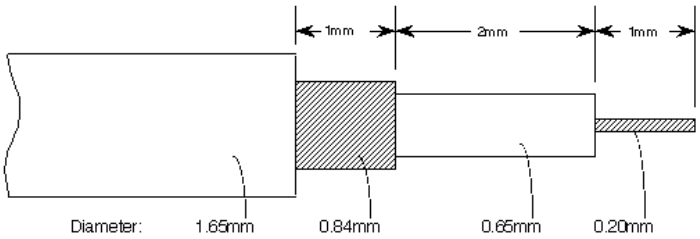

Fig. 1: Dimensions of the stainless steel coax and outer sheath used to generate the dipolar sources.

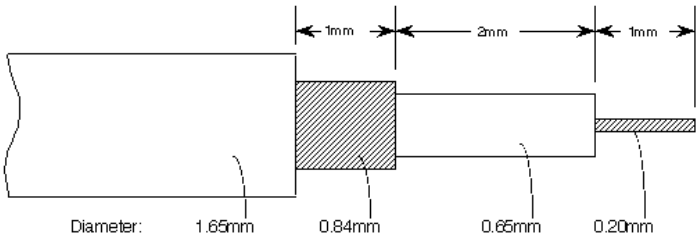

Fig. 1: Dimensions of the stainless steel coax and outer sheath used to generate the dipolar sources.

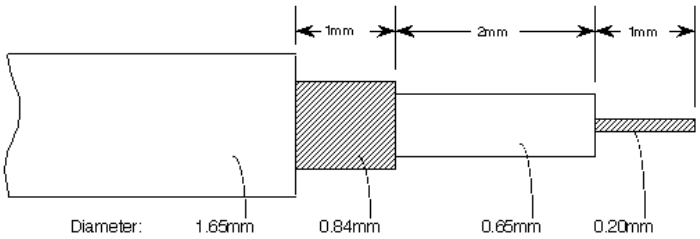

Fig. 1: Dimensions of the stainless steel coax and outer sheath used to generate the dipolar sources.

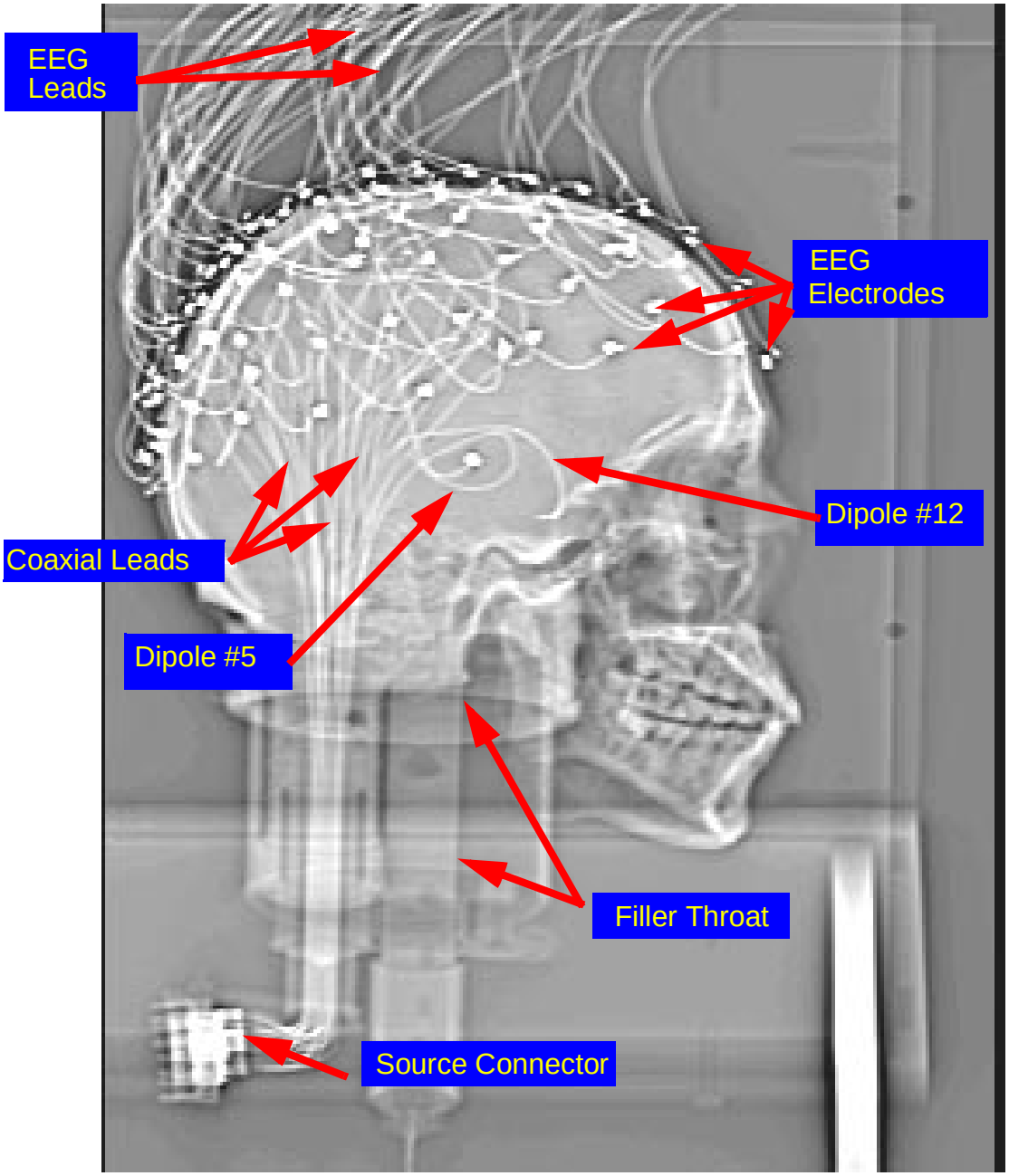

Fig. 2: X-ray projection of the skull phantom and EEG electrodes. The 32 coaxial cables that form the dipoles at the tips were inserted through the base. The other ends of the cables were connected with the driver through the source connector. The filler throat was used to fill/drain the brain volume of the phantom with a conductive gelatin. The EEG electrodes were affixed to a conductive latex "scalp" layer. Dipoles #5 and #12 are noted and discussed in the text.

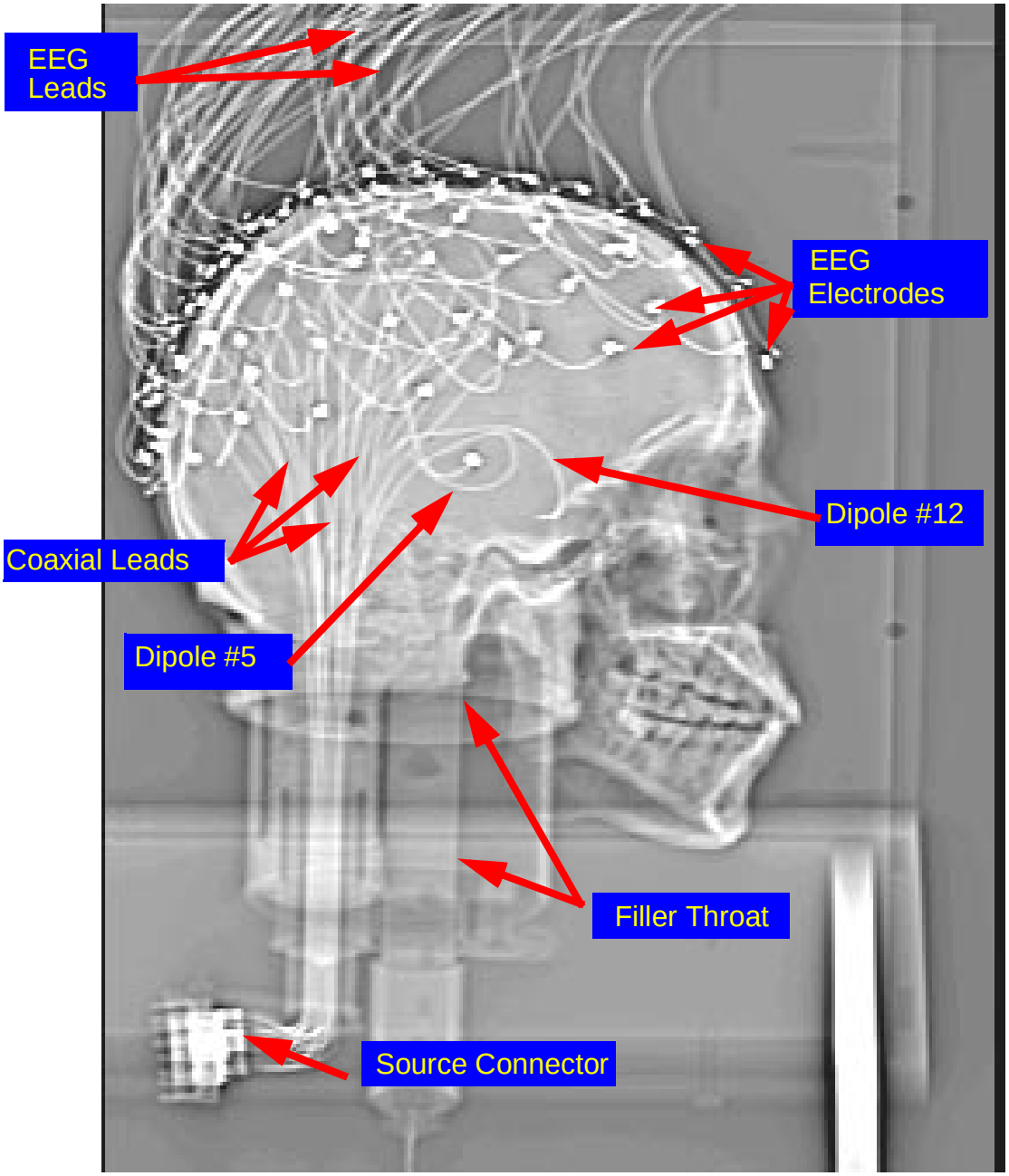

Fig. 2: X-ray projection of the skull phantom and EEG electrodes. The 32 coaxial cables that form the dipoles at the tips were inserted through the base. The other ends of the cables were connected with the driver through the source connector. The filler throat was used to fill/drain the brain volume of the phantom with a conductive gelatin. The EEG electrodes were affixed to a conductive latex "scalp" layer. Dipoles #5 and #12 are noted and discussed in the text.

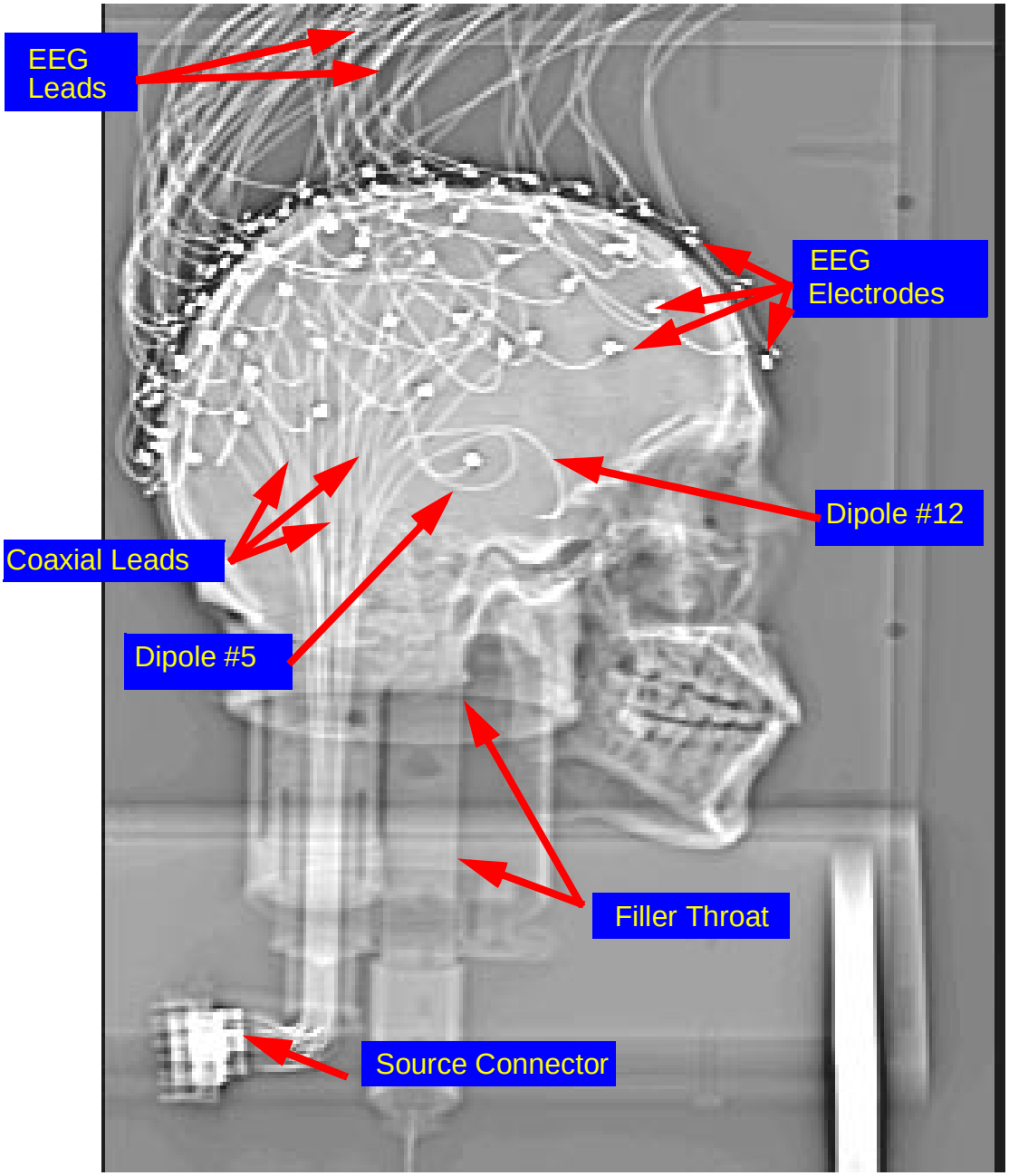

Fig. 2: X-ray projection of the skull phantom and EEG electrodes. The 32 coaxial cables that form the dipoles at the tips were inserted through the base. The other ends of the cables were connected with the driver through the source connector. The filler throat was used to fill/drain the brain volume of the phantom with a conductive gelatin. The EEG electrodes were affixed to a conductive latex "scalp" layer. Dipoles #5 and #12 are noted and discussed in the text.

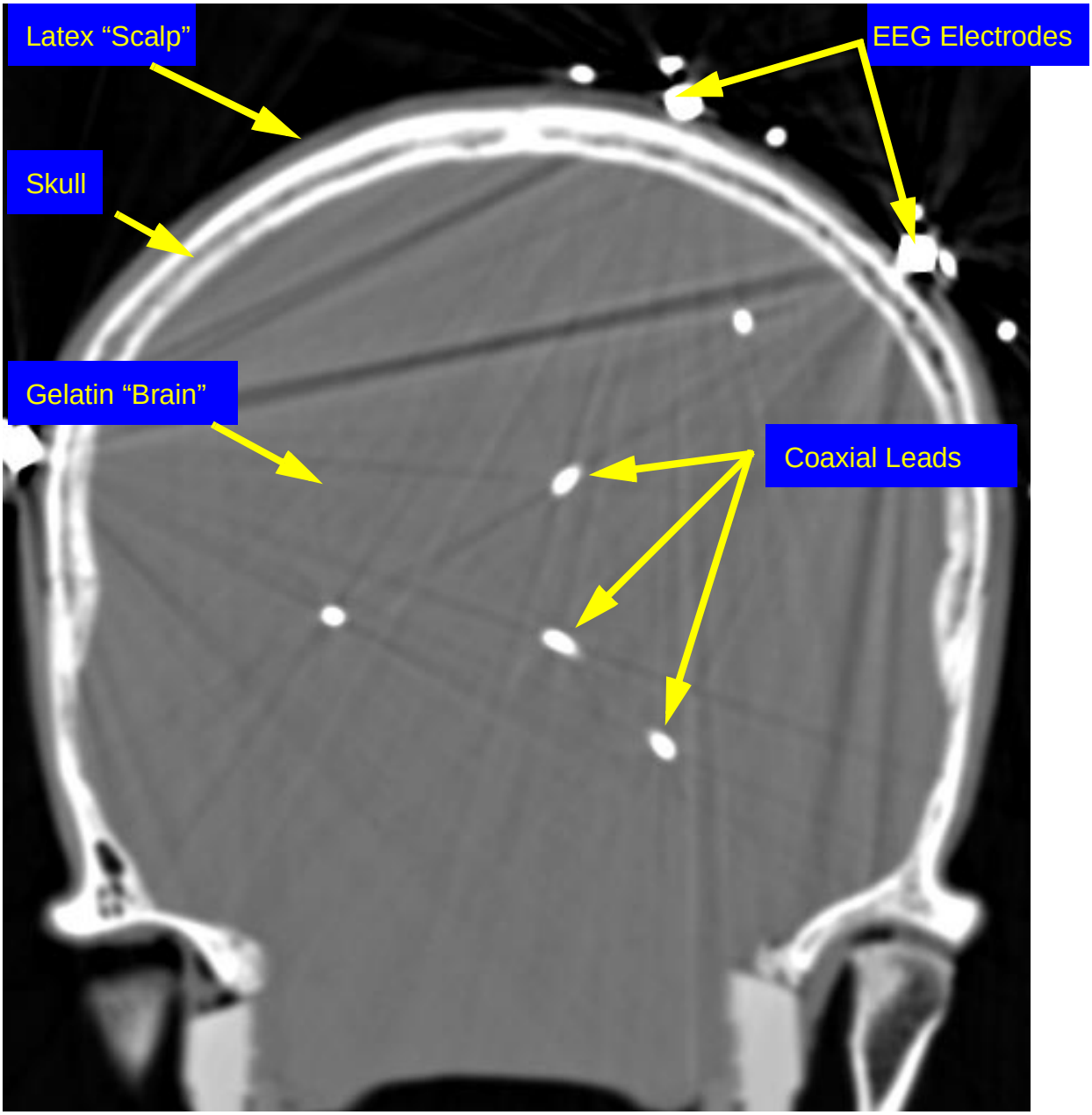

Fig. 3: X-ray Computed Tomography Slice shows the different compartments of the phantom, namely scalp, skull, and brain. Also visible are the coaxial leads and the EEG electrodes. The original CT data were acquired at 0.29 x 0.29 mm, with an interslice dimension of 2 mm. We isotropically resampled the data to a volume comprising 0.58 mm^3 voxels. The coaxial leads were traced through the volume to identify their dipolar tips and orientation.

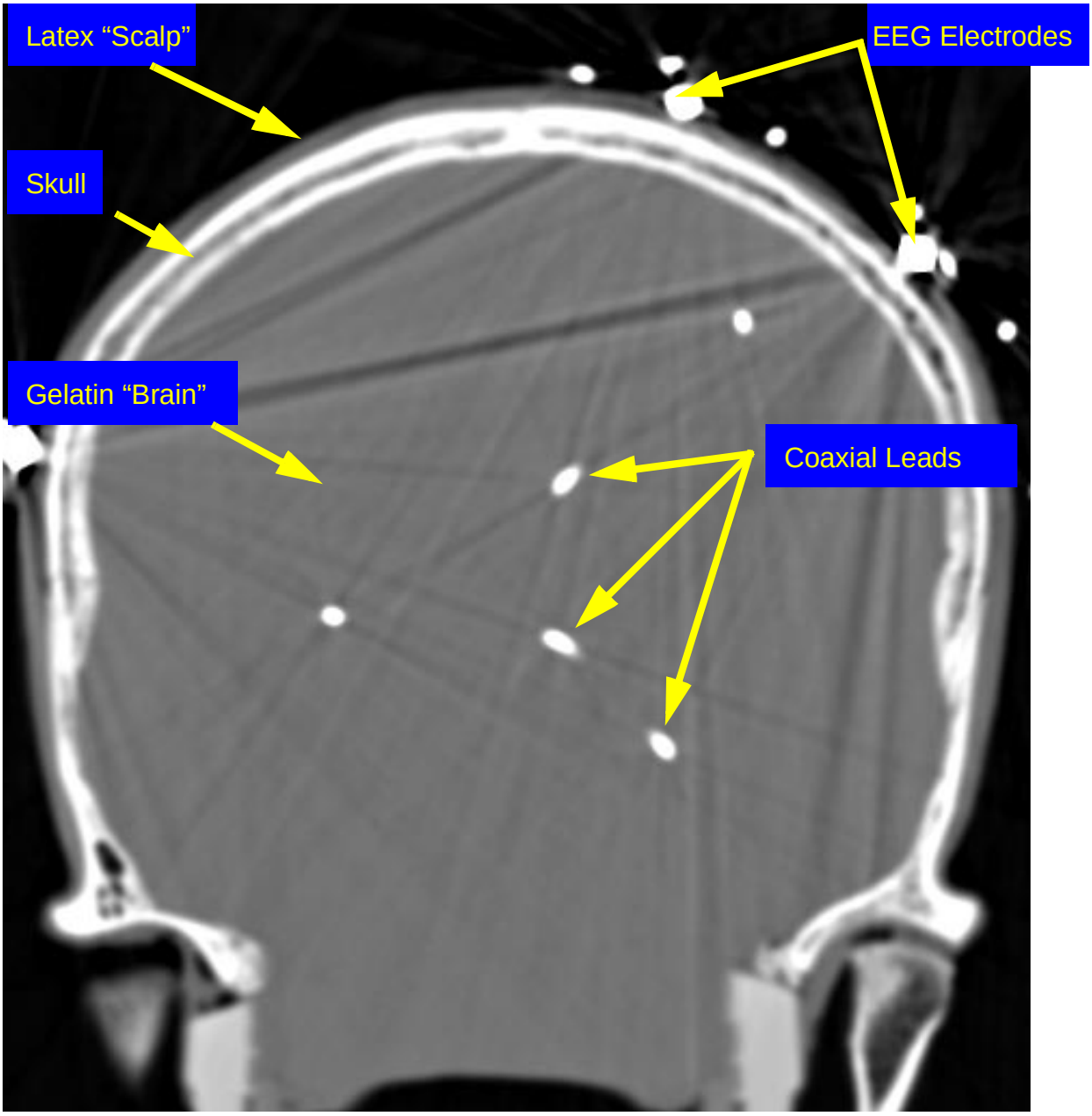

Fig. 3: X-ray Computed Tomography Slice shows the different compartments of the phantom, namely scalp, skull, and brain. Also visible are the coaxial leads and the EEG electrodes. The original CT data were acquired at 0.29 x 0.29 mm, with an interslice dimension of 2 mm. We isotropically resampled the data to a volume comprising 0.58 mm^3 voxels. The coaxial leads were traced through the volume to identify their dipolar tips and orientation.

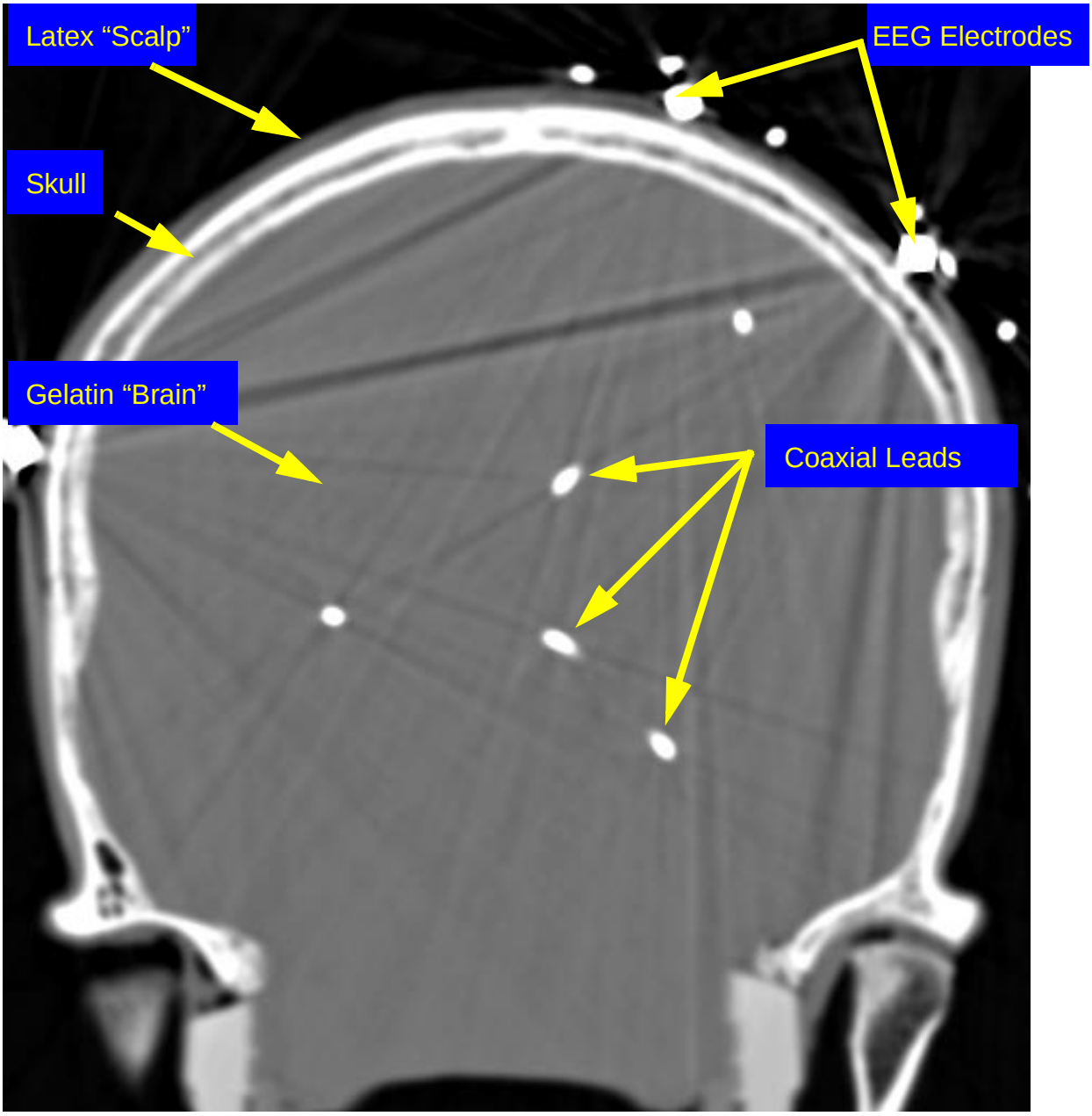

Fig. 3: X-ray Computed Tomography Slice shows the different compartments of the phantom, namely scalp, skull, and brain. Also visible are the coaxial leads and the EEG electrodes. The original CT data were acquired at 0.29 x 0.29 mm, with an interslice dimension of 2 mm. We isotropically resampled the data to a volume comprising 0.58 mm^3 voxels. The coaxial leads were traced through the volume to identify their dipolar tips and orientation.

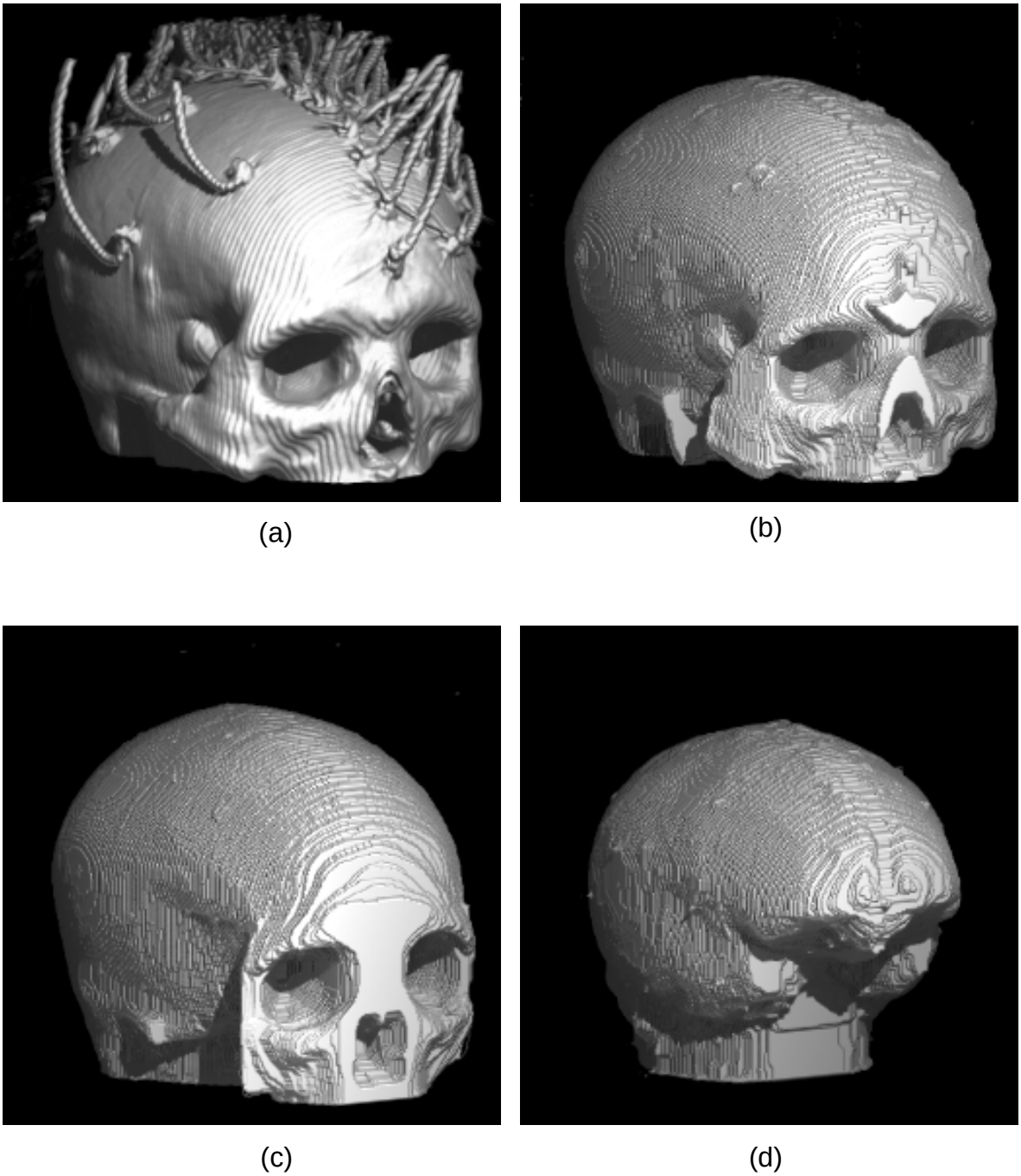

Fig. 4: CT surface extraction viewed from front-right. (a) The original scalp surface with the EEG electrodes; (b) Scalp surface after deleting the EEG electrodes; (c) Outermost skull surface; (d) Innermost skull surface.

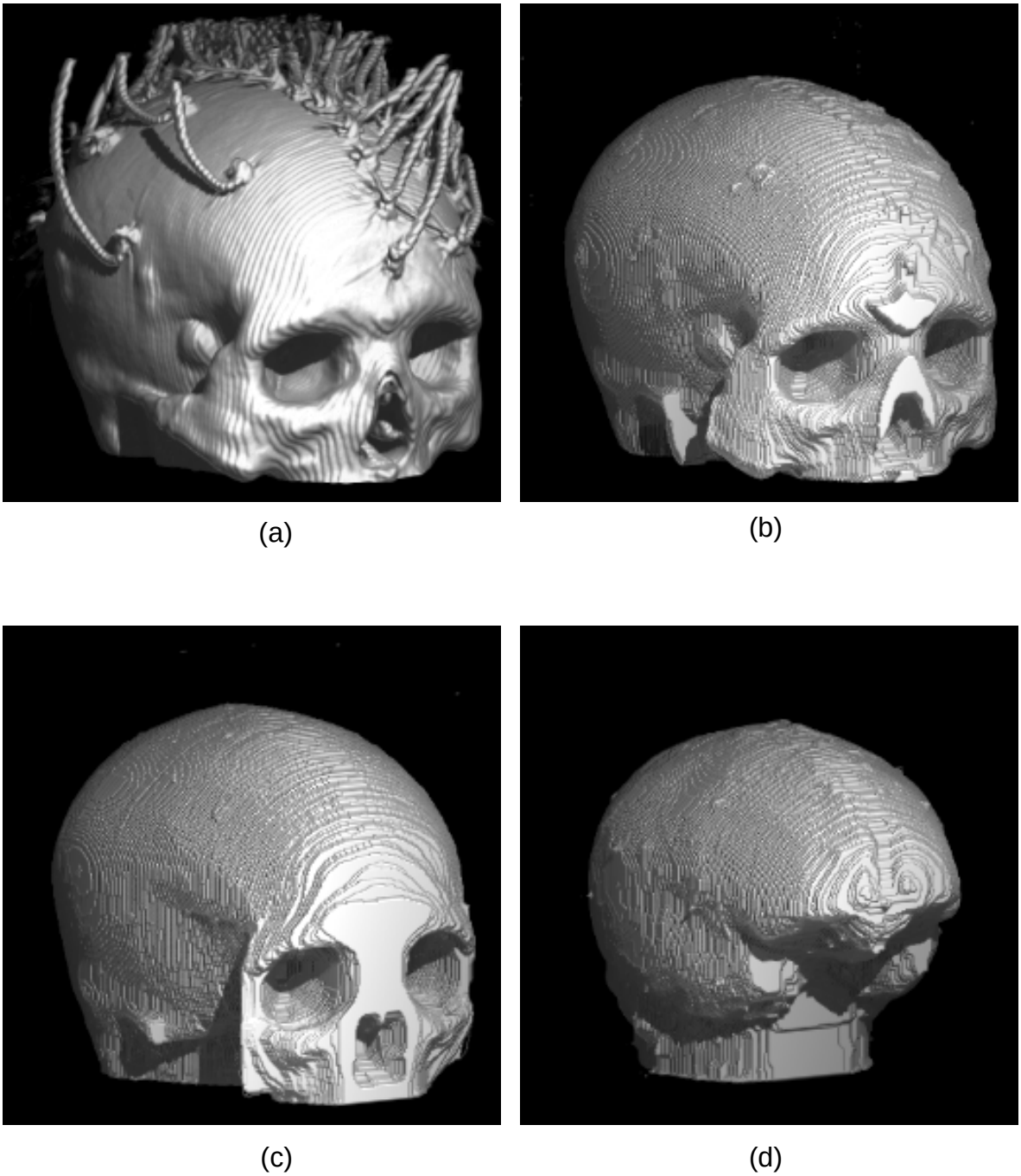

Fig. 4: CT surface extraction viewed from front-right. (a) The original scalp surface with the EEG electrodes; (b) Scalp surface after deleting the EEG electrodes; (c) Outermost skull surface; (d) Innermost skull surface.

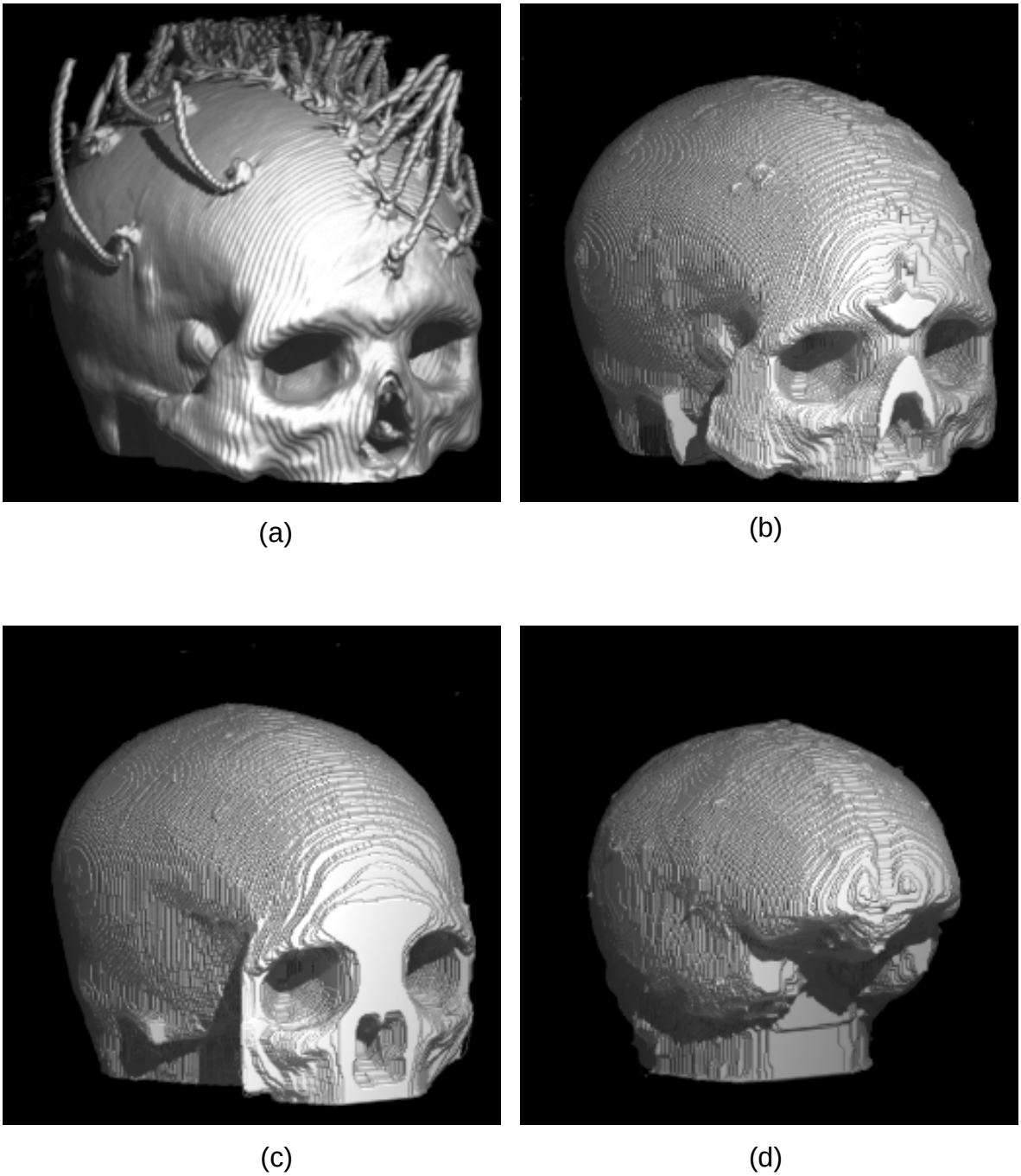

Fig. 4: CT surface extraction viewed from front-right. (a) The original scalp surface with the EEG electrodes; (b) Scalp surface after deleting the EEG electrodes; (c) Outermost skull surface; (d) Innermost skull surface.

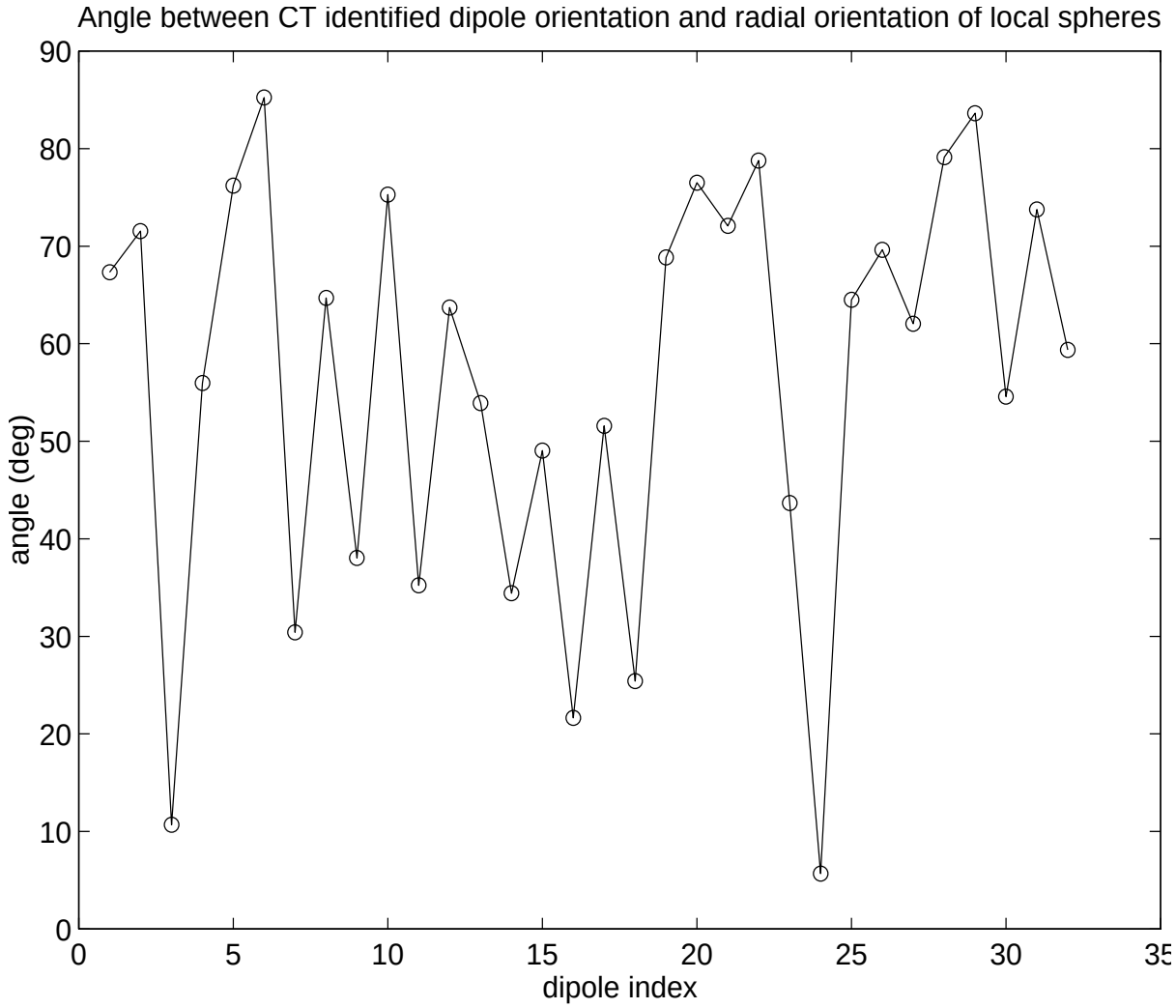

Fig. 5: The deviation of each of the 32 dipoles from a nominal radial orientation. The angles are measured relative to the radial vector pointing away from the center of the locally fitted spheres used in the spherical head models in Section 3**.**

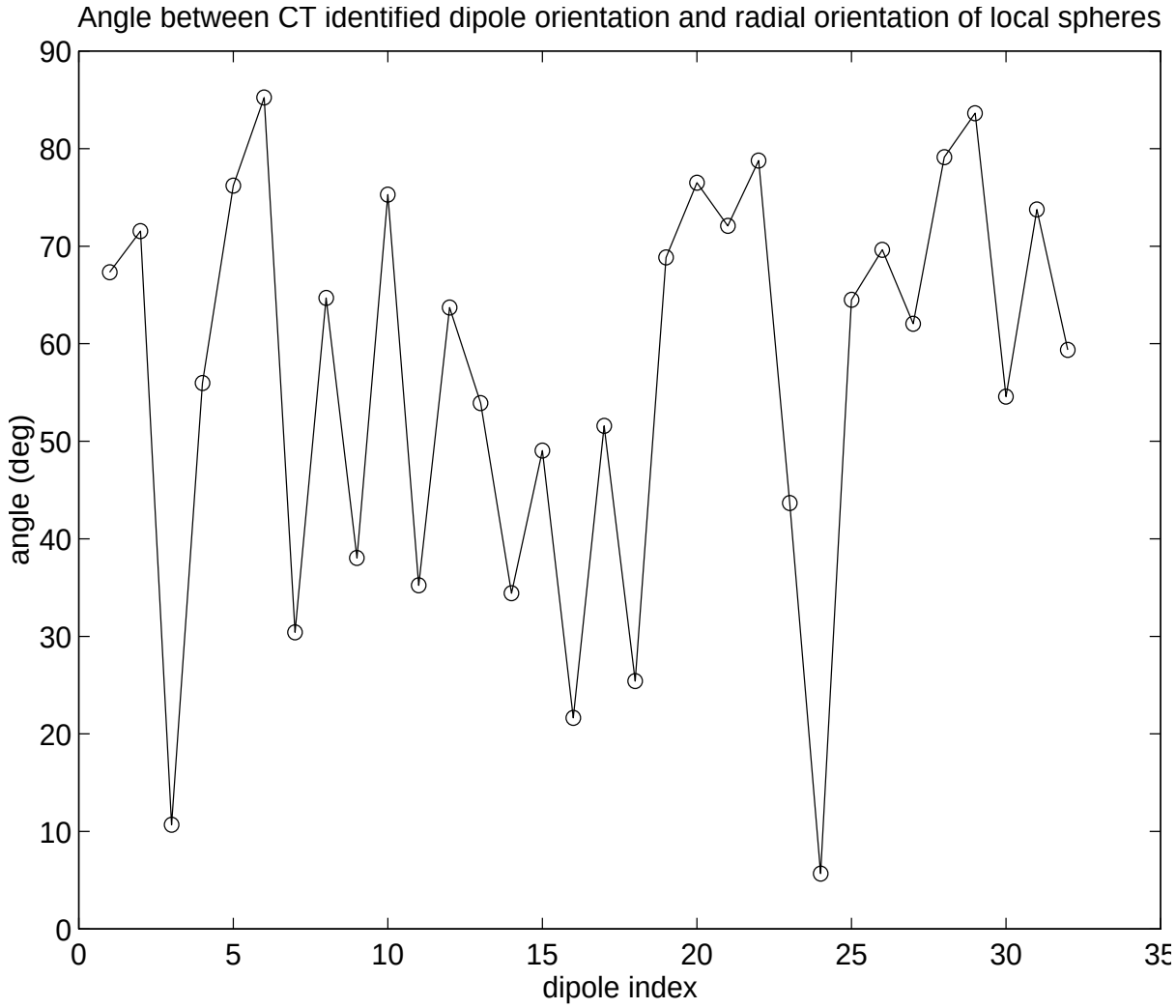

Fig. 5: The deviation of each of the 32 dipoles from a nominal radial orientation. The angles are measured relative to the radial vector pointing away from the center of the locally fitted spheres used in the spherical head models in Section 3**.**

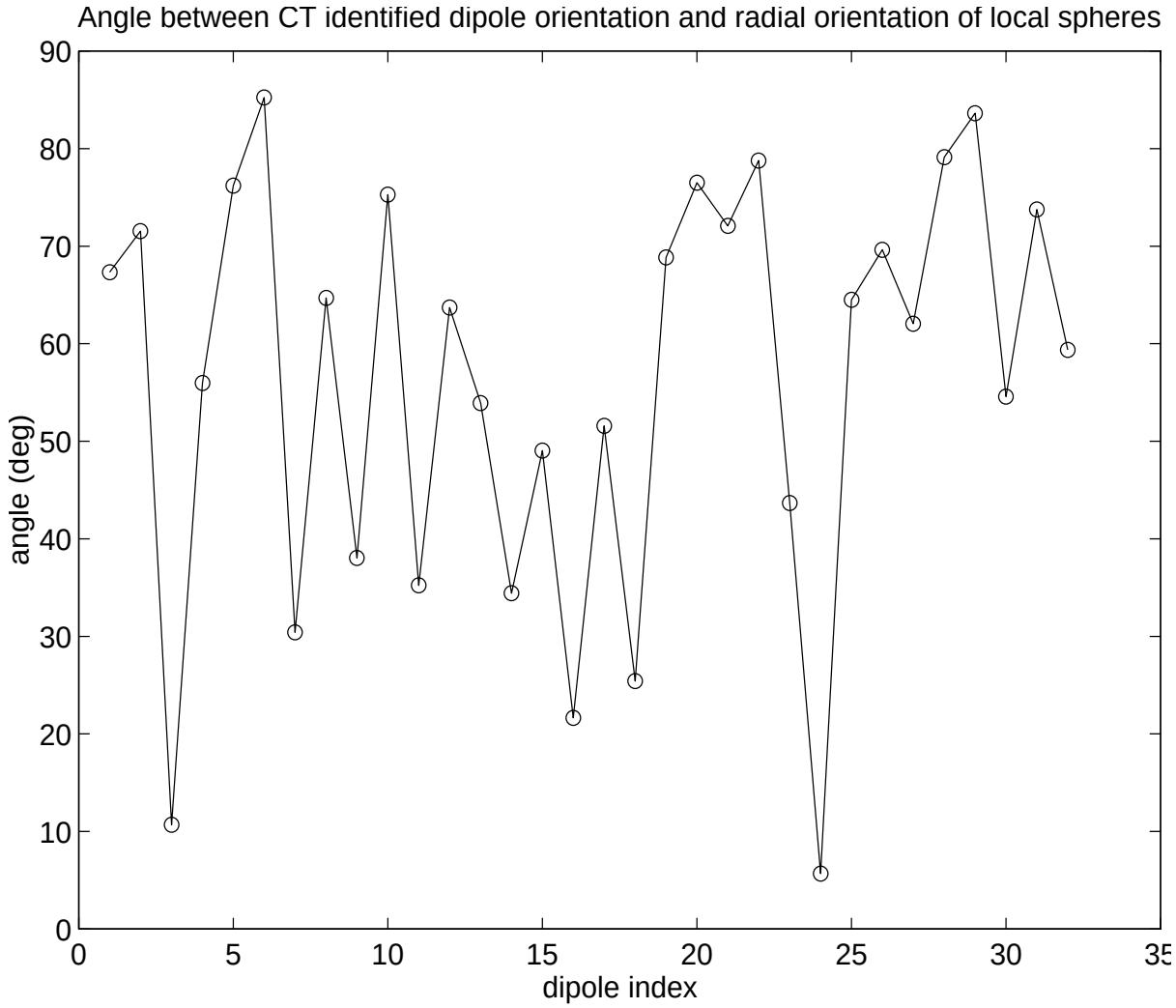

Fig. 5: The deviation of each of the 32 dipoles from a nominal radial orientation. The angles are measured relative to the radial vector pointing away from the center of the locally fitted spheres used in the spherical head models in Section 3**.**

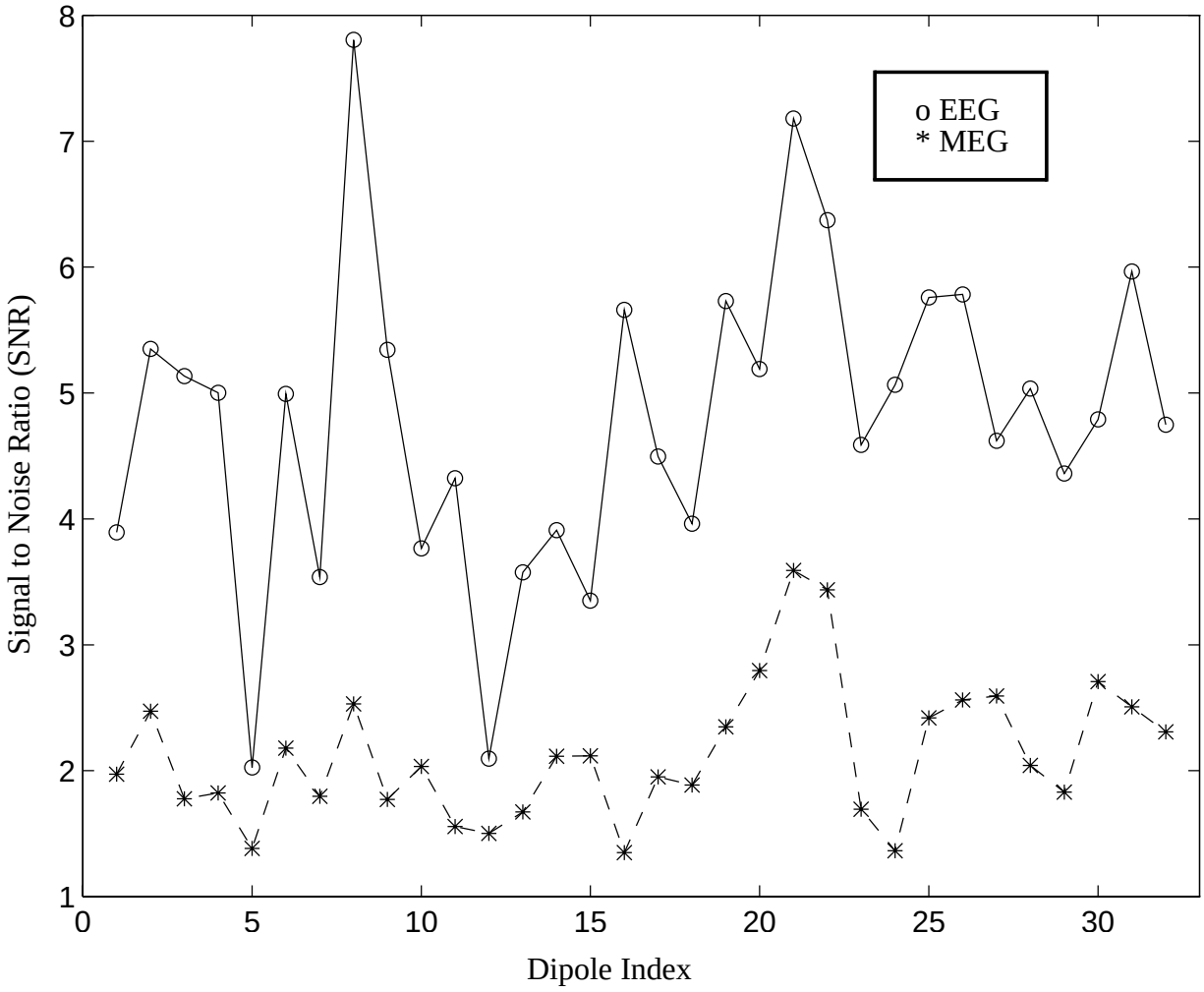

Fig. 6: The Signal to Noise Ratio (SNR) of the 32 dipoles plotted for EEG and MEG.

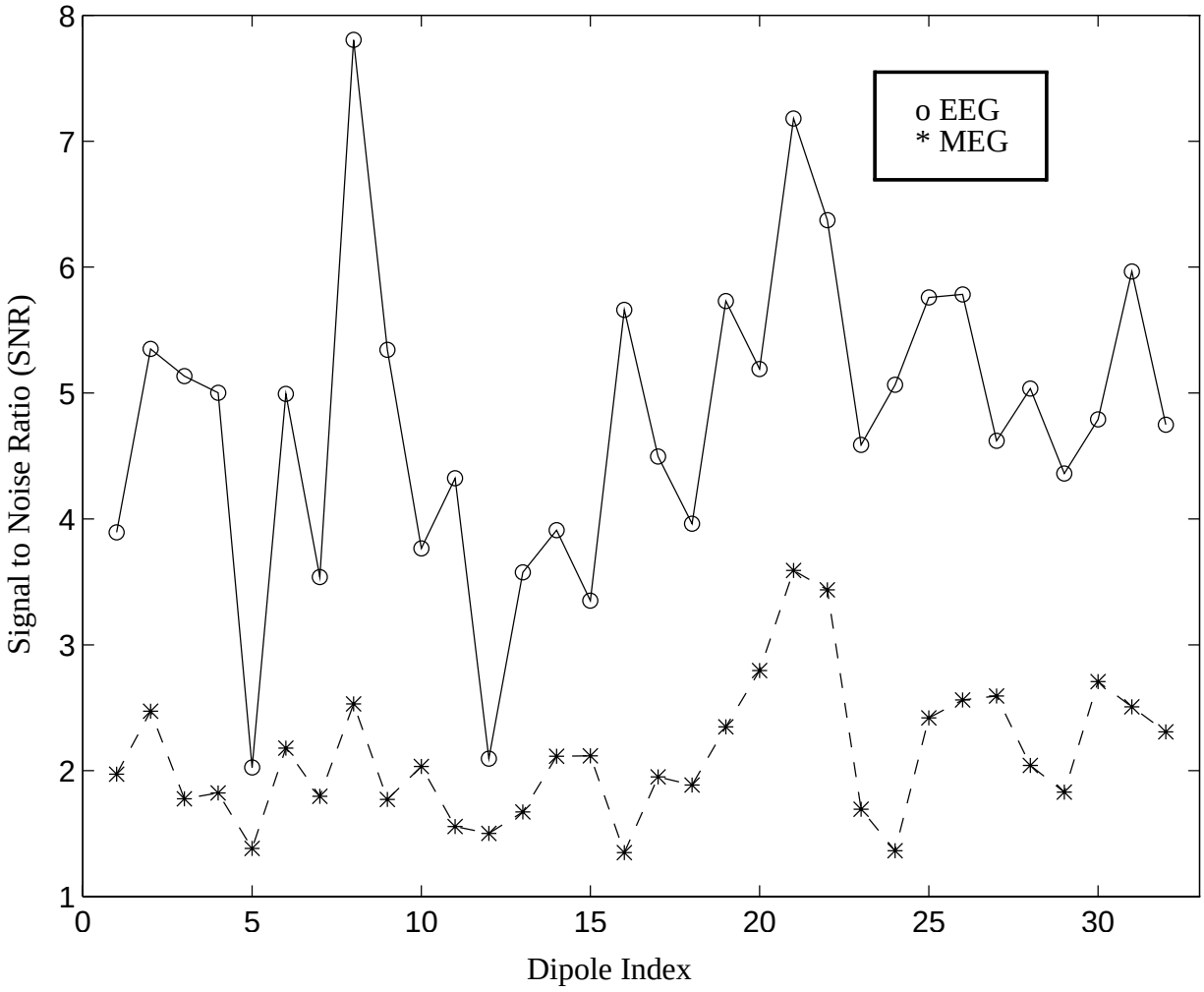

Fig. 6: The Signal to Noise Ratio (SNR) of the 32 dipoles plotted for EEG and MEG.

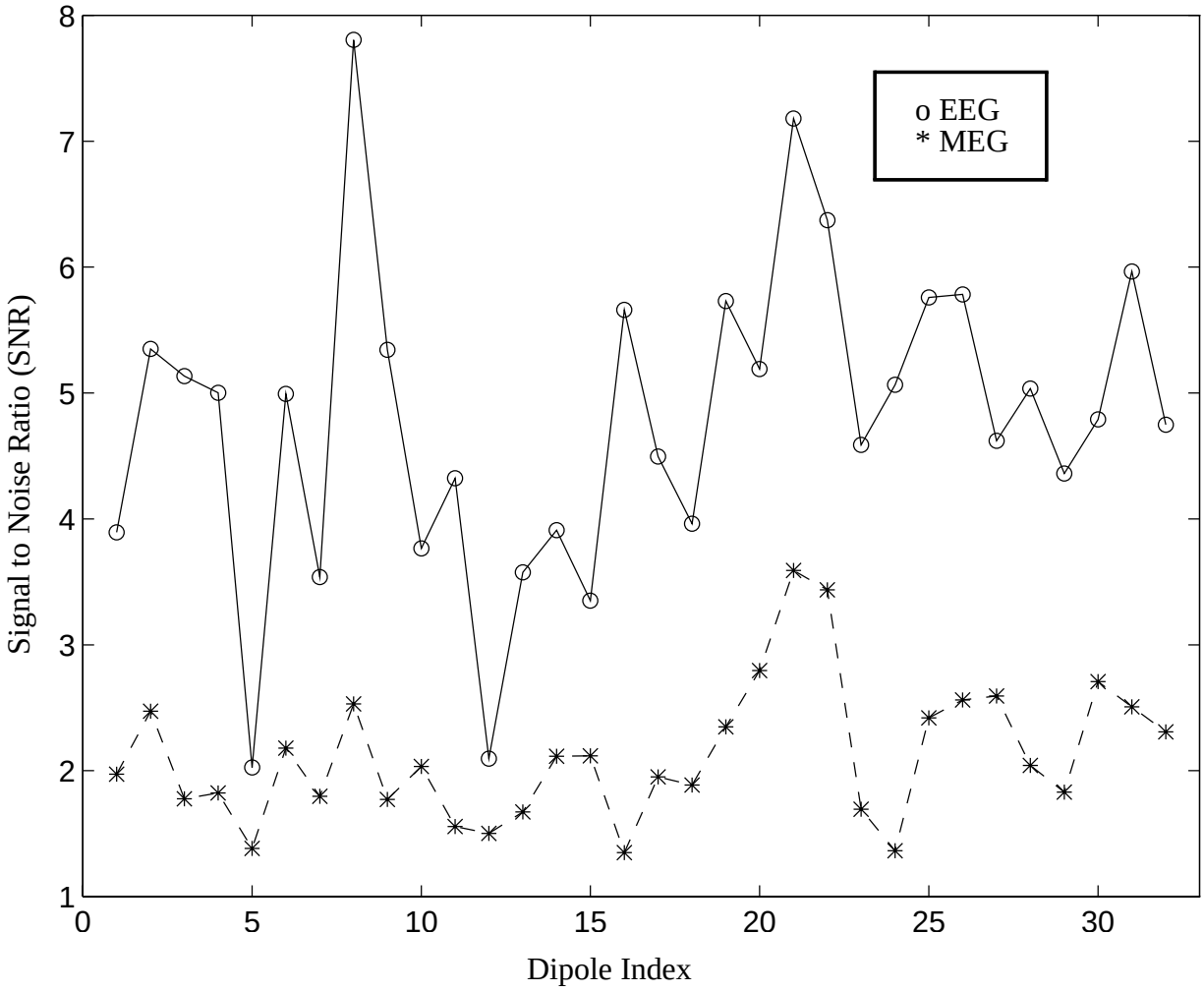

Fig. 6: The Signal to Noise Ratio (SNR) of the 32 dipoles plotted for EEG and MEG.

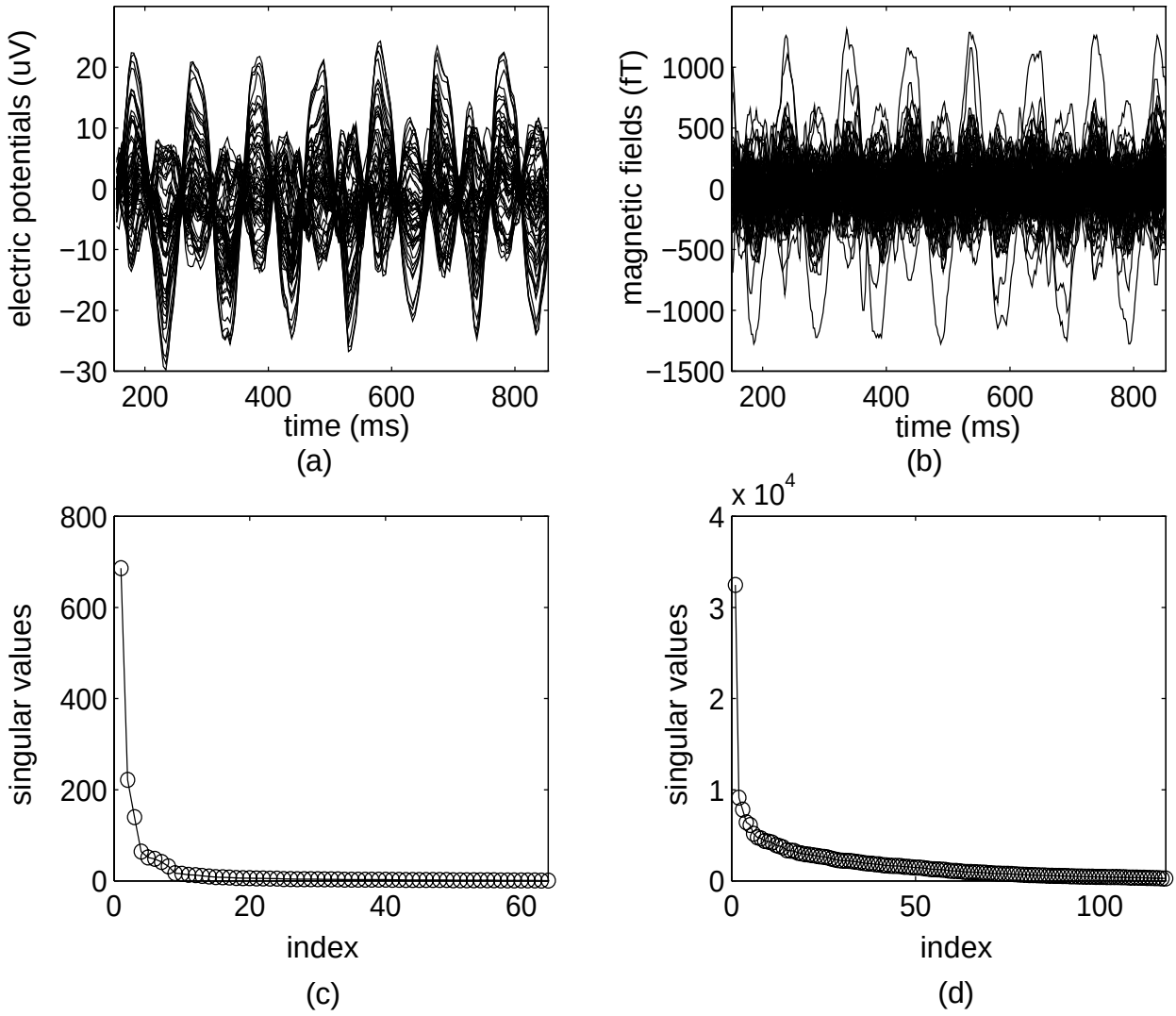

Fig. 7: EEG and MEG waveforms and their singular value plots for a representative dipolar source. (a) the EEG waveforms; (b) the MEG waveforms; (c) singular value plot of the EEG waveforms; (d) singular value plot of the MEG waveforms.

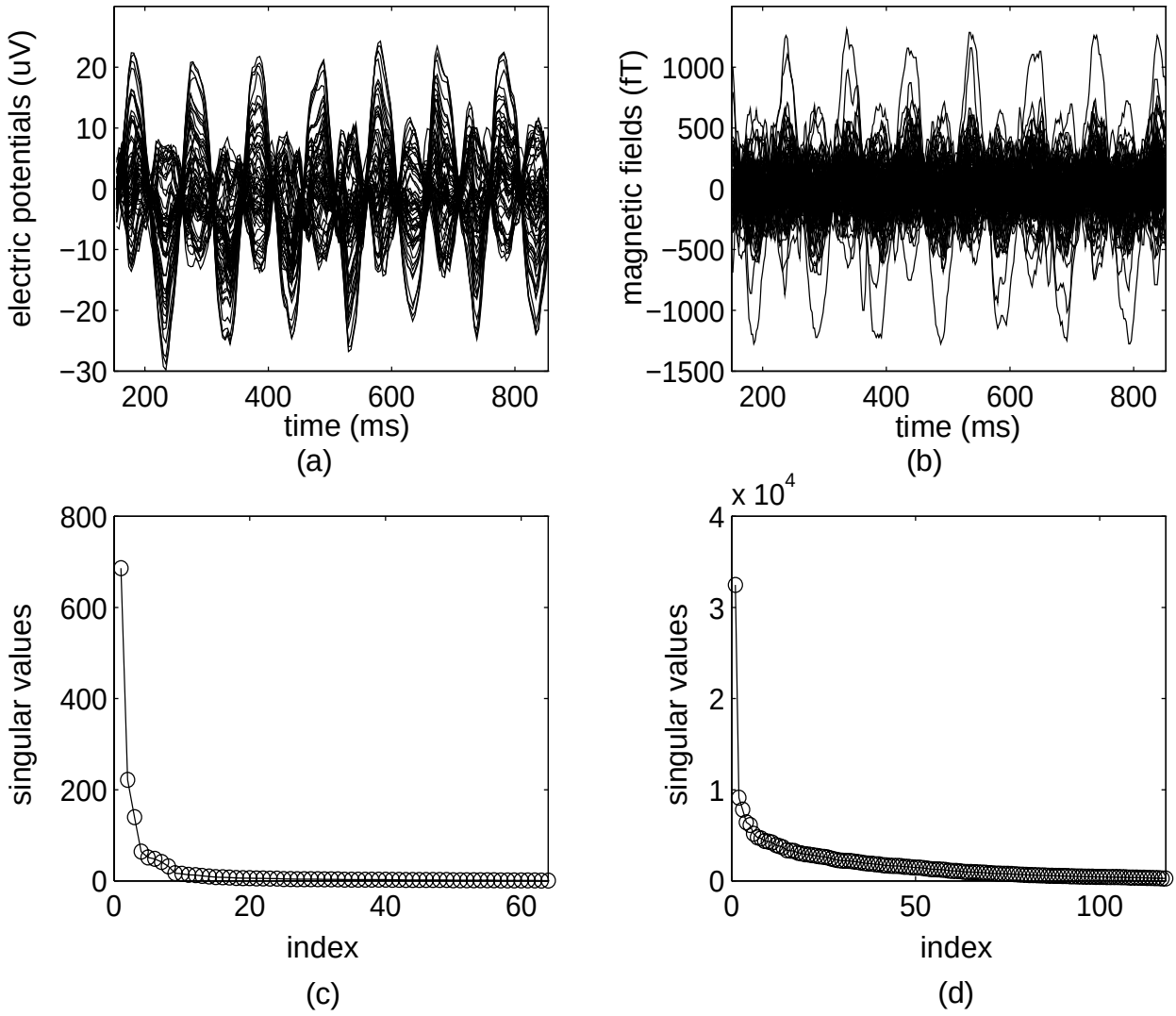

Fig. 7: EEG and MEG waveforms and their singular value plots for a representative dipolar source. (a) the EEG waveforms; (b) the MEG waveforms; (c) singular value plot of the EEG waveforms; (d) singular value plot of the MEG waveforms.

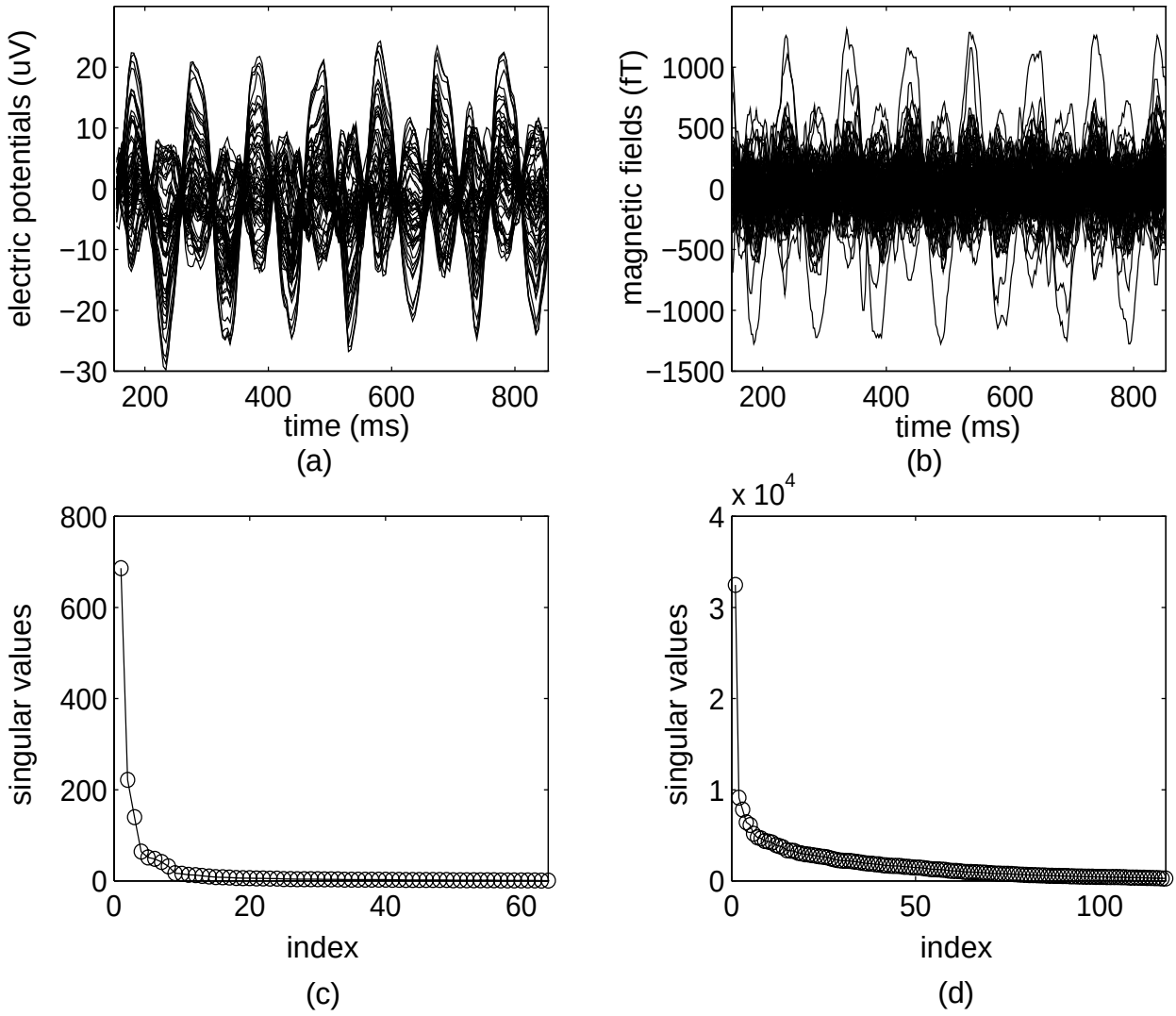

Fig. 7: EEG and MEG waveforms and their singular value plots for a representative dipolar source. (a) the EEG waveforms; (b) the MEG waveforms; (c) singular value plot of the EEG waveforms; (d) singular value plot of the MEG waveforms.

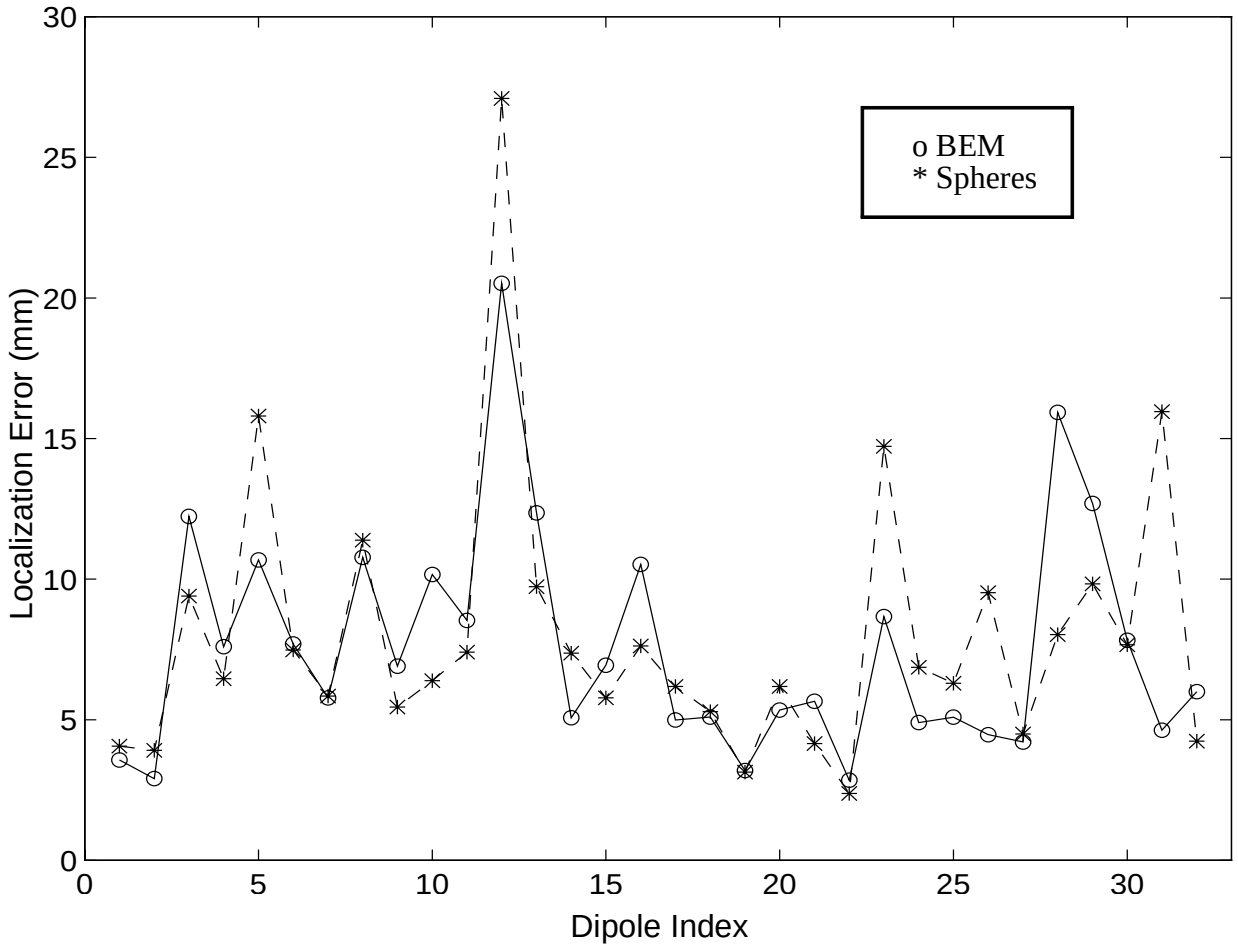

Fig. 8: The EEG localization errors for all the 32 dipole sources using a BEM approach and a locally fitted spheres model. The CT identified dipole locations are used as the "ground truth".

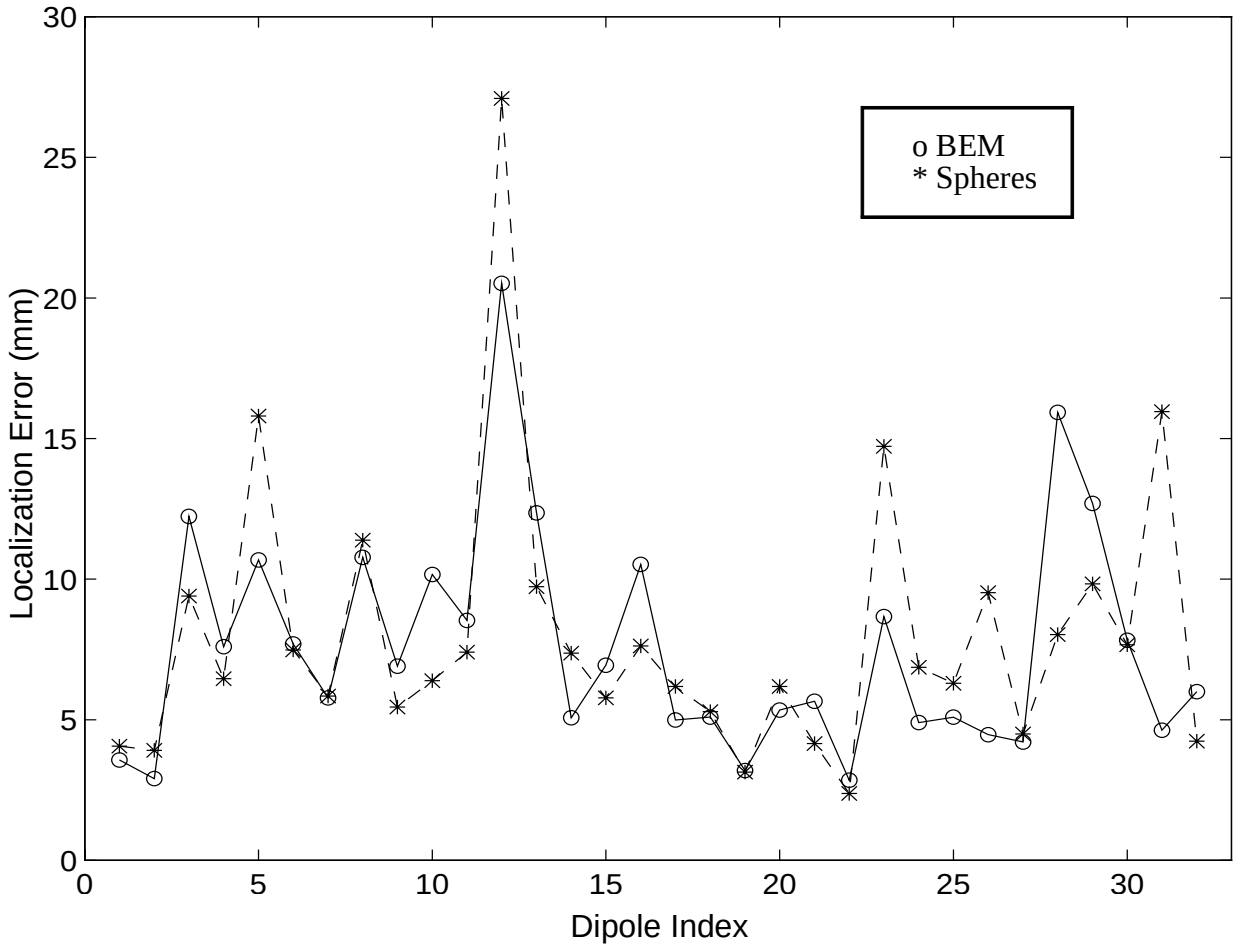

Fig. 8: The EEG localization errors for all the 32 dipole sources using a BEM approach and a locally fitted spheres model. The CT identified dipole locations are used as the "ground truth".

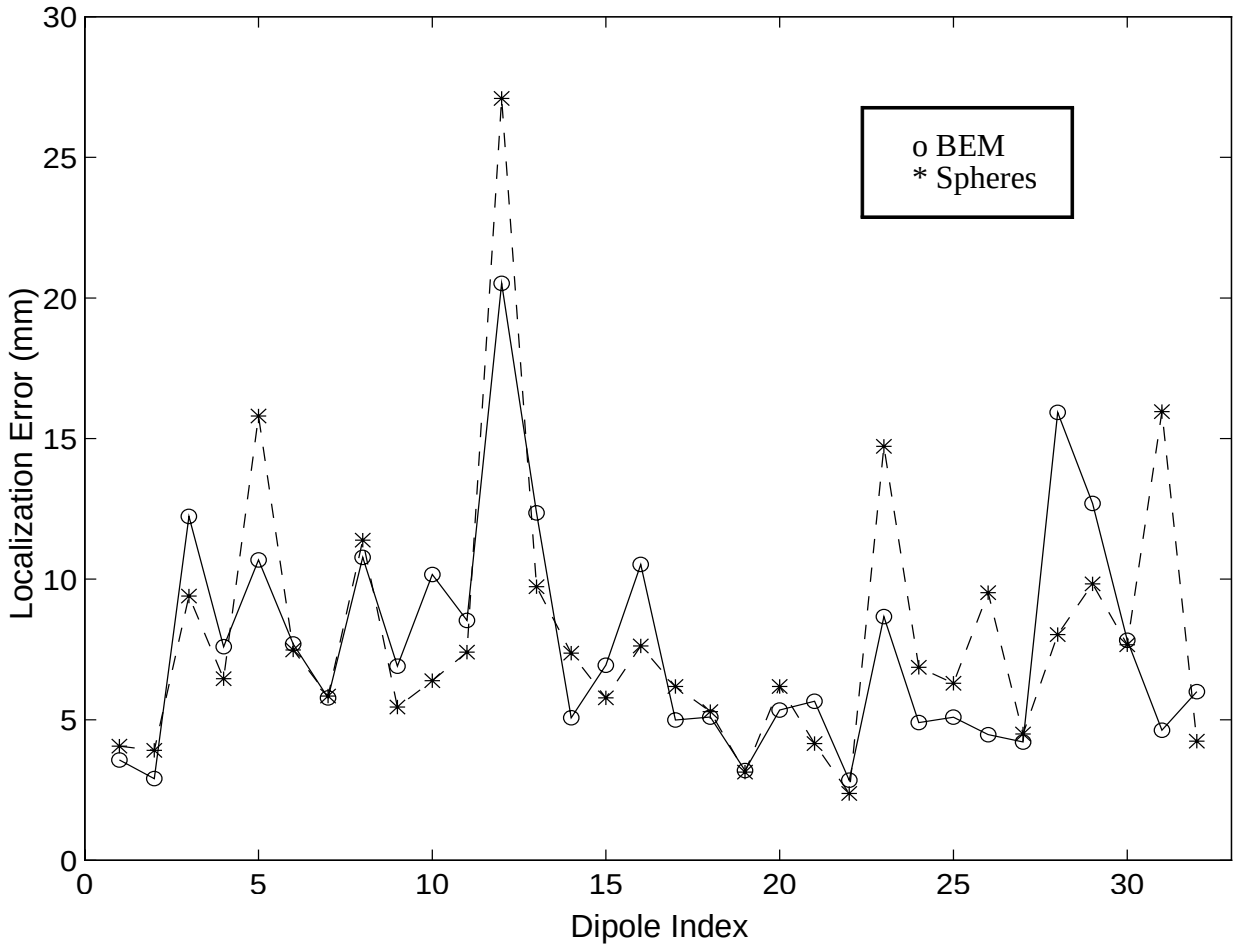

Fig. 8: The EEG localization errors for all the 32 dipole sources using a BEM approach and a locally fitted spheres model. The CT identified dipole locations are used as the "ground truth".

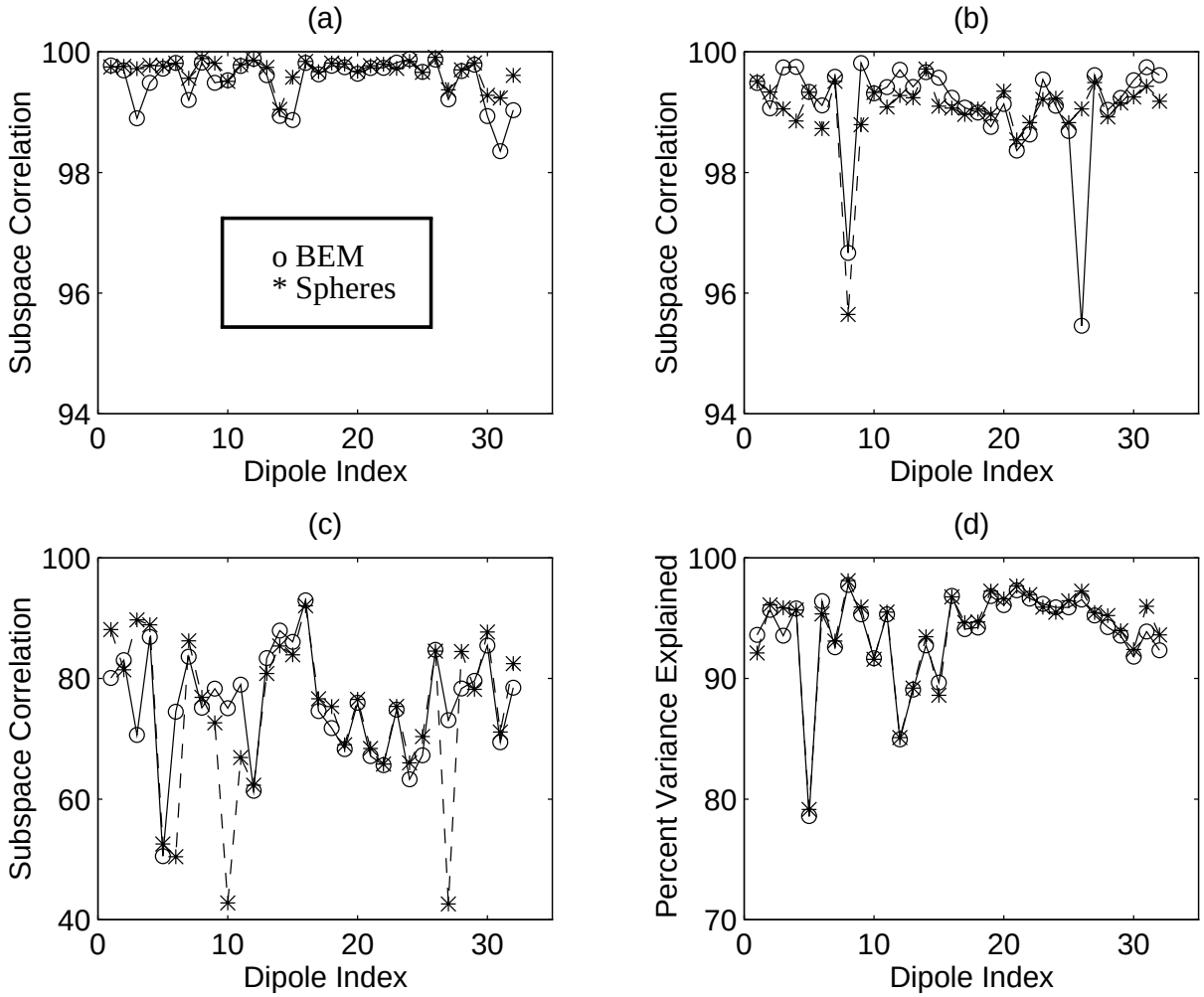

Fig. 9: The subspace correlations and percent variance explained (PVE) for the EEG solutions: (a) the subspace correlation for the first dipole model and the signal subspace; (b) the correlation for a second dipole; (c) the correlation for a third; (d) the percent variance explained for the EEG three-dipole fit.

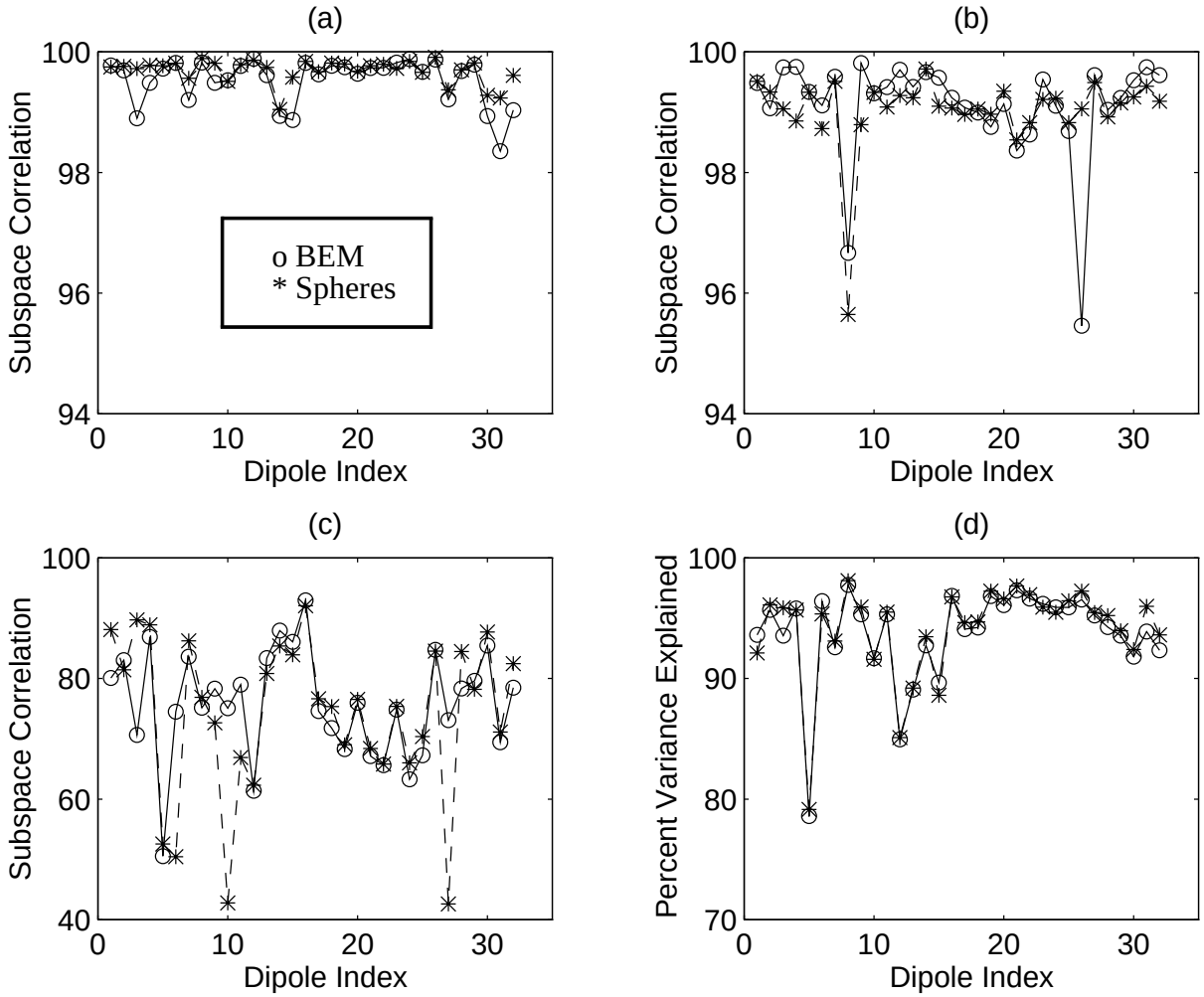

Fig. 9: The subspace correlations and percent variance explained (PVE) for the EEG solutions: (a) the subspace correlation for the first dipole model and the signal subspace; (b) the correlation for a second dipole; (c) the correlation for a third; (d) the percent variance explained for the EEG three-dipole fit.

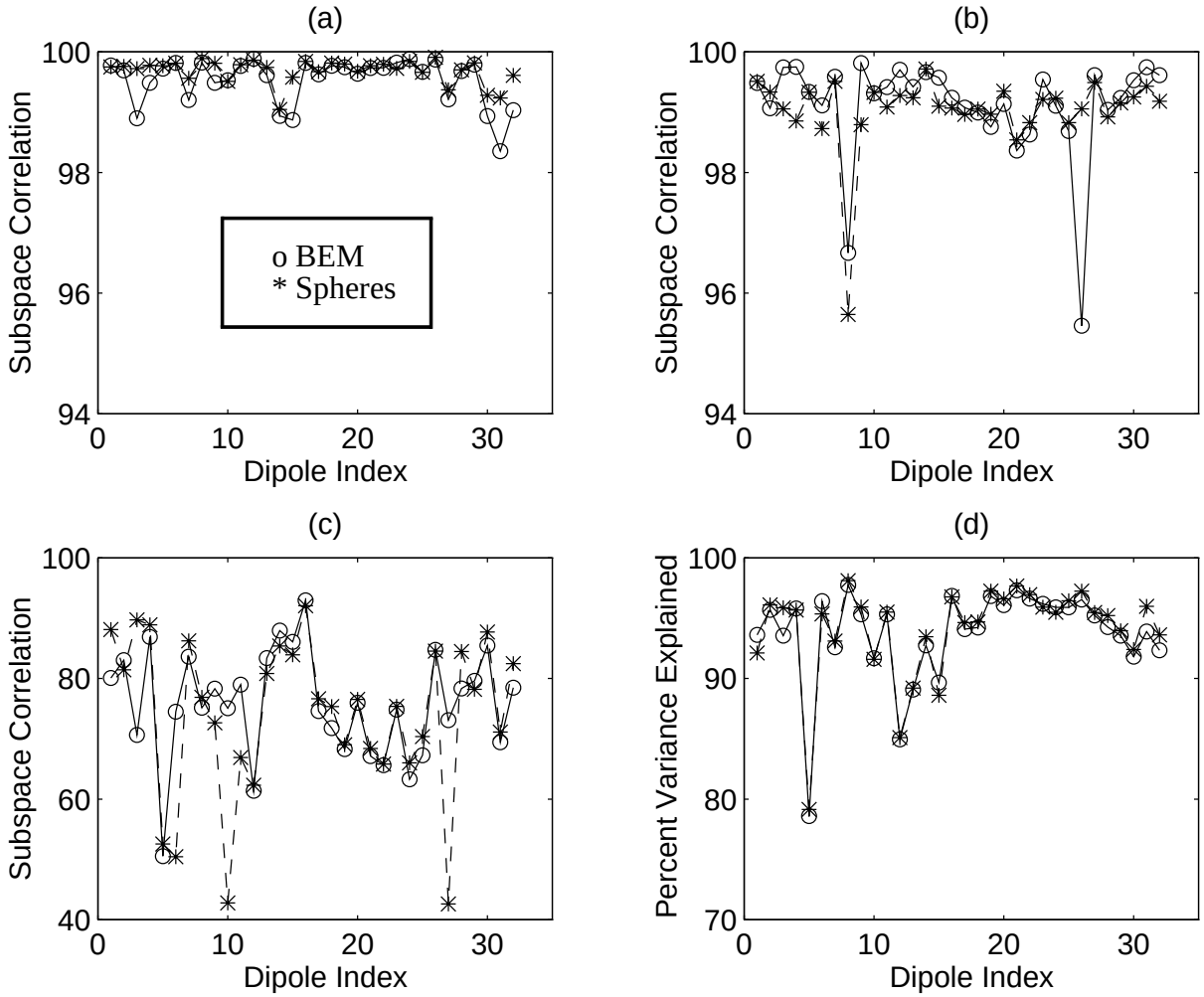

Fig. 9: The subspace correlations and percent variance explained (PVE) for the EEG solutions: (a) the subspace correlation for the first dipole model and the signal subspace; (b) the correlation for a second dipole; (c) the correlation for a third; (d) the percent variance explained for the EEG three-dipole fit.

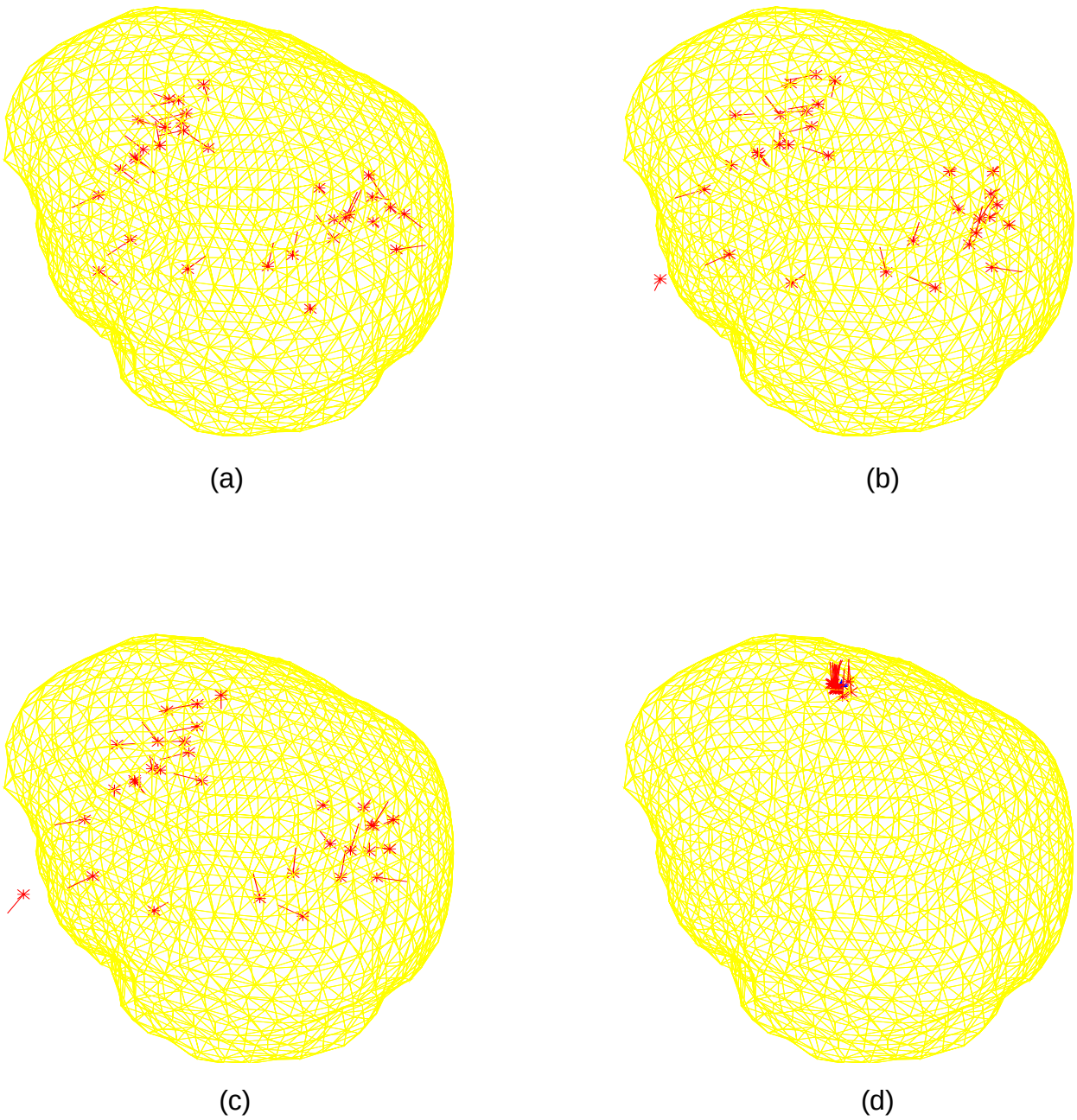

Fig. 10: Fitted dipole locations and orientations using EEG: (a) the 32 CT-identified dipole locations and orientations plotted in the tessellated inner skull surface; (b) the 32 fitted dipole locations and orientations using BEM; (c) the 32 fitted dipole locations and orientations using a two locally fitted sphere model; (d) the second identified dipolar sources, which form a cluster with radial orientation at the top of the head, under the reference electrode.

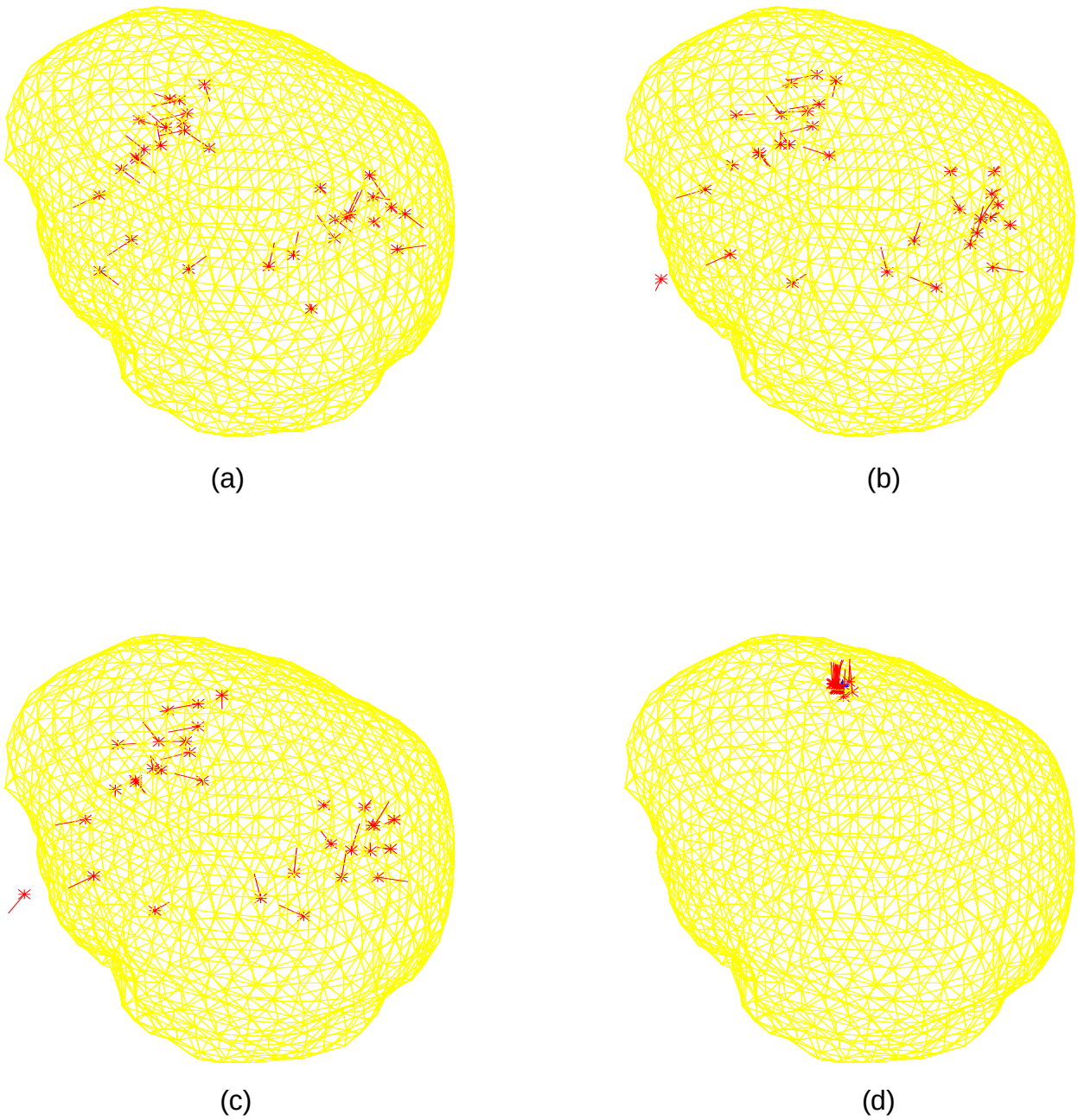

Fig. 10: Fitted dipole locations and orientations using EEG: (a) the 32 CT-identified dipole locations and orientations plotted in the tessellated inner skull surface; (b) the 32 fitted dipole locations and orientations using BEM; (c) the 32 fitted dipole locations and orientations using a two locally fitted sphere model; (d) the second identified dipolar sources, which form a cluster with radial orientation at the top of the head, under the reference electrode.

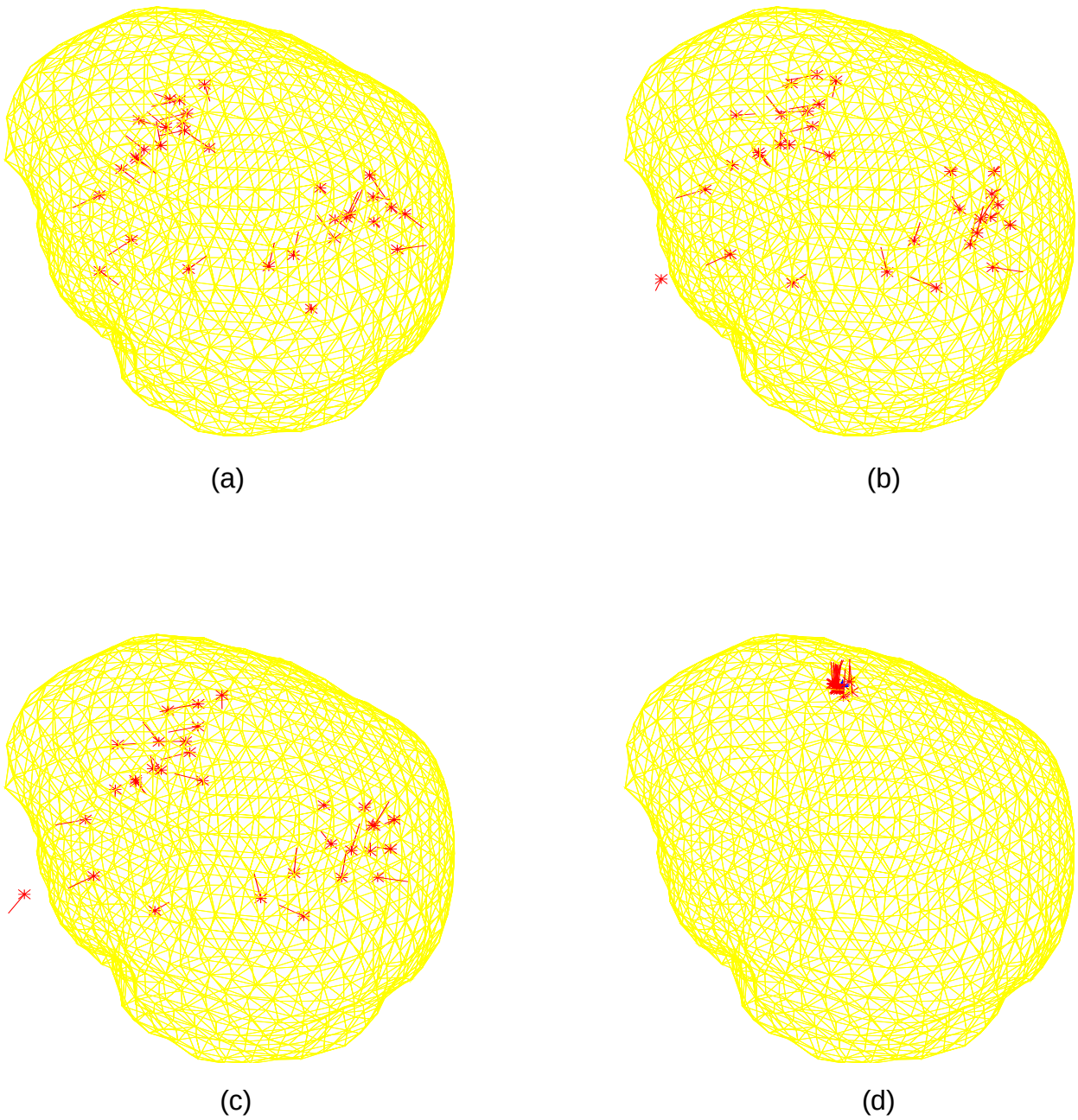

Fig. 10: Fitted dipole locations and orientations using EEG: (a) the 32 CT-identified dipole locations and orientations plotted in the tessellated inner skull surface; (b) the 32 fitted dipole locations and orientations using BEM; (c) the 32 fitted dipole locations and orientations using a two locally fitted sphere model; (d) the second identified dipolar sources, which form a cluster with radial orientation at the top of the head, under the reference electrode.

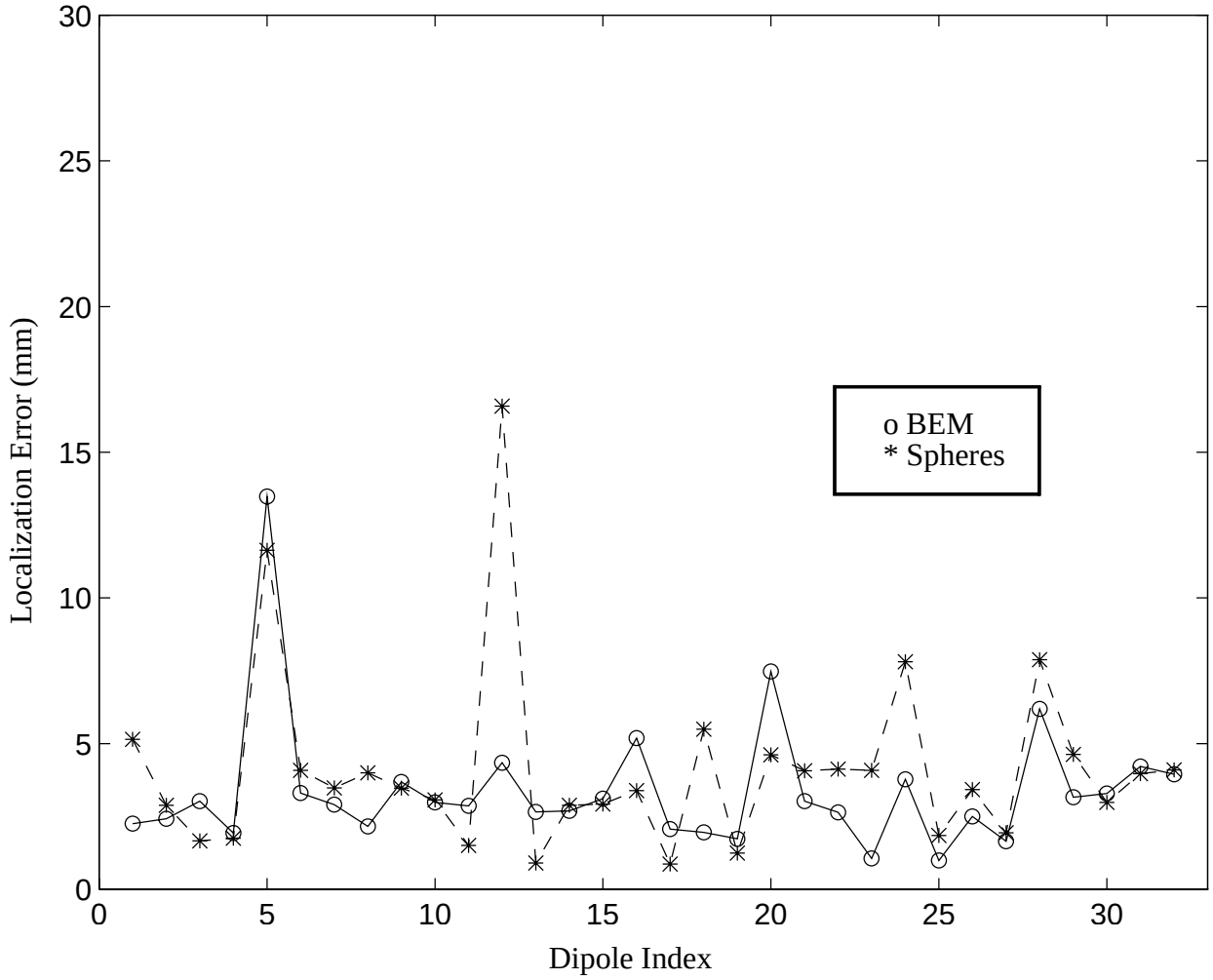

Fig. 11: The MEG localization errors for all the 32 dipole sources using a BEM approach and a locally fitted spheres model.

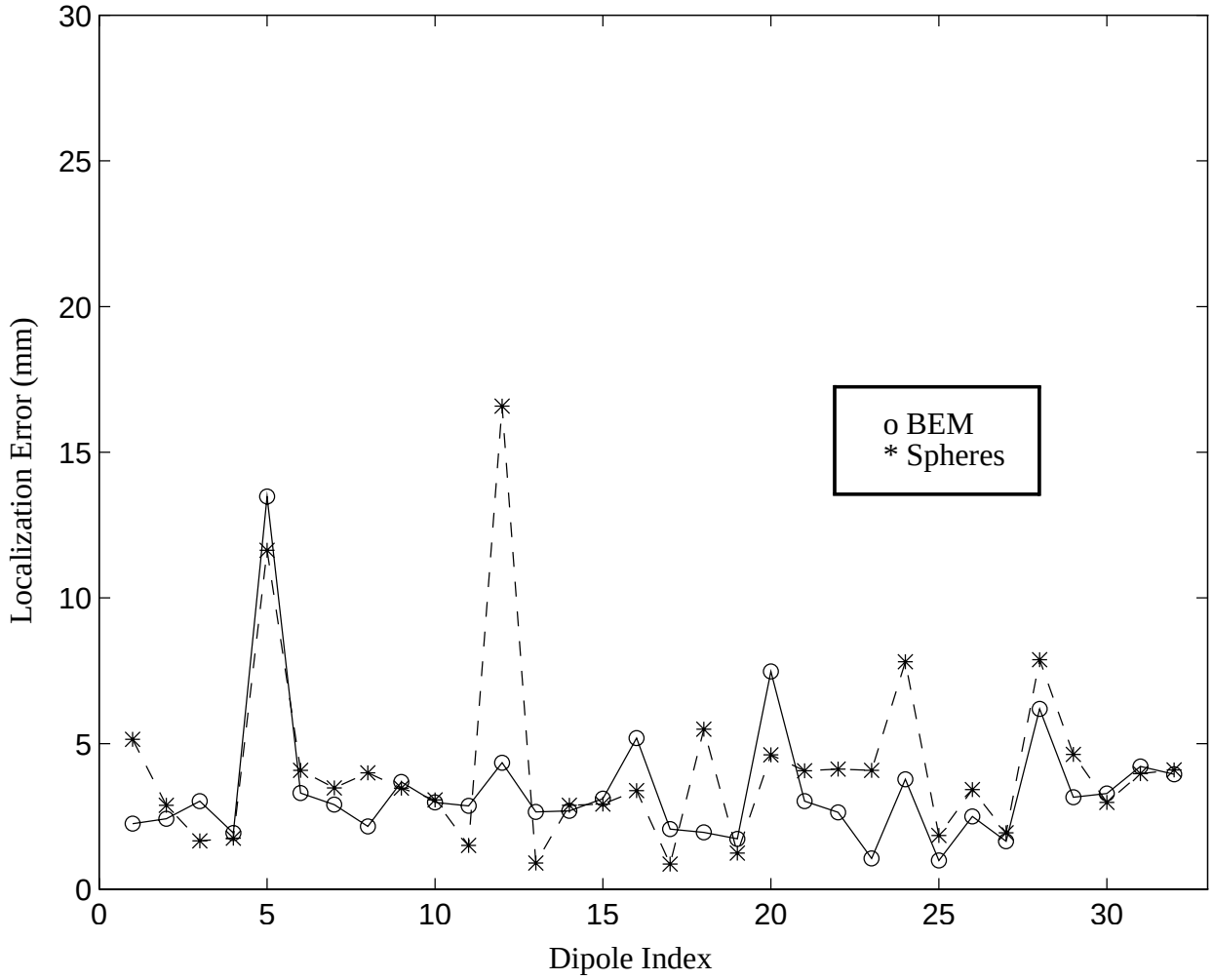

Fig. 11: The MEG localization errors for all the 32 dipole sources using a BEM approach and a locally fitted spheres model.

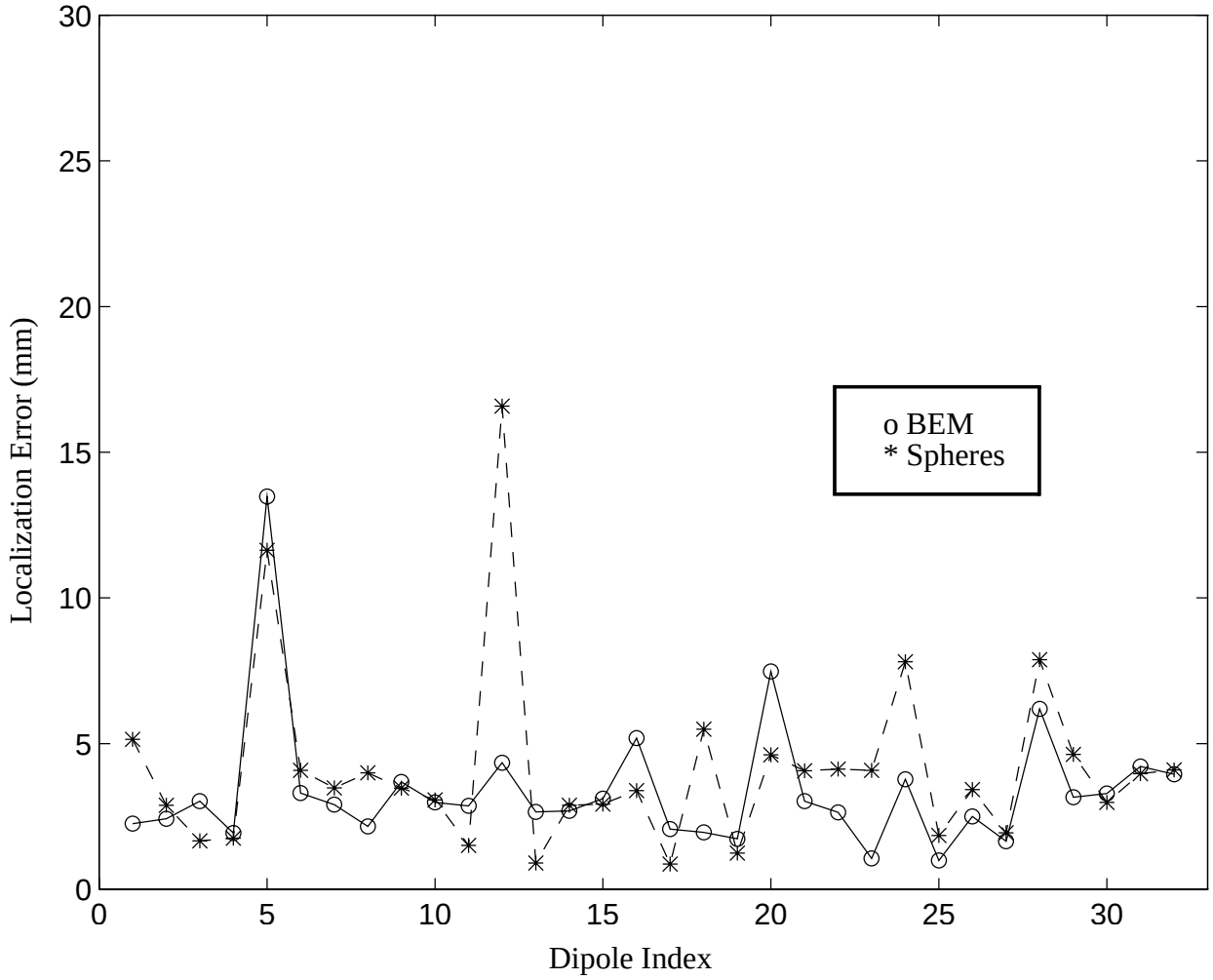

Fig. 11: The MEG localization errors for all the 32 dipole sources using a BEM approach and a locally fitted spheres model.

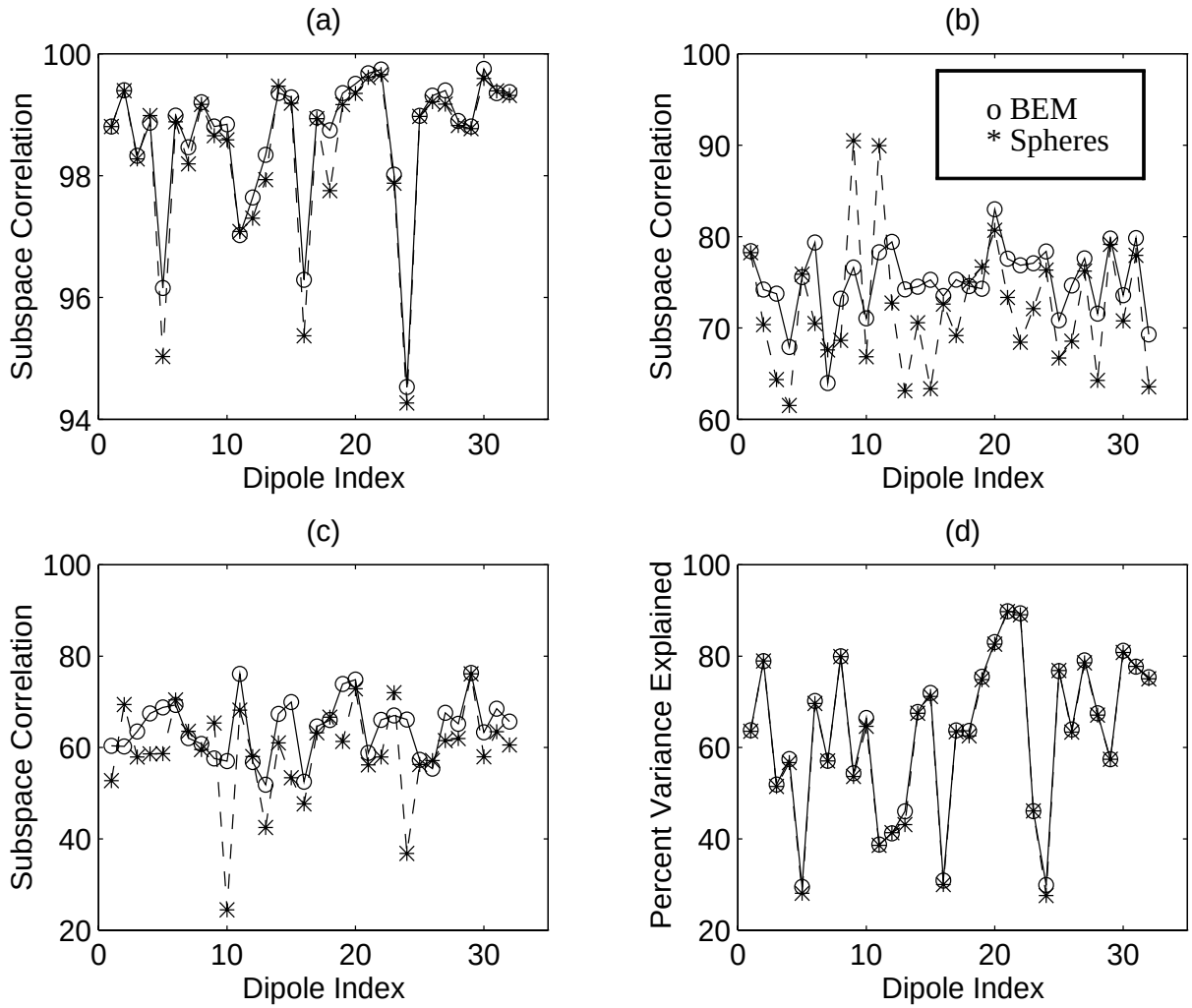

Fig. 12: The subspace correlations and percent variance explained for the MEG solutions. See Fig. 9 for plot descriptions.

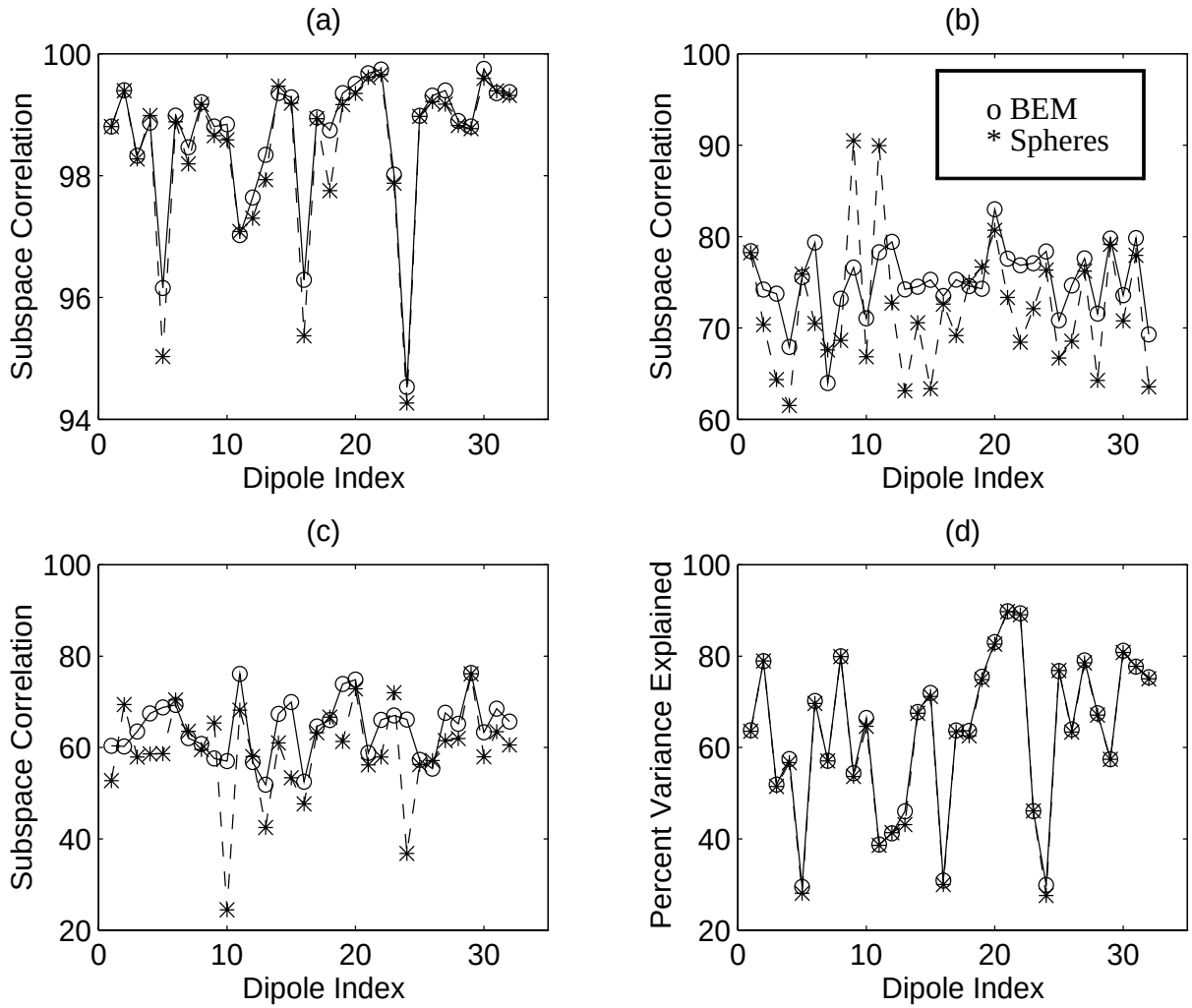

Fig. 12: The subspace correlations and percent variance explained for the MEG solutions. See Fig. 9 for plot descriptions.

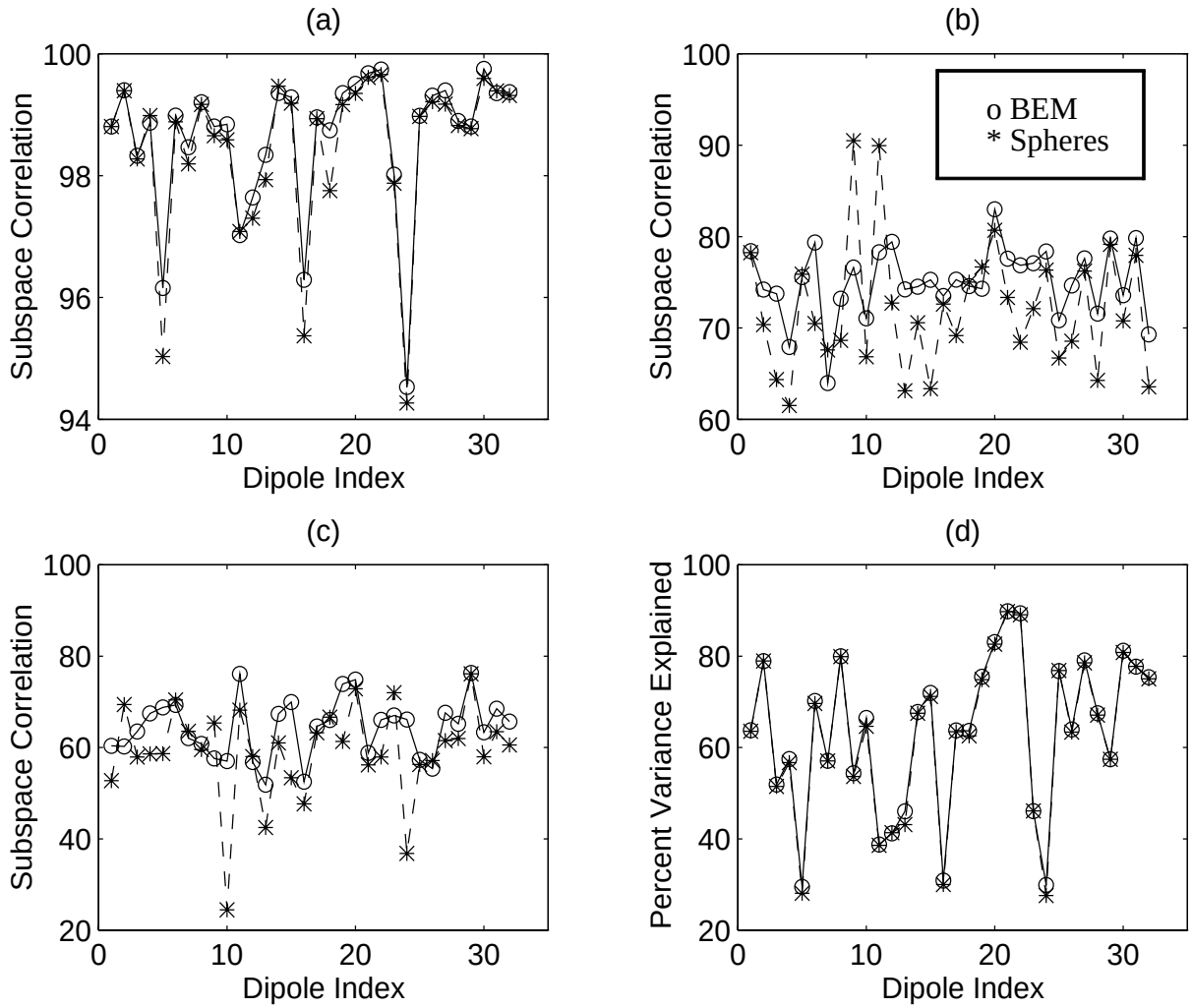

Fig. 12: The subspace correlations and percent variance explained for the MEG solutions. See Fig. 9 for plot descriptions.

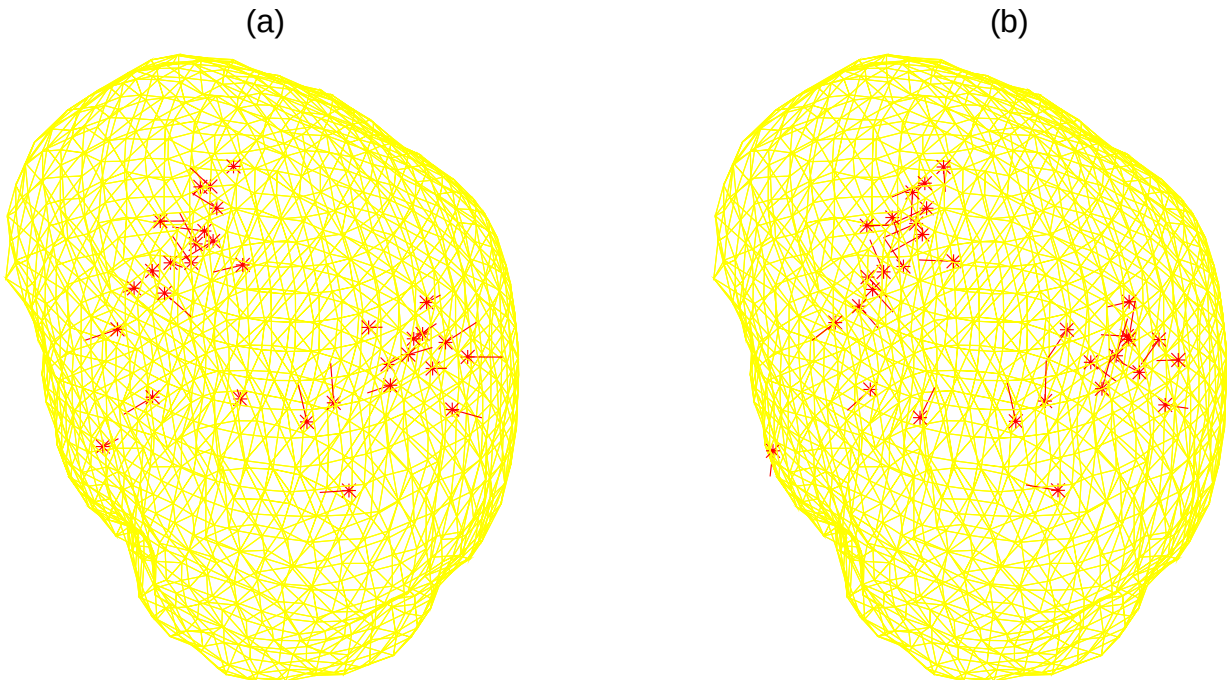

Fig. 13: The 32 MEG fitted dipole locations and orientations; (a) the 32 fitted dipole locations and orientations using BEM; (b) the 32 fitted dipole locations and orientations using a two locally fitted sphere approach. The true CT locations are given in Fig. 10(a).

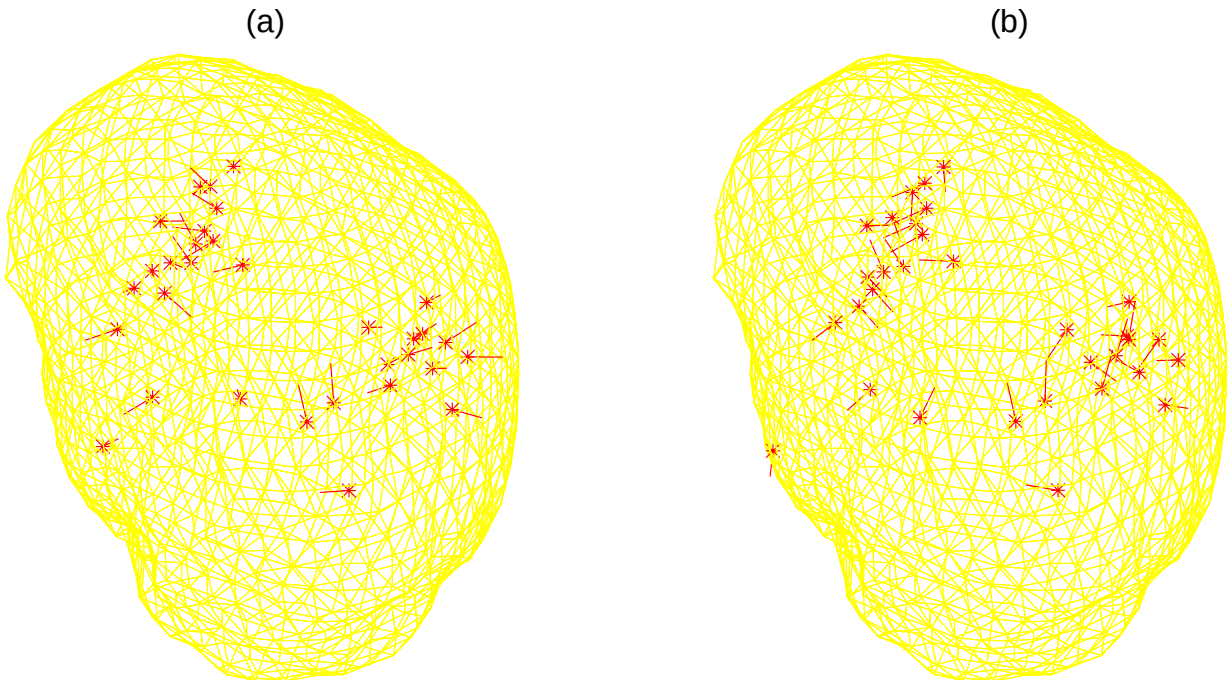

Fig. 13: The 32 MEG fitted dipole locations and orientations; (a) the 32 fitted dipole locations and orientations using BEM; (b) the 32 fitted dipole locations and orientations using a two locally fitted sphere approach. The true CT locations are given in Fig. 10(a).

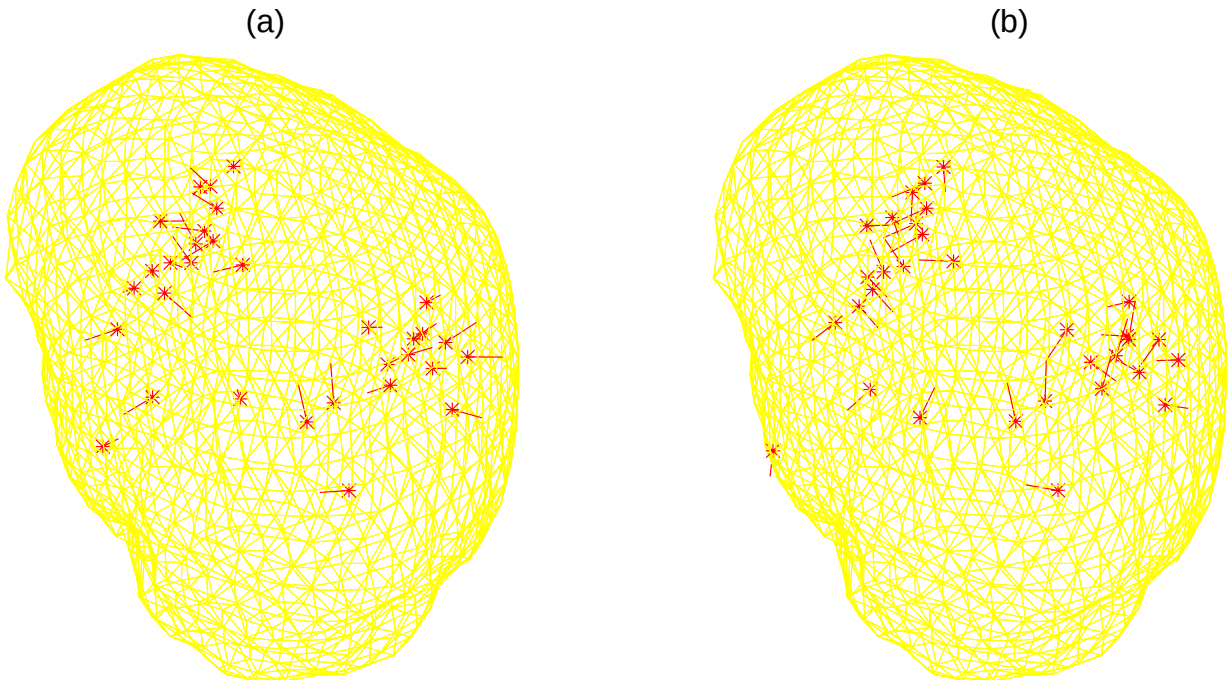

Fig. 13: The 32 MEG fitted dipole locations and orientations; (a) the 32 fitted dipole locations and orientations using BEM; (b) the 32 fitted dipole locations and orientations using a two locally fitted sphere approach. The true CT locations are given in Fig. 10(a).

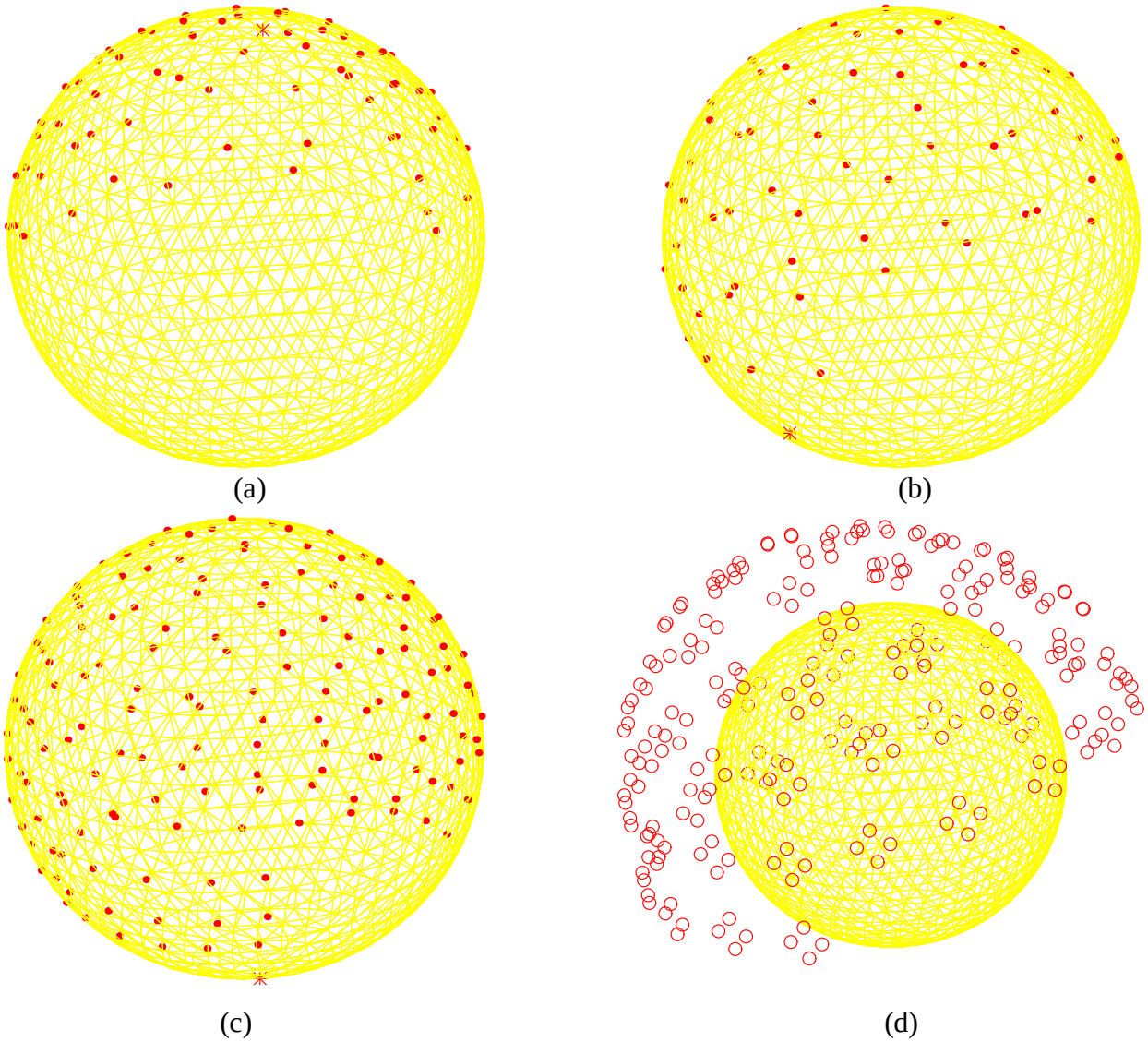

Fig. 14: The arrays used in the spherical head model simulations, as viewed from the upper front-right: (a) the simulated EEG array containing 64 channels to mimic the true EEG array used for the skull phantom (the array is plotted on the tessellated spherical scalp, and the asterisk is the reference electrode); (b) the simulated EEG array containing 61 channels, to mimic the 61 dual channel sites used in the Neuromag-122 MEG array (the reference is at the lower region); (c) a simulated array comprising 148 sensors about the upper hemisphere; (d) the Neuromag-122 MEG array.

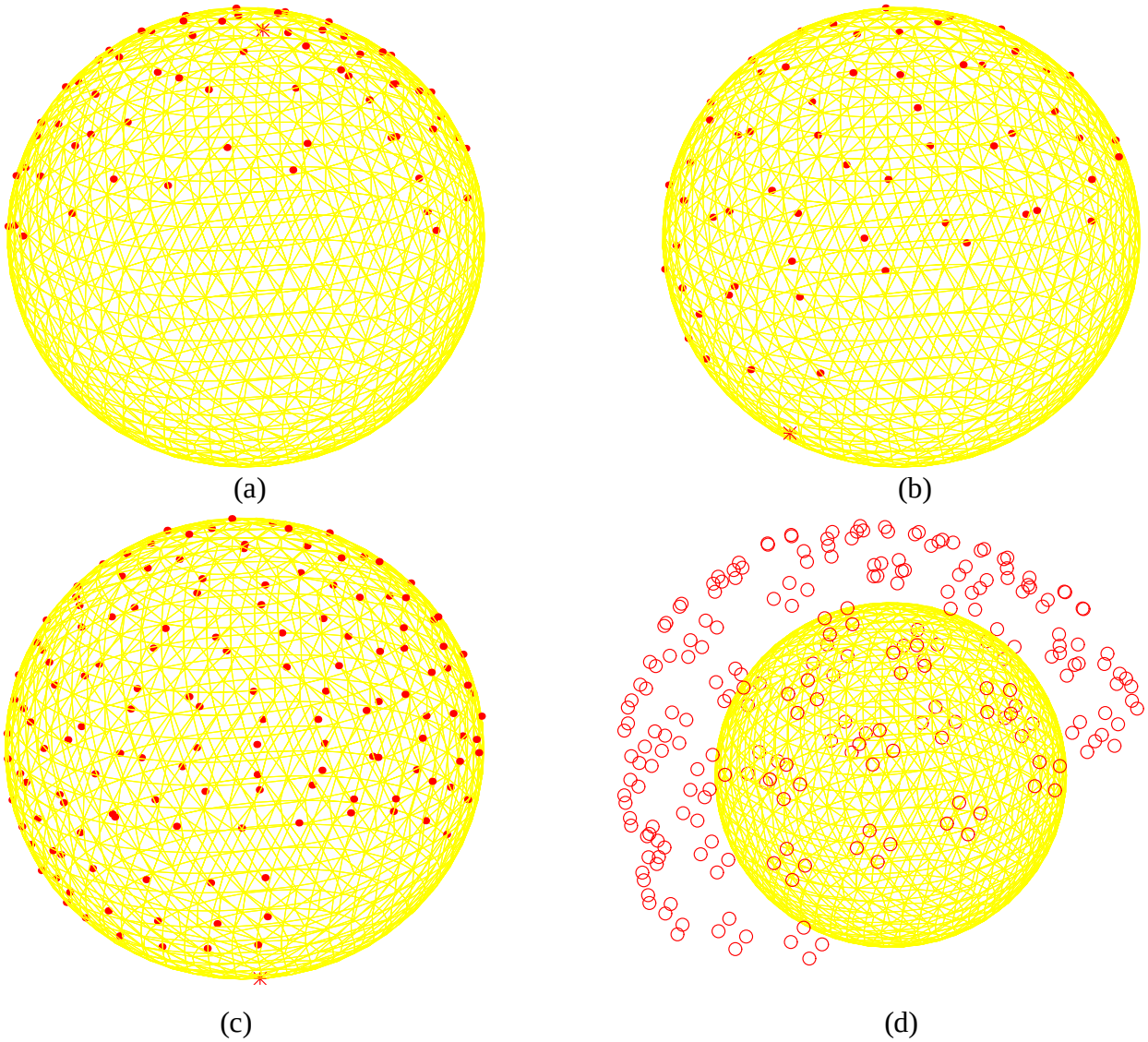

Fig. 14: The arrays used in the spherical head model simulations, as viewed from the upper front-right: (a) the simulated EEG array containing 64 channels to mimic the true EEG array used for the skull phantom (the array is plotted on the tessellated spherical scalp, and the asterisk is the reference electrode); (b) the simulated EEG array containing 61 channels, to mimic the 61 dual channel sites used in the Neuromag-122 MEG array (the reference is at the lower region); (c) a simulated array comprising 148 sensors about the upper hemisphere; (d) the Neuromag-122 MEG array.

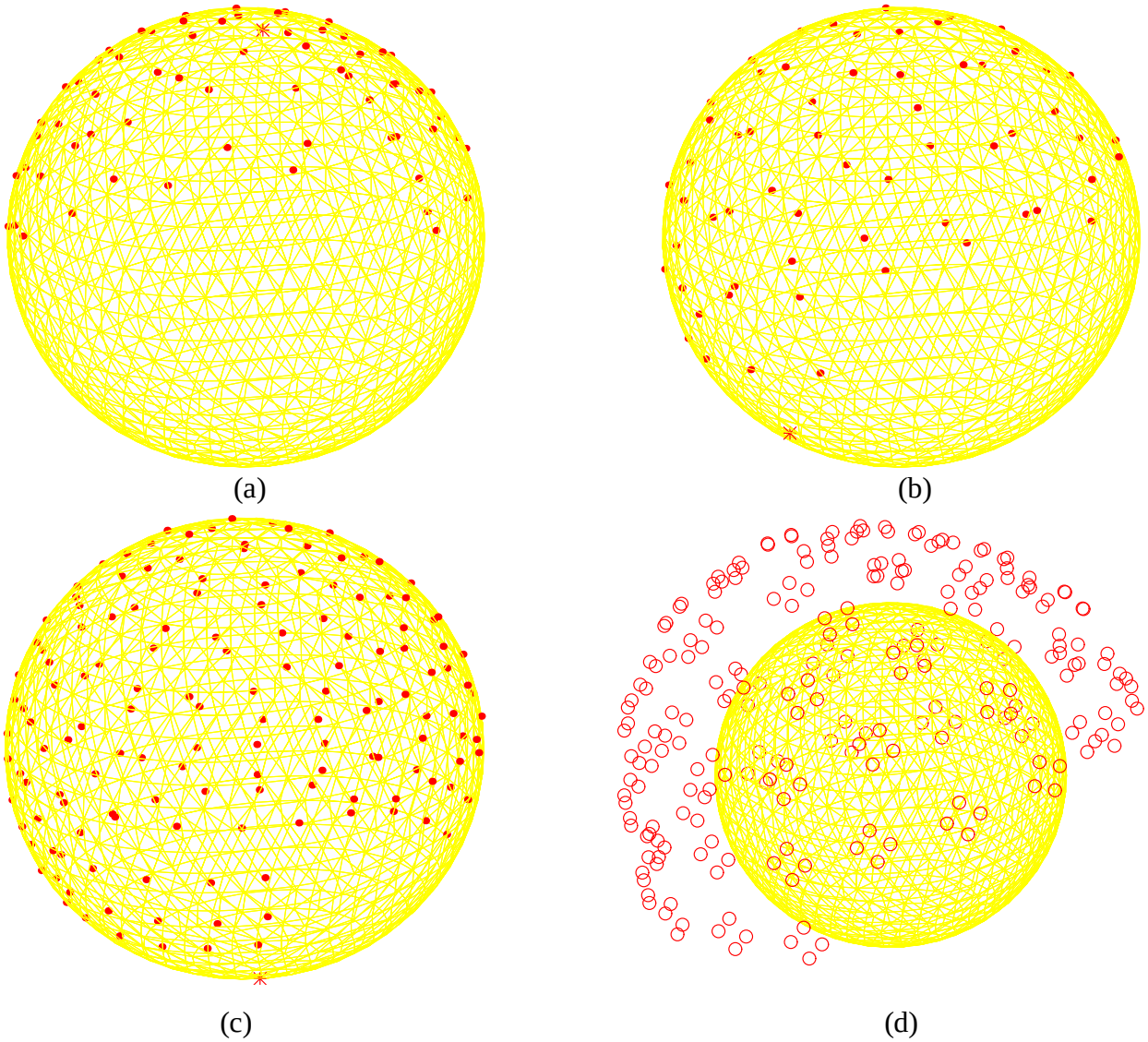

Fig. 14: The arrays used in the spherical head model simulations, as viewed from the upper front-right: (a) the simulated EEG array containing 64 channels to mimic the true EEG array used for the skull phantom (the array is plotted on the tessellated spherical scalp, and the asterisk is the reference electrode); (b) the simulated EEG array containing 61 channels, to mimic the 61 dual channel sites used in the Neuromag-122 MEG array (the reference is at the lower region); (c) a simulated array comprising 148 sensors about the upper hemisphere; (d) the Neuromag-122 MEG array.

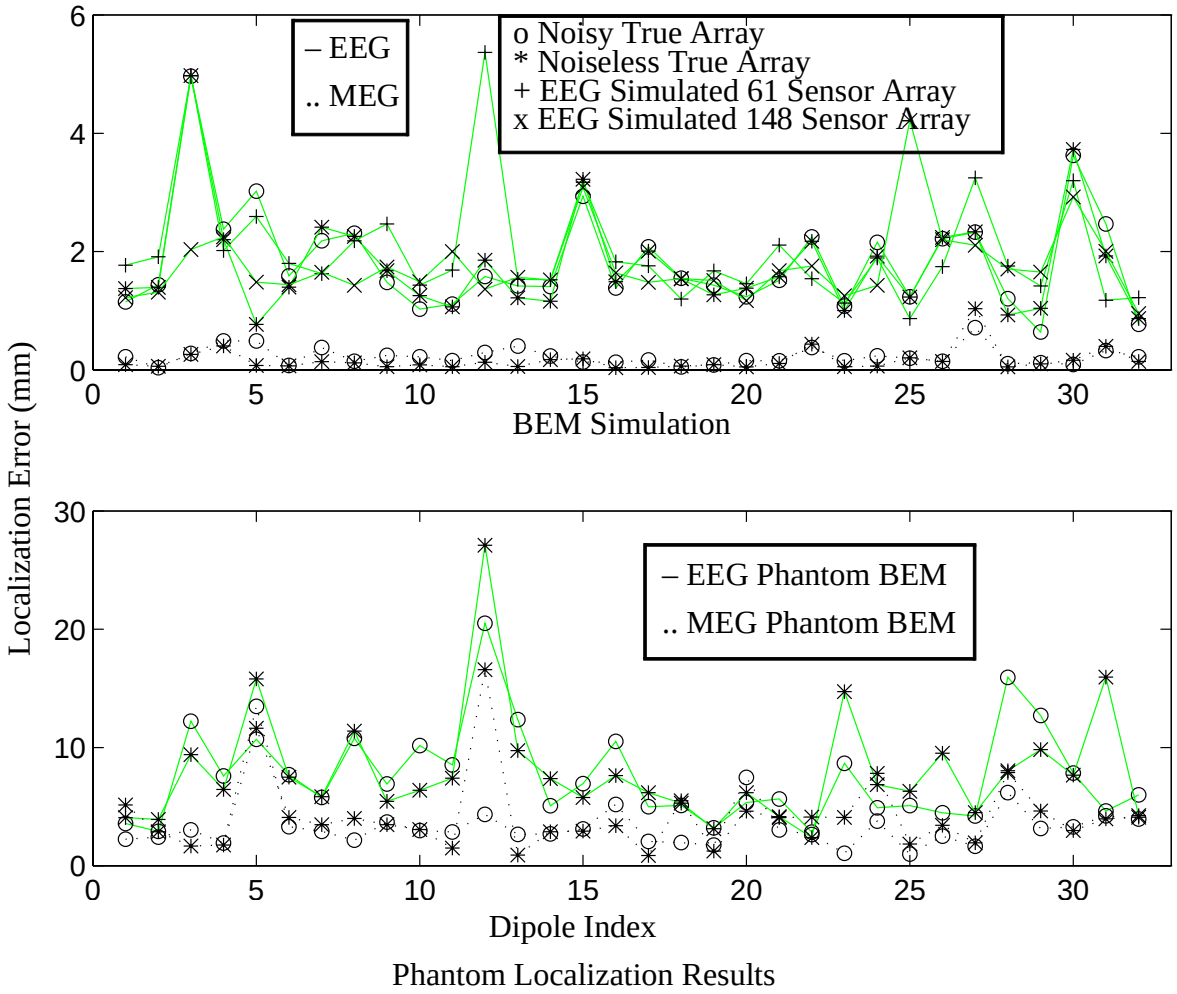

Fig. 15: Testing the BEM accuracy for EEG and MEG: (a) the simulation results for EEG and MEG, using a three sphere analytic solution for the forward model and a BEM on the inverse, for different array patterns and noise; (b) for comparison, the BEM localization results from the phantom (cf. Fig. 8 and Fig. 11).

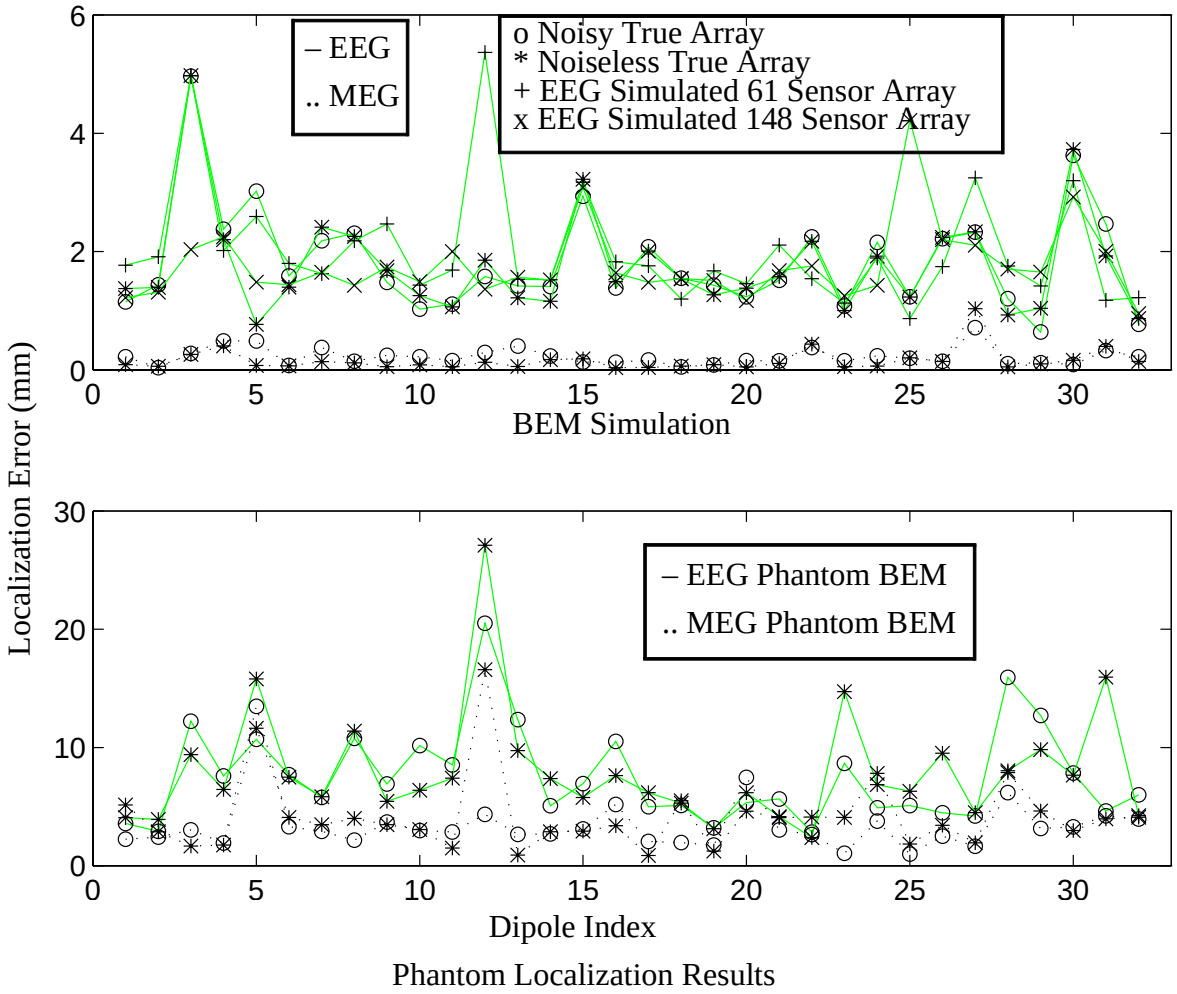

Fig. 15: Testing the BEM accuracy for EEG and MEG: (a) the simulation results for EEG and MEG, using a three sphere analytic solution for the forward model and a BEM on the inverse, for different array patterns and noise; (b) for comparison, the BEM localization results from the phantom (cf. Fig. 8 and Fig. 11).

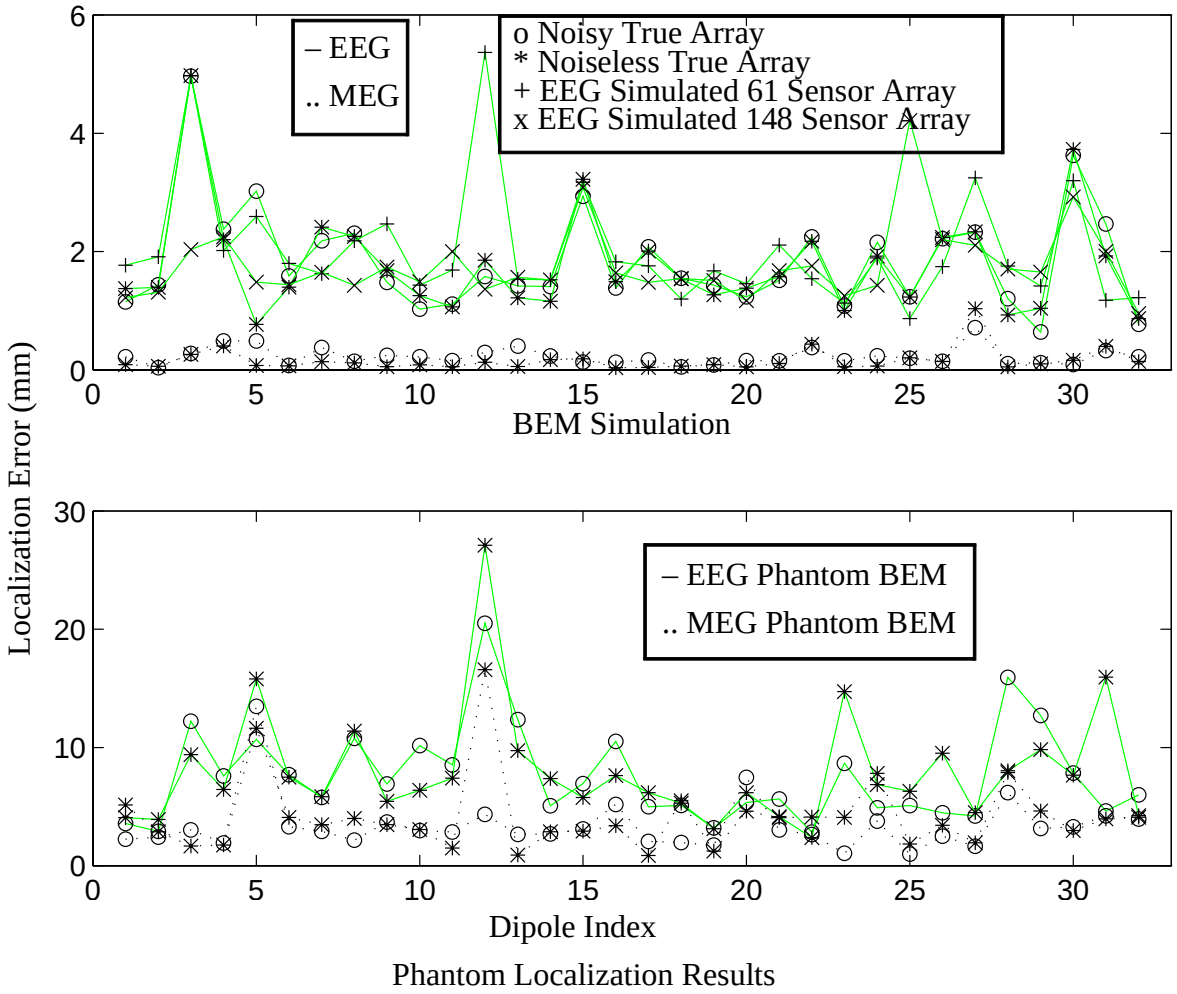

Fig. 15: Testing the BEM accuracy for EEG and MEG: (a) the simulation results for EEG and MEG, using a three sphere analytic solution for the forward model and a BEM on the inverse, for different array patterns and noise; (b) for comparison, the BEM localization results from the phantom (cf. Fig. 8 and Fig. 11).

Table 1: EEG and MEG mean localization errors. The simulations were generated using an analytic forward model calculation of three concentric spheres and a BEM for the inverse, with white noise added per the SNR displayed in Fig. 6. See Fig. 14 for simulation array patterns.

	EEG (mm)	MEG (mm)
Phantom, BEM Approach	7.62	3.40
Phantom, Locally Fitted Spheres Model	8.00	4.14
Noiseless Simulation, True Array Pattern	1.78	0.16
Noisy Simulation, True Array Pattern	1.85	0.23
Noisy EEG Simulation, Neuromag-122 pattern (61 Sensor) Array	2.04	–
Noisy EEG Simulation, 148 Sensor Array	1.77	–

Table 1: EEG and MEG mean localization errors. The simulations were generated using an analytic forward model calculation of three concentric spheres and a BEM for the inverse, with white noise added per the SNR displayed in Fig. 6. See Fig. 14 for simulation array patterns.

	EEG (mm)	MEG (mm)
Phantom, BEM Approach	7.62	3.40
Phantom, Locally Fitted Spheres Model	8.00	4.14
Noiseless Simulation, True Array Pattern	1.78	0.16
Noisy Simulation, True Array Pattern	1.85	0.23
Noisy EEG Simulation, Neuromag-122 pattern (61 Sensor) Array	2.04	–
Noisy EEG Simulation, 148 Sensor Array	1.77	–

Table 1: EEG and MEG mean localization errors. The simulations were generated using an analytic forward model calculation of three concentric spheres and a BEM for the inverse, with white noise added per the SNR displayed in Fig. 6. See Fig. 14 for simulation array patterns.

	EEG (mm)	MEG (mm)
Phantom, BEM Approach	7.62	3.40
Phantom, Locally Fitted Spheres Model	8.00	4.14
Noiseless Simulation, True Array Pattern	1.78	0.16
Noisy Simulation, True Array Pattern	1.85	0.23
Noisy EEG Simulation, Neuromag-122 pattern (61 Sensor) Array	2.04	–
Noisy EEG Simulation, 148 Sensor Array	1.77	–